SAHC

Safety Assessment of the Shah Mosque in Isfahan, Iran

Giacomo Destro Bisol

Portugal | 2019

ADVANCED MASTERS IN STRUCTURAL ANALYSIS
OF MONUMENTS AND HISTORICAL CONSTRUCTIONS

Master's Thesis

Giacomo Destro Bisol

Safety Assessment of the Shah Mosque in Isfahan, Iran

University of Minho

Portugal | 2019

ADVANCED MASTERS IN STRUCTURAL ANALYSIS
OF MONUMENTS AND HISTORICAL CONSTRUCTIONS

Master's Thesis

Giacomo Destro Bisol

Safety Assessment of the Shah Mosque in Isfahan, Iran

Portugal | 2019

DECLARATION

Name:	Giacomo Destro Bisol
Email:	dbisol@tiscali.it

Title of the Msc Dissertation:	Safety assessment of the Shah Mosque in Isfahan, Iran
Supervisor(s):	Paulo B. Lourenço, Ali Tavakoli Dinani
Year:	2019

I hereby declare that all information in this document has been obtained and presented in accordance with academic rules and ethical conduct. I also declare that, as required by these rules and conduct, I have fully cited and referenced all material and results that are not original to this work.

I hereby declare that the MSc Consortium responsible for the Advanced Masters in Structural Analysis of Monuments and Historical Constructions is allowed to store and make available electronically the present MSc Dissertation.

University:	University of Minho
Date:	17 / 07 / 2019
Signature:	

This page is left blank on purpose.

To my father.
To my mother and my sister for giving me the opportunity to complete this work.

This page is left blank on purpose.

ACKNOWLEDGEMENTS

First of all, I would like to thank my supervisors, Professor Paulo B. Lourenço And Professor Ali Tavakoli Dinani for wisely guiding me in this thesis.

I would also like to express my gratitude to Professor Javier Ortega for his constant help during these months.

I acknowledge the SAHC Consortium for granting me the opportunity to attend this Master and providing financial support.

I would also like to express my appreciation to all the SAHC lecturers, for their teaching and assistance.

To my SAHC friends and bestfriend.

My eternal gratitude to my family.

This page is left blank on purpose.

ABSTRACT

The structural analysis of monuments and historical construction has nowadays become a fundamental theme in order to preserve and maintain the cultural heritage for future generations. The target to achieve is to make the building live forever, but this goal, both from a technical point of view and from a scientific point of view, is rather complex. Furthermore, the theme of masonry structures, especially if they are located in seismic areas, has become an extremely actual subject. The study of complex monumental structures such as the Shah Mosque, the subject of this thesis, can and must become a useful research tool for the study of building heritage in general, aimed at reducing risk and protecting human life. This thesis focuses on the study of the structural stability of the Shah Mosque in Isfahan in Iran. The building was built in 1611, becoming an integral part of the urban transformation of the city of Isfahan, which became the new capital of Persia, by the will of the Safavid dynasty (whose dominion extended from 1501 to 1722). The mosque, which became a UNESCO heritage site since 1979, is characterized by an enormous hybrid bulbous double dome, formed by two shells, stiff masonry elements between the two domes and wooden elements. It can certainly be counted among the largest masonry bulb domes in the world, which are not yet fully known, especially in terms of static behavior. The research process is essentially based on four phases; (a) an initial state-of-the-art (b) a preliminary structural assessment, based on the information obtained in the literature (c) a series of in situ tests, aimed at characterizing the overall behavior of the structure and elastic properties of the material (d) a structural analysis aimed at understanding the performance of the building subject to gravitational loads and seismic action. During the thesis, attention will be paid, as far as the state-of-the-art is concerned, to the study of the genesis of the double dome, to the evaluation of the strengthening interventions suffered by the structure in the last century and to an evaluation of the previous structural analysis made on the Shah Mosque. As regards the tests carried out in situ, the study will focus on determining the dynamic properties of the structure and elastic properties of the constituent material, with particular attention to methods for evaluating the reliability of experimental data. Finally, with regard to the structural analysis, the interest will be directed to non-linear analysis. With particular regard to; (a) finite element modeling (b) material model (c) integration methods for iterative-incremental analysis (d) study of the results in terms of stress, strain and displacement. The results obtained allow to assess the performance of the building. As regards vertical loads, the structure seems to have an adequate safety level. Seismic analysis allowed to evaluate the main collapse mechanisms of the building, even if an implementation of this study in terms of expected earthquake and further analysis is strongly recommended. Finally, additional research to carry out on the structure will be proposed, in order to increase the level of knowledge on its static performance.

This page is left blank on purpose.

RESUMO

Análise de segurança da Mesquita do Xá em Isfahan, Irã.

A análise estrutural de monumentos e construções históricas tornou-se hoje um tema fundamental para preservar e manter o patrimônio cultural das gerações futuras. A meta a alcançar é fazer com que o edifício viva para sempre, mas esse objetivo, tanto do ponto de vista técnico quanto do ponto de vista científico, é bastante complexo. Além disso, o tema das estruturas de alvenaria, especialmente se elas estão localizadas em áreas sísmicas, tornou-se um assunto extremamente atual. O estudo de estruturas monumentais complexas como a Mesquita do Xá, objeto desta tese, pode e deve se tornar uma ferramenta de pesquisa útil para o estudo do patrimônio edilício em geral, visando reduzir riscos e proteger a vida humana. Esta tese enfoca o estudo da estabilidade estrutural da Mesquita do Xá, em Isfahan, no Irã. O edifício foi construído em 1611, tornando-se parte integrante da transformação urbana da cidade de Isfahan, que se tornou a nova capital da Pérsia, pela vontade da dinastia Safávida (cujo domínio se estendeu de 1501 a 1722). A mesquita, que se tornou patrimônio da UNESCO desde 1979, é caracterizada por uma enorme cúpula dupla híbrida bulbosa, formada por duas conchas, elementos de alvenaria rígidos entre as duas cúpulas e elementos de madeira. Pode certamente ser contado entre as maiores cúpulas de bulbo de alvenaria do mundo, que ainda não são totalmente conhecidas, especialmente em termos de comportamento estático. O processo de pesquisa é essencialmente baseado em quatro fases; (a) um estado inicial da técnica (b) uma avaliação estrutural preliminar, com base nas informações obtidas na literatura (c) uma série de testes in situ, visando caracterizar o comportamento geral da estrutura e propriedades elásticas do material (d) uma análise estrutural destinada a compreender o desempenho do edifício sujeito a cargas gravitacionais e ação sísmica. Durante a tese, será dada atenção, no que diz respeito ao estado da arte, ao estudo da gênese do duplo domo, à avaliação das intervenções de reforço sofridas pela estrutura no século passado e a uma avaliação da análise estrutural anterior feita na Mesquita do Xá. No que diz respeito aos ensaios realizados in situ, o estudo incidirá na determinação das propriedades dinâmicas da estrutura e das propriedades elásticas do material constituinte, com especial atenção aos métodos de avaliação da fiabilidade dos dados experimentais. Finalmente, no que diz respeito à análise estrutural, o interesse será direcionado para análise não linear. Com especial atenção para; (a) modelagem de elementos finitos (b) modelo de material (c) métodos de integração para análise incremental iterativa (d) estudo dos resultados em termos de tensão, deformação e deslocamento. Os resultados obtidos permitem avaliar o desempenho do edifício. No que diz respeito às cargas verticais, a estrutura parece ter um nível de segurança adequado. A análise sísmica permitiu avaliar os principais mecanismos de colapso do edifício, mesmo que uma implementação deste estudo em termos de sismos esperados e análise adicional seja fortemente recomendada. Por fim, serão propostas pesquisas adicionais para realizar a estrutura, a fim de aumentar o nível de conhecimento sobre seu desempenho estático.

This page is left blank on purpose.

RIASSUNTO

Valutazione della sicurezza strutturale della Moschea dello Shah in Isfahan, Iran.

L'analisi strutturale delle costruzioni storiche e monumentali è diventato oggigiorno un tema fondamentale al fine di preservare e conservare il patrimonio culturale alle future generazioni. L'obiettivo da perseverare è quello di far vivere per sempre l'edificio, ma tale obiettivo, sia da un punto di vista tecnico che da un punto di vista scientifico risulta piuttosto complesso. Inoltre, il tema delle costruzioni in muratura, specialmente se si trovano in zona sismica, è diventato un tema di estrema attualità. Lo studio di strutture monumentali complesse come ad esempio la Moschea dello Shah, oggetto di questa tesi, può e deve diventare uno strumento di ricerca utile allo studio del patrimonio edilizio in generale, finalizzato alla riduzione del rischio e alla protezione della vita umana. Questa tesi è incentrata sullo studio della stabilità strutturale della Moschea dello Shah ad Isfahan in Iran. L'edificio venne costruito nel 1611 divenendo parte integrante della trasformazione urbana della città di Isfahan, da poco diventata nuova capitale della persia, per volontà della dinastia Safavide (il cui dominio si è esteso dal 1501 al 1722). La moschea, diventata patrimonio UNESCO dal 1979, è caratterizza da un enorme doppia cupola a bulbo ibrida, formata da due gusci, elementi irrigidenti in muratura tra le due cupole ed elementi lignei. Essa è di certo annoverabile tra le più grandi cupole a bulbo in muratura al mondo, delle quali ancora non si ha una piena conoscenza, specialmente dal punto di vista del funzionamento statico. Il processo di ricerca di basa sostanzialmente su quattro fasi; (a) un iniziale stato dell'arte (b) una preliminare valutazione strutturale, basate sulle informazioni ottenute in letteratura (c) una serie di test in situ, finalizzati alla caratterizzazione del comportamento globale della struttura e delle proprietà elastiche del materiale (d) un'analisi strutturale finalizzata a capire le prestazioni dell'edificio soggetto ai carichi gravitazionali ed all'azione sismica. Durante lo svolgimento della tesi, l'attenzione sarà rivolta, per quanto riguarda lo stato dell'arte, ad uno studio della genesi della doppia cupola, alla valutazione degli interventi di rinforzo subiti dalla struttura nell'ultimo secolo ed a una valutazione delle precedenti analisi strutturali effettuate sulla Moschea dello Shah. Per quanto concerne i test effettuati in situ, lo studio sarà focalizzato sulla determinazione delle proprietà dinamiche della struttura e delle proprietà elastiche del materiale costituente, con particolare attenzione ai metodi per valutare l'affidabilità dei dati sperimentali. Infine, riguardo l'analisi strutturale, l'interesse sarà rivolto alle analisi non lineari. Con particolare riguardo a; (a) modellazione agli elementi finiti (b) modelli per la descrizione del materiale (c) metodi solutivi per analisi iterative-incrementali (d) analisi dei risultati. I risultati ottenuti consentono di valutare le prestazioni dell'edificio. Per quanto concerne i carichi verticali, la struttura sembra avere un adeguato livello di sicurezza. L'analisi sismica ha permesso di valutare i principali meccanismi di collasso dell'edificio, anche se un'implementazione di questo studio in termini di sisma atteso e di ulteriori analisi è fortemente raccomandato. Infine, si proporranno delle aggiuntive ricerche da effettuare sulla struttura, al fine di accrescere il livello di conoscenza sulle sue prestazioni statiche.

This page is left blank on purpose.

TABLE OF CONTENTS

LIST OF FIGURES

LIST OF TABLES

LIST OF EQUATIONS

1. INTRODUCTION

"The supreme Iranian art, in the proper meaning of the word, has always been its architecture. The supremacy of architecture applies to both pre and post Islamic periods."(Yarshater, 1983). Shah Mosque or Jameh Abbasi Mosque (fig 1.1), also known as Shah Mosque, is a Mosque in Isfahan, standing in the south side of Naghsh-e Jahan Square. This Mosque has been built during the Safavid period, ordered by the Shah Abbas I (or Abbas the Great) of Persia (Blake, 1999). The Shah Mosque of Isfahan is one of the everlasting masterpieces of architecture in Iran. It is one of the finest Islamic edifices in the world, topped with an imposing bulbous double-shell dome with 22.65m span and 52m height.

Figure 1.1 The Shah Mosque in Isfahan, Iran (Photo by author, 2019)

1.1 Context and motivation

Given the value of the building and its unquestionable importance, a structural assessment seems necessary to determine its safety level in order to establish an adequate maintenance measures and if a reinforcement project is necessary. For this purpose, structural analysis is a fundamental tool to obtain adequate information regarding the condition of the structure, but certainly cannot by itself provide enough information. In general, the requirements for the structural analysis are:

- Geometry, historical structures are often characterized by a very complex geometry. They often include straight or curved members. They combine curved 1D members (arches, flying arches) with 2D members (vaults, domes) and 3D ones (fillings, pendentives...). They combine slender members with massive ones (massive piers, walls buttresses, foundations...). However, today numerical methods (such as FEM) do afford a realistic and accurate description of geometry (Roca et al., 2010,302).
- Material Behavior, historical or traditional materials such as earth, brick or stone masonry and wood are characterized by very complex mechanical and strength phenomena still challenging our 3 modeling abilities. In particular, masonry is characterized by its composite character (it includes stone or brick in combination with mortar or day joints), a brittle response in tension (with almost null tensile strength),

a frictional response in shear (once the limited bond between units and mortar is lost) and anisotropy (Roca *et al.*, 2010: 301).

- Morphology, a more significant problem lays in the characterization and description of the internal morphology of structural members and their connections. Structural members are often non-homogeneous and show complex internal structures including several layers, filling, material, cavities, metal insertions and other possible singularities. Connections are singular regions featuring specific geometric and morphological treats. The transference of forces may activate specific resisting phenomena (contact problems, friction, eccentric loading). Modeling morphology and connections in detail may be extremely demanding from a computational point of view (Roca *et al.*, 2010: 302).
- Actions, historical structures may have experienced (and keep on experiencing) actions of very different nature, including the effects of gravity forces in the long term, earthquake, environmental effects (thermal effects, chemical or physical attack), and anthropogenic actions such as architectural alterations, intentional destruction, inadequate restorations... Many of these actions are to be characterized in historical time.
- Effects linked to the construction process, during the construction of the building many problems can be occurred due to design errors or to processing errors. This mistake can strongly affect the building during its entire life.
- Existing imperfections and damage existing and general alterations may affect very significantly the response of the structure. Damage and deformation are to be modeled, as present features of any existing structure, to grant adequate realism and accuracy in the prediction of the actual performance and capacity. Damage encompasses mechanical cracking, material decay (due to chemical or physical attack) or whatever phenomena influencing on the original capacity of materials and structural members (Roca *et al.*, 2010: 303).
- The interaction of the structure with the soil, the global behavior of the building can be strongly affected by the soil (changing for example the response under seismic actions). Another phenomena to keep under control are settlements, one of the main problems in historical construction.
- History, it is an essential dimension of the building and must be considered and integrated in the model. The following effects linked to history may have had influence on the structural response and existing damage: Construction process, architectural alterations, additions, destruction in occasion of conflicts (wars...), natural disasters (earthquake, floods, fires...) and long-term decay or damage phenomena. History constitutes a source for knowledge. In many occasions, the historical performance of the building can be engineered to obtain conclusions on the structural performance and strength. For instance, the performance shown during past earthquakes can be considered to improve the understanding on the seismic capacity. The history of the building constitutes a unique experiment occurred in true scale of space and time (Roca *et al.*, 2010: 303).

1.2 Methodology and scope of the work

As stated, in order to make a reliable assessment of the structure, it is necessary to have a full picture of the building. Structural analysis of historical structures constitutes in fact a multidisciplinary, multifaceted activity requiring a clever integration of different approaches and sources of evidence (Roca *et al.*, 2010: 301). For this purpose and in order to gather the necessary information for the safety evaluation of the Shah Mosque, in this thesis, it was decided to carry out:

1) Historical research, it is important as it leads us to understand structural performance of the building along with monitoring, inspection and structural analysis. This research is focused on typological and historical geneses of the building (in terms of construction methods, interventions made on the building and actions suffered by the structure during its life) with particular emphasis in double-shell domes. The dome is a hierarchically priority element in eastern architectural history that influences subsequent developments in the area.

2) Morphological, material and geometric characterization, to this end, the information found in the literature will be used first to perform a preliminary structural analysis, subsequently, in order to obtain more reliable results, through inspections and tests additional information will be collected.

3) Validation of the model, through the experimental data it will be possible to calibrate the model, obtaining for example, information about its dynamic properties. Finally, the results obtained before and after the implementation with the experimental data will be compared.

4) Structural Analysis, after having collected enough data, it will be possible to perform an evaluation of the building, also taking into consideration the seismic action, through structural analysis. The main objectives of this evaluation will be to understand the possible causes of damage (diagnosis), establish the conditions of the structure (safety level) and, if necessary, establish an adequate strengthening strategy.

2. HISTORICAL RESEARCH

The building is part of a complex in Isfahan, planned to be the heart of the Safavid capital, with the square Naqsh-e jahān (in Persian Meidān Naqsh-e jahān, means: "the image of the world") in the center. This huge square is flanked on each side by four monumental buildings (fig 2.1) linked by series of arcades of two stories: to the north, the Portico of Qeyssariyeh (1602-1619), to the south, the Royal Mosque (1611-1629), to the east, the Mosque of Sheykh Lotfollah (1602-1618) and to the west, the pavilion of *Ali Qapu* a small *Timurid* palace (15th century)(Dinani, 2019: 51).

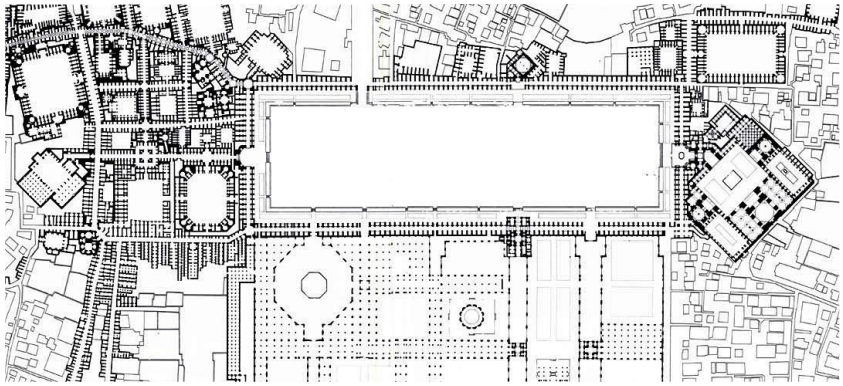

Figure 2.1 The Naqsh-e Jahān square (Herdeg, 1990)

In fact, the Royal Square of Isfahan is claimed to be "the most relevant monument of Persian socio- cultural life during the Safavid period" (*ICOMOS Report of the Bureau*, 1979).

2.1 History of the building

The construction of Shah Mosque started in 1611 and was completed in 1629. In 1979, it became together with Naghsh-e Jahan Meidan a World Heritage Site. This monument has been an integral part of the commercial redevelopment of the town- square of Isfahan during the Safavid age. The Safavid age has long been recognized as a period of special interest in the history of Iran in the Islamic era (1501-1736). This is a period of rare dynastic continuity and stability, military might, artistic brilliance and economic prosperity. The two centuries of Safavid rule were also important in laying the foundation for the emergence of the modern state of Iran (Dinani, 2019: 49). During this period a series of city improvement operations were established (fig 2.2) which can be divided into two main steps, as detailed next.

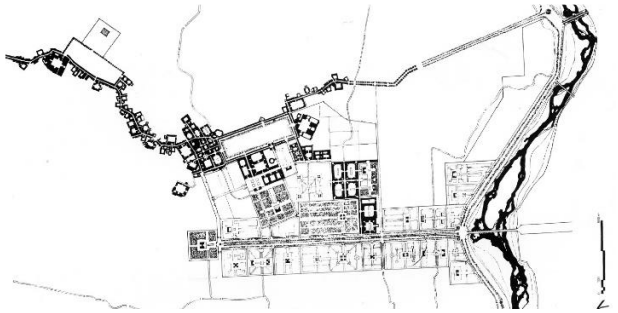

Figure 2.2 Urban development in Safavid period (Ardalan and Bakhtiar, 1973)

The first urban development step began from 1598 to 1611 which is called "establishing processes" that programmed Isfahan as a capital city, meaning works required by the definition of Isfahan as an imperial center, with the palace complex, the *meidan* area, and the royal pleasance (a secluded garden). The second urban development step is called "sumptuous". Projects such as the Shah Mosque were made to celebrate the grandeur of the Safavid state under Shah Abbas's reign. Indeed, the Royal Mosque, became the greater project in the *meidan* (Dinani, 2019). From the architectural viewpoint, the Mosque represents a classic Persian four *eyvan* plan (an *eyvan* is a rectangular hall or space, usually vaulted, walled on three sides, with one end entirely open) with a domed chamber over the *meḥrāb* sanctuary (fig 2.3 and fig. 2.4) (the *meḥrāb* is a semicircular niche in the wall of a Mosque that indicates the direction of Mecca and hence the direction that Muslims should face when praying). In many ways, however, this building represents an exceptionally creative response to a series of pressing needs and pre-existing urban constraints. In fact, for example, the principal façade of the Mosque had to remain flush with the southern side of the *meydān*, while at the same time orientating its *meḥrāb* correctly.

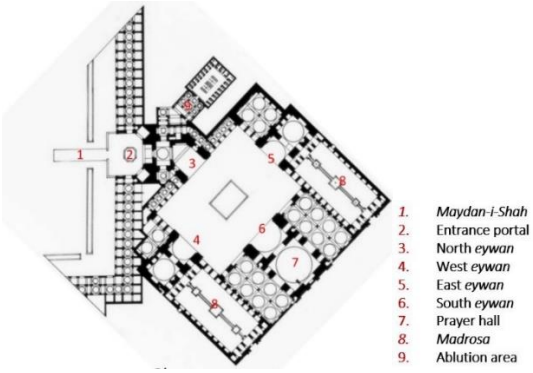

Figure 2.3 Plan of the Shah Mosque (Coste, 1867)

Regarding the construction material, further to the use of brick as a main material, the discovery of a marble quarry in the vicinity of Isfahan provided the usage of the stone for covering only the inner walls, a local but scarce material (Dinani, 2019).

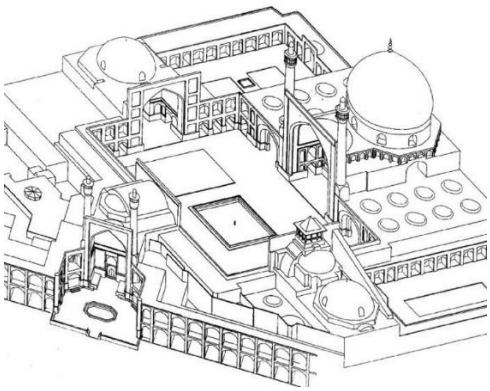

Figure 2.4 Axonometric View of the Shah Mosque (Archive Center of Tehran Shahid Beheshti University, 1996)

2.2 Past structural intervention

During the recent centuries, there have been several restorations on Shah Mosque, mainly repairing mosaic faience and strengthening of the structure. The first restoration for which there is information is for sure that one of the 1932. The first conservation report, for the Mosque, is a Persian text containing all the planning and proceedings for restoration and renovation of Isfahan monuments. In this report (Maaref-I Salnameh-I Esfahan, 1936), it is possible to find a brief story of the first renovation about Shah Mosque in 1932. The report points out that a deep crack appeared in the south *eyvan* faced to the dome, which resulted in a danger of collapse. The report points out that a deep crack had appeared in the south *eyvan* faced to the dome (probably due to an earthquake in 1844), which resulted in a danger of collapse. This was one of the reasons why a financial plan for the Shah Mosque was planned, it was supported by charity funds, almost 110000 *Rials* served by Municipality, Ministries of Education and Finance between 1932 and 1933. In 1932, 1 *Rial* was equal to the 0.0732 grams of gold. Currently, the average gold price (2016-18) is about 36 Euro/gram, thus the budget of 360000 *Rials* may be translated to about one million of Euro (Dinani, 2019). Hossein Moarefi, as a maestro in restoration, at the time claimed that the acceleration of the construction process, due to the large number and time limitation of Safavid projects, could be the main reasons of the structural weakness in some parts of the Mosque However, he did not neglect the role of the earthquake of 1844 in the structural performance of the monument (Varjavand, 1976). The proposal of intervention for the South *eyvan* and dome proposed by Moarefi included (Maaref-I Salnameh-I Esfahan, 1936; Varjavand, 1976):

- Preparing a wooden scaffolding with 32 m height.
- Collecting and coding all the remaining tiles.
- Connect the two Minarets through a steel tie to reduce their displacement (fig2.5).
- Stabilizing the *eyvan* with a net of three steel I-beams in the right and two others in the left side (fig 2.5).
- Re-assembling old tiles with pins and new ones without pins.
- Applying I-beams steel rings with 90 m perimeter on the extrados of the outer dome in the position of the traditional encircling wooden ties system.

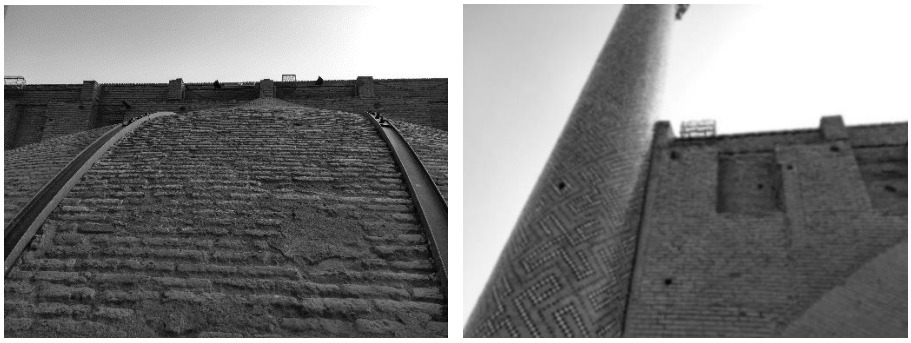

Figure 2.5 Structural strengthening of the south *eyvan* (right) connection between the two minarets (Photo by author, 2019)

It is possible to say that this intervention of I-beams and cables was done in order to avoid the out of plane mechanism of the facade of the south *eyvan*. In addition, the foundation of the east dome has been reinforced and the cracks restored as well as the roof of the Mosque, which was paved by bricks (Dinani, 2019).

2.3 The double dome

It has generally been recognized that domes whether as single domical buildings or in large complexes of buildings have played a significant role in Islamic architecture. They are considerably different in size and type (fig2.6). The double-shell domes (dome whose two shells have noticeable distances) are the majority of Islamic domes and had gradually developed from the early Islamic epochs through to the late Islamic era developed from the early Islamic epochs through to the late Islamic era (Ashkan and Ahmad, 2010). Regarding the double-shell dome types, two subdivision groups have been defined based on how these two shells are composed together (Pirnia, 1987, 1991). Generally speaking, one type is slightly doubled, as the profile of both domes follows up with a short distance from each other. Another type refers to the double dome with different domical curvatures manifesting important in-between space including radial stiffener walls and wooden elements (Dinani, 2019).

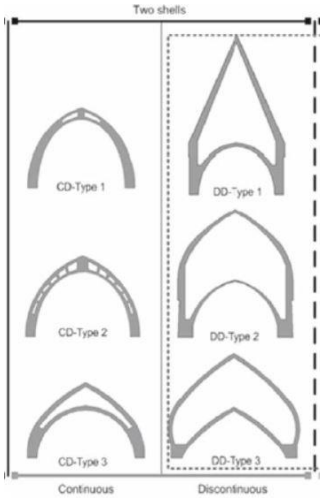

Figure 2.6 Typologies of double dome in Persia (Ashkan and Ahmad, 2010)

In this regard, the dome over the Sultan Bakht Aqa mausoleum in Isfahan (1351-52 A.D.) was the earliest known example of the double-shell dome where the external and internal shells basically exhibited different profiles with radial stiffeners (fig. 2.7) (Ashkan and Ahmad, 2009).

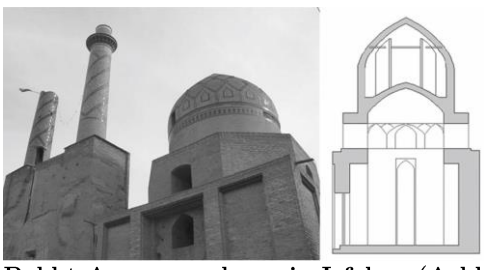

Figure 2.7 Sultan Bakht Aqa mausoleum in Isfahan (Ashkan and Ahmad, 2010)

2.3.1 Constituent elements of the double dome

The most common prototype of double-shell domes consists of:

- The external shell**,** (the most importance component and the most visible part of dome). It is the only architectural item that was conceptually found in synonymous during the several Islamic epochs. The bulbous external dome is the most prominent shape of the double-shell domes in the last generation of the Islamic domes that were appeared, especially, since the Safavids dynasty in the Middle East and central Asia. This external shell has a longer diameter than the drum that it rests on and its height value usually surpass its width. Its thickness is usually proportionally reduced from its base to the top (Ashkan and Ahmad, 2010).
- Internal shell**,** this covers the internal domical chamber and has a simple geometric shape, compared to the external shell. In fact, it is necessary that its geometric shape fully conformed with the external shell for transferring forces from the upper components to the transition tier in order to stabilize the dome structure (Ashkan and Ahmad, 2010).
- Drum**,** used by the designers to make the building as high as possible Its thickness must be sufficient to transfer and neutralize the vertical thrust of the external shell to the lower parts, especially, the internal shell.
- Internal stiffeners with or without wooden elements, these are specific characteristics of such domes. Generally speaking, they were built in the space between the two shells (fig 2.8) for the main purpose to support the external dome. Their settings and sizes strongly depends on the dome span.

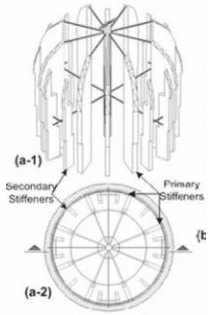

Figure 2.8 Example of internal stiffeners with the wooden struts in Sultan Bakht Aqa (Ashkan and Ahmad, 2010)

After having listed the constituent elements of the double domes, it is important to stress its indisputable advantages. One of the main virtues of discontinuous double-shell domes is the separation of the weathering surface from the internal shell, thereby, providing substantially improved weather protection (Mainstone, 2001). From the structural point of view, the double-dome technique allows the use of thin shells, reducing the overall weight. In fact, the construction method was extremely successful, despite the seismic hazard in the Middle East and central Asia. Architecturally, double-domes permitted an increase in the external size and height of the dome thereby making it more imposing without the necessary increase in its internal height which improved its aesthetical meaning and splendor (Hillenbrand, 1994).

2.3.2 Construction method

Most domes were constructed from quasi-brittle materials, such as stone, mud brick and baked brick. Sometimes, fragile ceramics were utilized, not only to embellish the exterior faces of the external shell and the drum, but also to prevent the penetrations of rain and snow. The method for erecting the discontinuous double-shell dome (fig 2.9) involves, first, the building of the internal shell within the main roof. The drum and the stiffeners were then built together on the lower components. The last task is to set the wooden struts in the devised holes between the radial walls and then to close the external shell (Ashkan and Ahmad, 2010). In bulbous domes, the directions of the bricks' courses are almost always perpendicular to the generated curve of the dome surface in both the external and internal shells. The thickness of both shells was also gradually reduced in height to decrease the weight of the shells and to limit the use of material. Regarding the design, the role of mathematicians cannot be overlooked. In fact, the main efforts aimed to define and formulate 'an exact geometric method' (fig 2.7) rather than to determine certain proportions, not only for the dome designs, but also, for the arches and vaults shapes (Ashkan and Ahmad, 2010). Regarding the masonry domes in Iran, they are constructed without centering, based on special techniques subtly reflected in the structure assemblage. This feature results in a juxtaposition of the masonry and wooden elements, and a techno-poetic fulcrum, namely the *Shahang-Hanjar* (Pirnia, 1991) technique. This contains a vertical wooden column (fig 2.10) established in the center of the dome with radial timbers fixed to the structure and an *Ardakan* chain radially adjusted. This simple system plays both roles of scaffolding and building guidance. The outer dome and walls, which correspond to this 'productive machine' for the structure, are simultaneously erected (Dinani, Sadeghi and Lourenco, 2019)

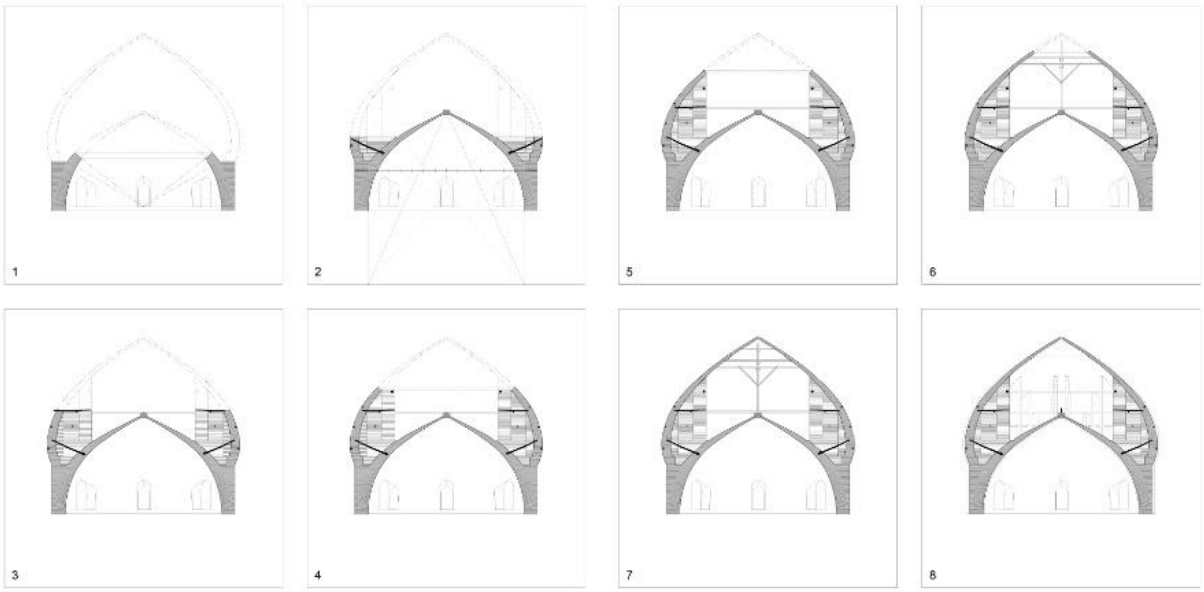

Figure 2.9 construction sequences of the Shah Mosque (Dinani, 2019)

Figure 2.10 The vertical column in the Shah Mosque substituted with a metallic element (photo by author, 2019)

2.3.3 The double dome of the Shah Mosque

The Shah's dome as a hybrid double dome (HDD) is a composite structure of brick double dome with radial stiffener walls, wooden ties arranged in radial, circumferential or diagonal positions adopted in the building construction and the structural system (Dinani *et al*, 2019). It adopts the slightly bulbous shape for the outer dome and a pointed dome for the inner dome (fig 2.11). Regarding the dimensions, the outer diameter of the drum is 26.3 m. The upper dome is 52 m high from the ground and 24.3 m from the spring point of the inner dome. The lower dome is 38 m high from the ground level and 13.3 m from its springing with a huge space between the two domes with the height of 11.3 m.

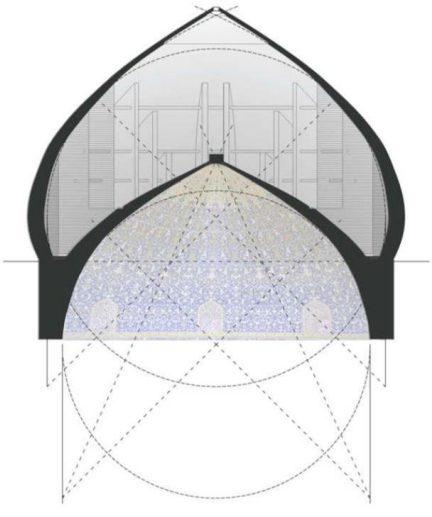

Figure 2.11 Double dome of the Shah Mosque in Isfahan (Dinani, 2016)

The thickness of the lower dome varies from 1.70 m (base) to 0.25 m (top). At the height of 4 m from the springing of the dome, the thickness reaches a maximum of 2.20 m, as the drum merges to the inner dome to make a platform for placing the outer dome. In the outer dome the thickness of its profile is from 1.10 m to 0.30 m (Dinani, 2019). Regarding the dome of the Shah Mosque, a fundamental role is played by radial stiffeners (fig 2.12) walls which have an essential role in subtlety, stability and construction of Persian bulbous dome. This Dome is composed by 32 radial walls with thickness of 40 cm and variable height, 9 of that are height of 12.6 m, 8 are

height 10.6 m and 15 are height 7. To retain horizontal thrust the walls lock to the outer dome and embedded wooden elements (although the structural effect of these elements appears poor) join them to the inner dome. Therefore, the structural role of the integrated walls into the domes cannot be ignored. It is clear how these stiffeners give a structural contribute keeping the thrust line of the outer dome within the wall (Dinani, 2019) that otherwise, due to the bulb shape of the dome it could come out of the dome section, causing the possible loss of equilibrium (how the static theorem of the limit analysis state).

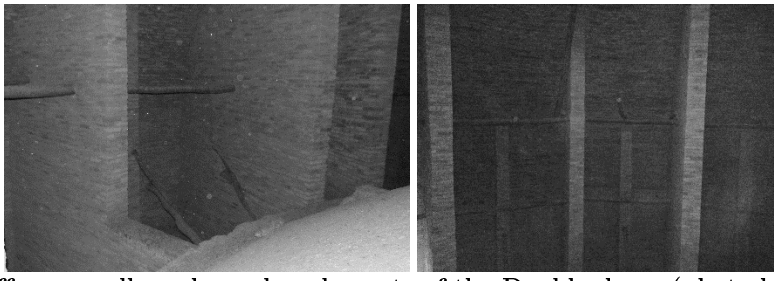

Figure 2.12 Stiffeners walls and wooden elements of the Double dome (photo by author, 2019)

Other important components that cannot not be mentioned are the various wooden elements present in the dome (tab 2.1). For the construction process and structural reasons, wooden members of double dome are either exposed or embedded, in both circumferential and radial arrangements (fig 2.12). On the extrados of the outer dome, an encircling wooden ties system is laid under the layer of the faience tiles. These wooden chains locked together might be inserted during the construction to balance the horizontal thrusts of the outer dome. There are 42 circumferential elements as scaffolding connecting the walls in three levels, which are not anchored. Moreover 15 diagonal elements interlock the shortest stiffeners walls into the inner dome (Dinani *et al.*, 2019: 90).

Type	Plane	Position in plan / Position in section	Connection form	Dimensions	No	Structural or Non-structural element
Radial	xy	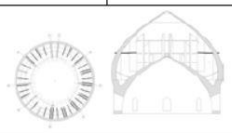	Cantilevered wooden element	L: 340 cm D: 10 cm	33	Non-structural element, only constructive component
Circumferential elements	xy	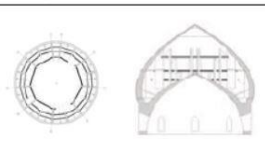	Both sides are embedded in the masonry but not anchored	L: 170, 380 cm D: 16 cm	17	Non-structural element, only constructive component
				L: 160, 330 cm D: 20 cm	16	
				L: 125, 540, 560 cm D: 25 cm	7+2	
	xy	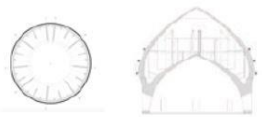	Wooden chains are locked together	85 m, 83 m, 75 m	3	Structural element
	xz	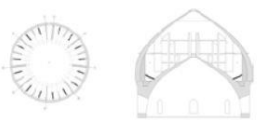	Both sides are embedded in the masonry and fixed	L: 360 cm D: 20 cm	15	Structural element

Table 2.1 Typology and function of the wooden elements (Dinani, 2019)

2.4 Historical seismicity of the Isfahan region

The study of the seismicity of the area is of fundamental importance, first to better understand the actions suffered by the structure during its lifetime, second to have an idea about the future actions that the structure will have to resist. This information is also essential to assess the safety level of the building and to plan a possible strengthening design. The city of Isfahan, the fourth largest city in Iran with a population of about 2 million, is located about 100 km from the main Zagros Thrust (fig 2.13) in central Iran in an area of subdued seismic activity. Seismic catalogues show that Isfahan was hit by earthquakes several times, with the loss of thousands of lives. But the examination of all available seismological, tectonic, historical and field data shows unambiguously that during its known history the city of Isfahan was never destroyed by an earthquake (Ambraseys, 1979).

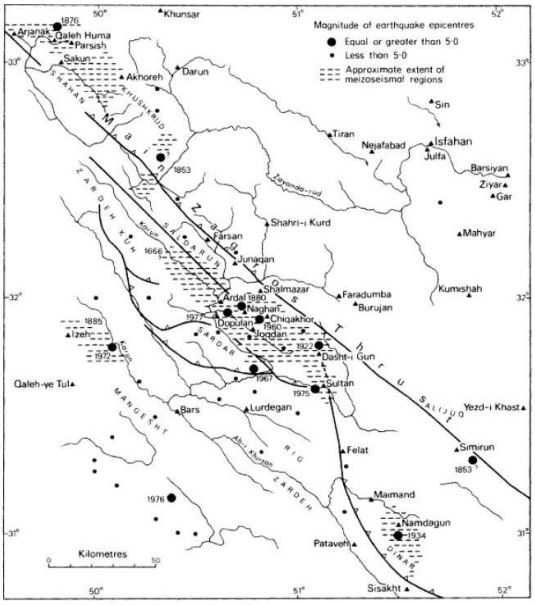

Figure 2.13 Map of Isfahan and Chahar Mahal (Ambraseys, 1979)

It is then clear that there are doubts about the seismic events suffered by the city of Isfahan. Although some historical sources show the existence of destructive earthquakes, the current seismicity assessment techniques seem to deny these sources. It therefore seems appropriate to evaluate some past seismic events in order to understand the probability that an earthquake will hit the city of Isfahan.

2.4.1 Earthquakes in Isfahan

The earliest account of allegedly destructive earthquakes in the Isfahan region can be shown to be inaccurate, and the inclusion of these events in modern works of reference is the result of an uncritical use of the available source material. In fact, these earthquakes are reported by few or sometimes single sources, often many years after the seismic event. It is therefore important to remember the lack of reliability of this data. Among the main seismic events stated, it is possible to include:

- 853 AD, which is the first earthquake that allegedly have affected Isfahan. This event seems to have been devastating for the city causing countless damages and thousands of victims. However, this event is reported by a single source about a thousand years after. There is no clear evidence that Isfahan was destroyed in the middle of the 9th century by an earthquake.
- 1344 AD, for this event we have the earliest explicit statement for a damaging earthquake in Isfahan. It is documented that the city of Isfahan was shaken by a mighty earthquake which ruined its walls and some of the houses, and about 20 people were killed beneath the ruins. Also, for this case, only one source of information is available.
- 1778 AD, an earthquake almost totally destroyed Kashan. The shock was strongly felt in Isfahan, about 150km from the epicenter, but without any evidence that it caused damage.
- 1844 AD, an earthquake shock was felt in Isfahan which originated from a damaging earthquake 120km north of the city, which ruined the region of Kuhrud. In Isfahan, the shock caused no damage except to a small part of the Jameh Mosque. This building, already structurally weakened, was cracked by the shock and its two minarets were detached from the main body of the edifice (Ambraseys, 1979), making strengthening necessary (fig 2.14). Furthermore, as a result of this event, damage also occurred in the Shah Mosque, the earthquake caused the cracks on the semi-dome of the *eyvan* (Dinani, 2019).

Figure 2.14 Reinforcement of the Jameh Mosque, Isfahan (Photo by author, 2019)

Other earthquakes to take into account are those of 1853 AD in the district of Buriari and of 1868 AD, in Dasht-i Kavir, felt in Isfahan but there are no documents attesting damage following these events. In the 20th century, several earthquakes hit the region around Isfahan (see annex A). The most relevant is the one of the 1977. This earthquake killed 366 people in the region of Naghan and several villages were ruined. Most of the damage was sustained by poorly built adobe houses. But the shock seems not to have been felt in Isfahan (Ambraseys, 1979).

2.4.2 Seismic hazard and risk

There is little doubt that the occurrence of destructive earthquakes in Isfahan is rare, considering that it was one of the most important cities on a major trade route in Iran and that its history is well covered in different sources. The available long-term historical and recent instrumental information confirms that whenever an earthquake has been felt in Isfahan, it has been when a serious shock had occurred at some considerable distance from the city. In this case, some slight movement of the ground was felt which occasionally caused concern but rarely caused serious damage. Earlier writers praising Isfahan point out that earthquakes seldom occur there. This is a conspicuous fact attributed to the beauty of the city together with its tall, slender buildings, houses two to three storeys high, and free-standing minarets (Ambraseys, 1979). As a matter of fact, a large number of the most splendid Saljuq minarets, standing up to 50 m high, have survived for seven centuries in Isfahan and around the city. These are not to be found in other major towns in Iran, such as Tabriz, Shiraz, Tehran, Kerman or Qazvin. All the references to destructive shocks in Isfahan can be shown to be illegitimate and the result of an uncritical use of early and more recent source of information (Ambraseys, 1979). The only exception is the one genuine reference to earthquake damage in 1344. It is therefore possible to state that the Isfahan region is an area with low seismic hazard, but risk is moderate to high, given the presence of vulnerable buildings of important cultural value, namely tall minarets and the imposing bulbous domes. It therefore seems appropriate to study the effect of seismic action in the safety of the Shah Mosque in Isfahan.

2.5 An overview on the previous structural analysis on the Shah Mosque

Shah Mosque has been a subject of structural analysis by Hejazi (1997, 2005), Mirghaderi (2005), Kalantari (2017) and Dinani (2019). Hejazi and Mirghaderi's work (fig 2.15) was a quantitative research. Although the model analyzed different scenarios by removing the structural elements such as radial walls, the model has not considered the wooden elements, openings on the drum, soil properties and entire part of the building. The numerical results have not considered the existing condition of the building such as the damages and crack patters but also the historical performance of the building. According to their results, the double dome of Shah Mosque is the most vulnerable one when compared to single domes in Isfahan and the stiffener walls played a crucial role in the stability of the double dome against earthquake (Hejazi, 2005). The research done by Kalantari in 2016 applied only linear analysis for the Shah's double dome due to its self-weight. Based on that, he proposed structural strengthening by extending the radial walls towards the center, which increase the weight of the dome, to reduce the deformation of the upper part of the dome.

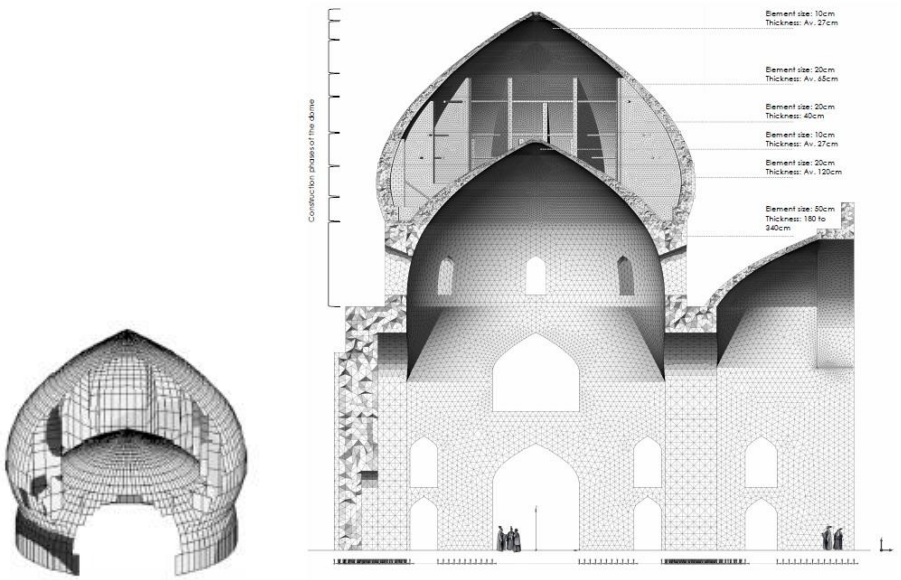

Figure 2.15 (left) FE model of the Shah's double dome for seismic analysis (Hejazi, 2005) (right) FE Model by considering the construction phases and encircling ties system(Dinani, 2019).

An important tool, for the subsequent phases, is the study of the previous structural analysis carried out on the mosque by Dinani in 2019 which is the main resource in this field. Dinani's research was considerable in terms of approach, inquiries, modeling method, and results. The investigation combined historical evidence, crack patterns, and numerical analysis to understanding the structural behavior and proposing a strengthening for the double dome. He performed a deep study of the mosque, analyzing, first of all of all the material property of the structure (this data will be used in the next section). Subsequently, he studied the response of the mosque, with particular attention to the hybrid double dome, subjected to vertical (Fig. 2.16 and 2.17) and horizontal loads through nonlinear analysis. Then he proposed cable net strengthening for the double dome of the Shah Mosque (Fig. 2.16 and 2.17).

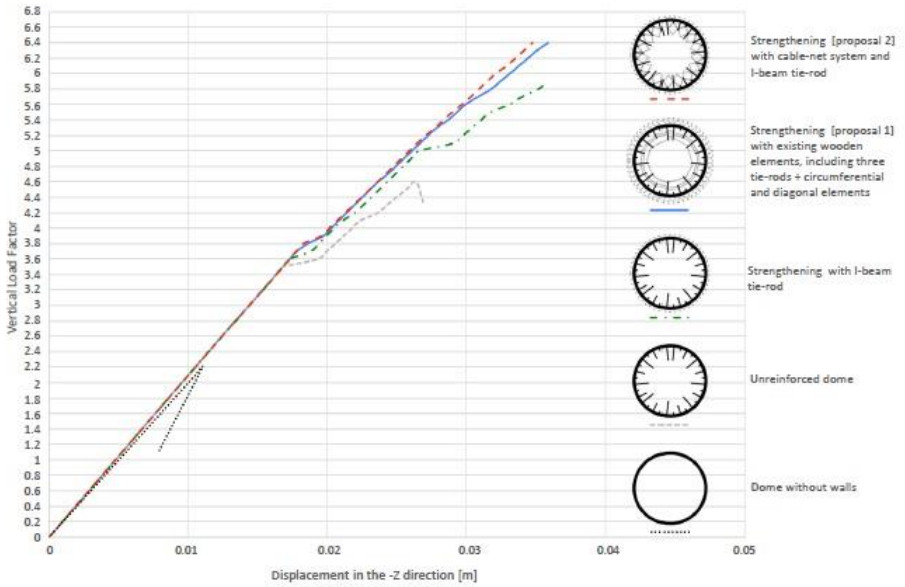

Figure 2.16 Capacity curve due to the vertical loading for the double dome with and without walls, masonry double dome with steel tie-road and two strengthening proposals (Dinani, 2019)

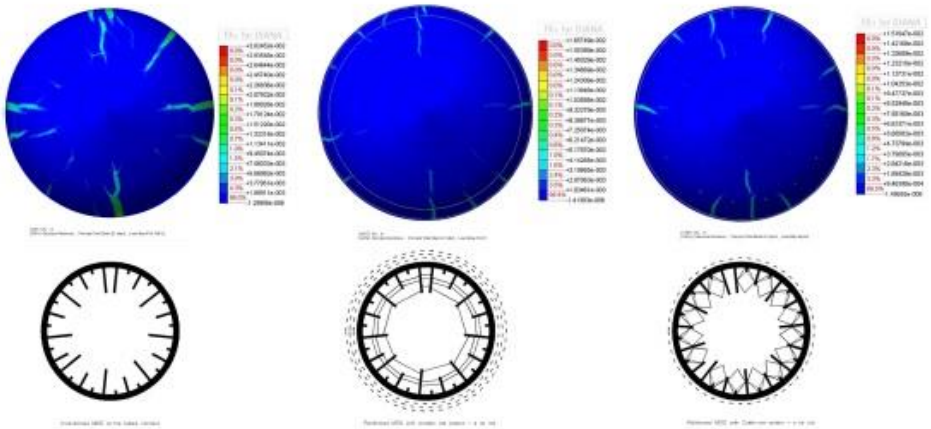

Figure 2.17 Maximum principal strains E1 due to the vertical loading, damage pattern at end of the capacity curve, load 6.4 of self-weight for unreinforced dome compared with two strengthening proposals

He also indicated that the eyvan had faced with the overturning façade. It was discussed that an integration between historical evidences, inspection and analytical model's results (fig 2.18) showed that the semi dome of the eyvan had presented the restrained deformation of a crack during the inspection, which had reported in Salnameh of 1937. Meanwhile, the mode shape configuration of both the 1st and 4th modes and maximum displacement proves the possibility overturning façade and anticipating the crack pattern which is so akin to the current situation of the semi-dome.

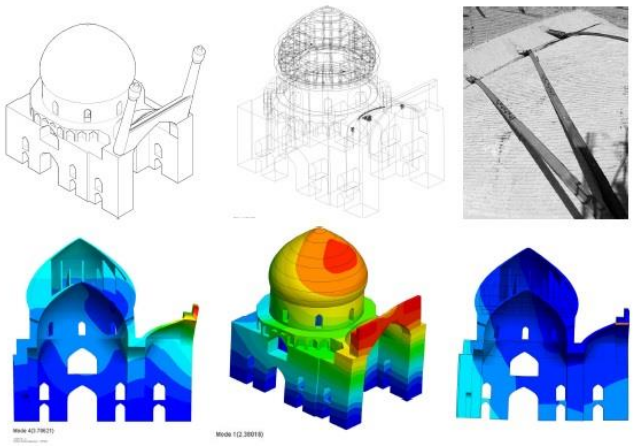

Figure 2.18 An integration between historical evidences, inspection and analytical model's results (Dinani, 2019)

He summarized the results of the vertical overloading analyzing the crack pattern on the outer dome (fig 2.19) and on the radial walls for the. Regarding the cracks on the outer shell: (a) vertical cracks appear where mostly biggest radial walls are underneath (b) diagonal cracks grow from the vertical ones in the upper part of the dome, influenced by the structural performance of the upper portion (c) on the trace of the top of the stiffener walls of height 10,6 and 7 meter, cracks spread through the crown (d) around the outer dome where it reaches the max diameter, cracks appear as a belt due to the maximum horizontal thrust of the babuls dome. With respect to the cracks on the radial walls: (a) cracks are present in the intersection of the walls and outer dome, mostly those height 10,6 meter and 7 meter (b) cracks appear on the corner of the L shape, for the stiffener walls height 10,6 meter (Dinani, 2019).

Figure 2.19 Maximum principal strains E1 due to the vertical loading, damage pattern at end of the capacity curve (Dinani, 2019)

He discussed also the performance of the building under seismic action, focusing in the response of the double dome. The seismic response of the double dome is studied along with the longitudinal direction through a pushover analysis, kept only the dome with non-linear property. Aimed to find vulnerable part of the dome in the seismic action as well as the role of the stiffener walls connecting two domes. The pushover in Y+ direction shows how the structure can withstand to the 40% of the gravitational load applied in the horizontal direction. The dome has an extensive stiff behavior above the drum where the stiffener walls are located. However, the vulnerable part is the drum or lower portion of inner dome where there are 8 openings in the dimension of 180 x 380 cm (fig 2.20).

The pushover in X+ shows results quite similar to the previous one. In fact, given the geometric symmetry of the dome, the response appears analogous with the push over in the Y direction, damage around the north window then occurs (fig 2.20). As before, the capacity of the structure to resist an horizontal load is around the 40% of the gravitational load. (Dinani, 2019) conclude his study with a safety evaluation: "*For the Shah's MDD the safety factor is equal to 2 for the PGA of 0.2g, and 1.15 for the PGA of 0.35g.*"

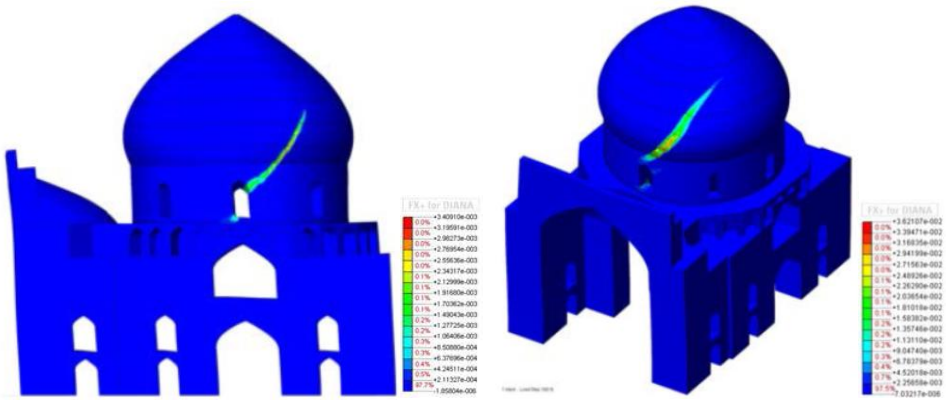

Figure 2.20 Maximum principal strain at load factor 0,4 (left) pushover analysis +Y (right) pushover analysis +X (Dinani, 2019)

According to the brief review of the previous analysis, this research, in the next steps, attempts to calibrate the model based on (Dinani, 2019) and considering the nonlinear material properties not only for the double dome but also for the entire FE model.

3. PRELIMINARY STRUCTURAL ANALYSIS WITH A PROVISIONAL MODEL

As mentioned, structural analysis is a fundamental tool for safety evaluation, so it was decided to prepare a finite element model (on which is possible perform linear and non-linear analysis), in order to obtain a first idea on the performance of the structure and to have a greater knowledge during the phase of in situ tests. This was based on the geometrical model provided by (Dinani, 2019). It is also important to remember that in professional practice it is often complicated, for economic reasons and time constraints, to perform adequate in situ tests in order to obtain sufficient experimental data to calibrate a FE model. A comparison between the performance of the structure, analyzed first with the properties available in the literature and then with the real data collected in situ, through the tests, is therefore of interest. A further reason for the study of the model even before the collection of experimental data in a faraway location (such as Isfahan) is that for complex structures (such as the Shah Mosque) numerical models can be rather complicated, as some geometrical details are missing and some modeling assumptions need in situ validation. In this chapter, some general suggestions on the analysis of large structures will be also made, obtained during the preliminary study of the Mosque (with particular reference to the Diana finite element software).

3.1 Numerical model

The numerical model of the Shah Mosque in Isfahan was prepared using the software DIANA (DIsplacement ANAlyser)(DIANA FEA BV, 2019). A first FE model (both on the pre/post-processor Midas FX + and the DIANA FEA finite element software) was provided by Dr. Ali Tavakoli Dinani as stated above. During this thesis it was decided to exploit the geometric model on Midas FX+ by importing it onto the FEM DIANA software, where a new FE model was made.

3.1.1 Units

DIANA software gives the output in the units that the user can chose for the input. A consistent system of units must be defined and all data must be entered in units from that system (DIANA FEA BV, 2019). The unit system used in the modeling is contained in tab. 3.1.

Unit	*Length*	*Mass*	*Time*	*Velocity*	*Acceleration*	*Force*	*Stress*	*Energy*
Derivation	l	m	t	lt^{-1}	lt^{-2}	mlt^{-2}	$ml^{-1}t^{-2}$	$ml^{2}t^{-2}$
Unit system(m,t,kN)	m	t	s	m/s	m/s^{2}	kN	kPa	kJ

Table 3.1 Units in DIANA

3.1.2 Model geometry

The analysis of historic masonry buildings is a complex task. In general, there are two major steps required when facing this kind of engineering problems: idealization of the geometry and idealization of the materials (Lourenço and Pereira, 2018). Regarding the idealization of the geometry and according to the scope of the study, the main volume of the Mosque was modelled, (fig 3.1). The stiffness of the remaining parts of the adjacent structure will be taken into account during the next chapter, when, with the experimental data, it will be possible to calibrate the model and better understand the stiffness provided by the adjacent parts of the Mosque.

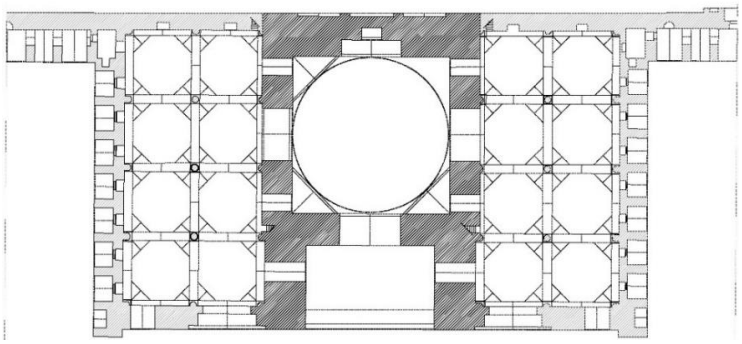

Figure 3.1 Plan of the Shah Mosque, in dark gray the part of the building studied (Isfahan ICHTO archive)

The geometrical model was prepared in Midas FX+. The walls present several thicknesses (from 5.0 to 0.2 m) and, to take into account the variability of geometric structural elements, different model parts have been used in order to have a better control during the discretization of the mesh. (fig 3.2). About the boundary conditions, it was decided to use a fixed support at the base of the structure (fig 3.2), which is allowed to rotate upon cracking.

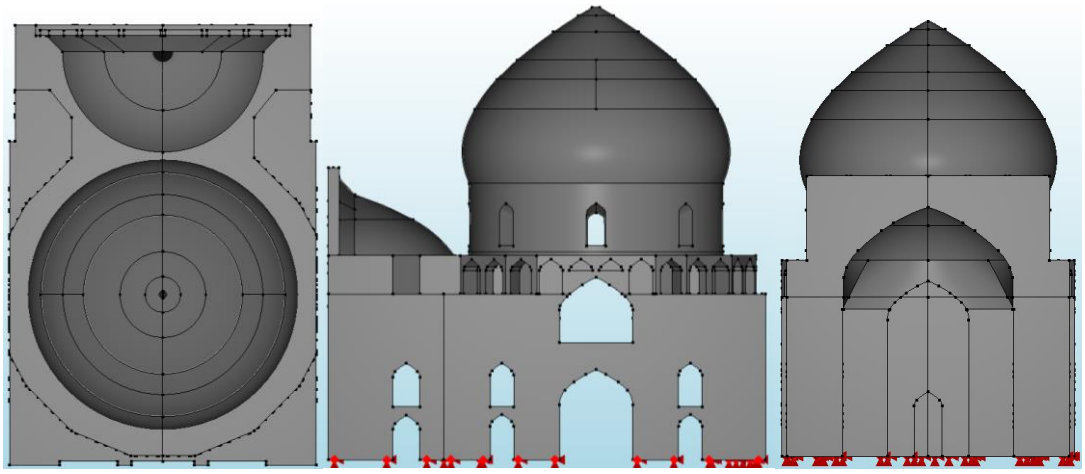

Figure 3.2 Geometric model of the Shah Mosque

Regarding the idealization of the material, the analysis of masonry structures built from a large number of units and joints (such as the Shah Mosque) can only be carried out with a macro-mechanical based finite element model which essentially considers masonry material as a homogeneous continuum and further establishes proper phenomenological constitutive laws.

Although micro-modelling, which takes into account the bond between the bricks and the mortar, gives a closer response to reality, the macro-modelling is used for complex models and, as long as the material is well calibrated, the approach can lead to good results.

3.1.3 Element type

When using a FE software, there are several different types of elements available to idealize the geometry. Some types are more relevant for general applications, while others have a more limited application. In the specific case of historic masonry structures, the geometry can usually be idealized in different ways, namely using linear elements (truss or beam elements), plane "two-dimensional" elements (usually shell elements), or fully three-dimensional elements (solid elements). Solid elements are general purpose elements and, usually, the most adequate. However, because of their tendency to produce large systems of equations, these elements need to be applied carefully. Solid elements are characterized by the following properties: the stress condition is three-dimensional, the loading may be arbitrary and the dimensions in three axial directions X, Y and Z are of the same order of magnitude. Typical applications of solid elements are the analysis of voluminous structures like concrete foundations, thick walls and floors (as in the case of the Mosque) and soil masses. Solid elements are three-dimensional general-purpose elements in which the displacements can be the translations in the three general directions (u_x, u_y, and u_z)(DIANA FEA BV, 2019). It seems that fully three-dimensional elements (3D) are the most appropriate type of element for historic structures. However, these are usually time consuming (considering the time used to prepare the model, perform the actual calculations, and analyze the results) (Lourenço and Pereira, 2018). For the complexity of the structure, to the detriment of the computational burden, the numerical model has been generated by solid (3D type), in order to get an accurate result. For meshing the 3D solid in DIANA, a four-node tetrahedron solid of type TE12L has been used (fig 3.3).

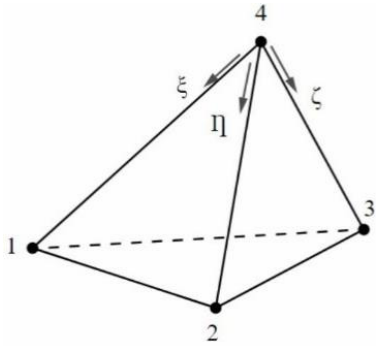

Figure 3.3 TE12L element (DIANA FEA BV, 2019)

The TE12L element is a four-node, three-side isoparametric solid tetrahedron element. It is based on linear interpolation and numerical integration. The shape functions can be expressed as shown in eq. 3.1. These polynomials yield a constant strain and stress distribution over the element volume (by default Diana applies a 1-point integration scheme).

$$u_i(\xi, \eta, \zeta) = a_0 + a_1\xi + a_2\eta + a_3\zeta$$

Equation 3.1 Shape function for TE12L element (DIANA FEA BV, 2019)

3.1.4 Mesh definition

The model is discretized over space in a certain number of elements. Generally, the more refined the mesh is, the more accurate the finite element solution is. However, more elements also entail longer computation times. Mesh design must take into account several pros and cons (DIANA FEA BV, 2019). The shape and size of the elements have an important impact on the solution. Attention should be paid to the discretization of the mesh, giving a fair compromise between accuracy and computational efforts, to obtain reasonable solution, in particular when non-linear static or dynamic analysis are performed. Still, according to the FE theory, as the mesh gets finer, it gets closer to the true solution (Lourenço and Pereira, 2018). In fact, here, the geometric model has been prepared in order to assign the mesh size as a function of the size of the element (fig 3.4). Furthermore, the mesh has been refined around discontinuous zones (edges and faces) (fig 3.4). This approach is adopted in order to reduce the number of elements but at the same time to obtain a fine mesh in the structural elements with small dimensions. The full FE model contains 294'782 nodes and 1'412'622 elements with the different mesh sizes from 0,7 meter in the body of the building to 0,2 meter in the upper part of the domes.

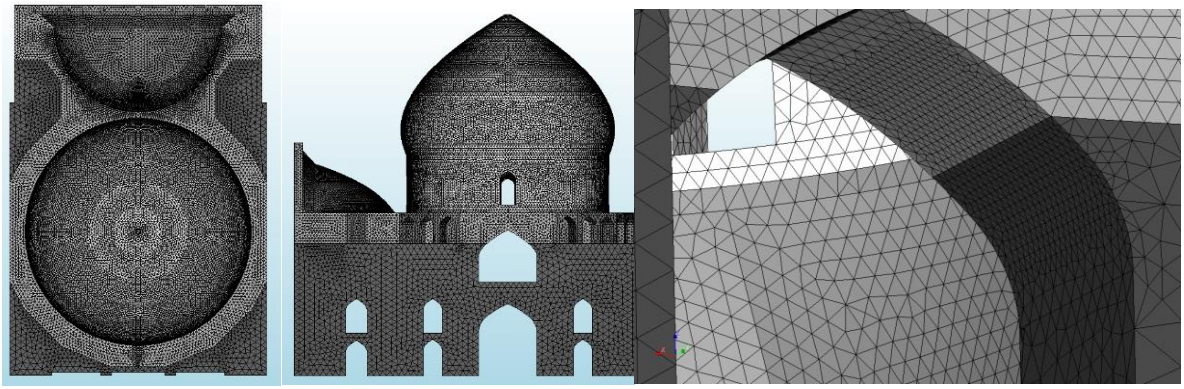

Figure 3.4 Meshed model in DIANA

3.1.5 Material property

Regarding the properties of the material, the values provided by (Dinani, 2019) will be used. The properties and strength of the masonry brick of the Shah's dome are derived from a basic cell of masonry surveyed from the building, as it strongly depends upon the properties of the constituents of brick and mortar and construction technique. In order to characterize the properties of the masonry, a micro-modelling approach has been used. The basic cell in the Shah Mosque (fig 3.5) contains bricks and mortar with dimension of 270x140x250 mm where the size of the brick, as the unit, is 250x 250x50 mm with 2cm for the head and bed joints (Dinani, 2019).

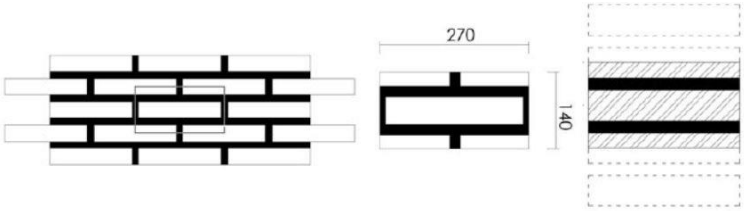

Figure 3.5 Basic cell in the Shah Mosque (Dinani, 2019)

As explained in (Dinani, 2019), the basic material properties of brick and mortar are referred to the local sources (Hejazi and Mehdizadeh Saradj, 2012) and in particular to the technical report of structural damages (Kavak Consulting Engineers, 2009) for the Si-o Se Pol bridge (1602) constructed in the same period in Isfahan. Subsequently, the physical and mechanical characteristics of the brick masonry has been achieved for the Shah dome based on its basic unit (tab 3.2) (Dinani, 2019). Here, ρ is the specific mass, **E** is the Young's modulus, ν is the Poisson's ratio, $\mathbf{f_c}$ is the compressive strength, $\mathbf{G_c}$ is the compressive fracture energy, $\mathbf{f_t}$ is the tensile strength and $\mathbf{G_f}$ is the tensile fracture energy.

	ρ (kg/m^3)	**E** (MPa)	ν	$\mathbf{f_c}$ (MPa)	$\mathbf{G_c}$ (N/mm)	$\mathbf{f_t}$ (MPa)	$\mathbf{G_f}$ (N/mm)
Brick	1330	5300	-	15,5	-	1,25	-
Mortar	1600	1300	-	6,0	-	0,50	-
Masonry	1420	2830	0,2	5,8	9,2	0,28	0,008

Table 3.2 Material properties of the Shah Mosque (Dinani, 2019)

3.1.6 Material model

Masonry has a non-linearbehavior and manifests a nonductile post-peak softening behavior, which consists of a gradual strength decrease of the material under a continuous increase of deformation. This characteristic is typical of quasi-brittle materials (Lourenço, 1996). Fig. 3.6 shows characteristic stress displacement diagrams in uniaxial tensile and compressive behavior.

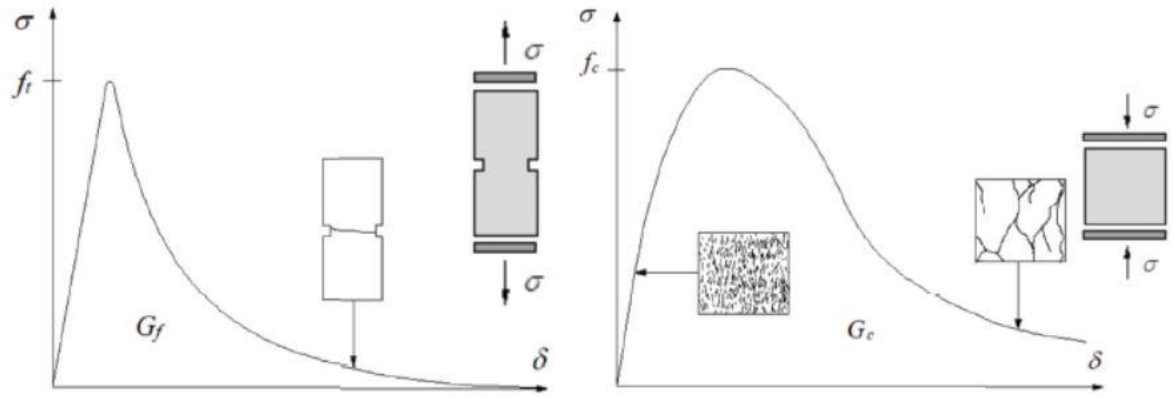

Figure 3.6 Diagrams showing characteristic stress displacement of quasi-brittle materials under uniaxial loading: (left) tensile behavior (right) compressive behavior (Lourenço, 1996)

It is important to choose an adequate constitutive model in order to take into account the tridimensional non linear behavior of material. With regard to the assessment of masonry structures considering non-linearbehavior of masonry, DIANA FEA has different possibilities for the constitutive models (considering only macro-modeling approaches). In this thesis, it is been decided to use the Total Strain-Based Crack model (TSBC) with a rotating crack formulation to evaluate the performance of the Mosque. The constitutive model based on total strain is developed along the lines of the modified compression field theory, originally proposed by (Vecchio and Collins, 1986). Like the multi-directional fixed crack model, the total strain based

crack models follow a smeared approach for the fracture energy. The smeared crack models consider cracking as a distributed effect with directionality and the cracked material is simulated as a continuous medium with anisotropic characteristics (DIANA FEA BV, 2019). Although these models were born for reinforced concrete, they give good results also for masonry under the assumption of isotropic material. The TSBC model available in DIANA can describe both the tensile and the compressive behavior of a given material with one stress-strain relationship. This stress-strain relationship under tensile behavior can be idealized using several different approaches, including constant, linear, exponential and brittle. For the assessment of the Shah Mosque, it is been decided to use the exponential stress-strain relation (fig 3.7). Regarding the compressive behavior, it can be idealized also using different approaches, such as elastic, constant and parabolic. Here, the parabolic law is used (fig 3.7) (Lourenço and Pereira, 2018).

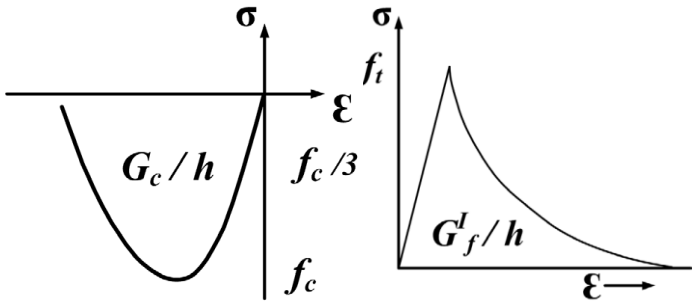

Figure 3.7 Parabolic law for compression (left) exponential law for tensile (right)(DIANA FEA BV, 2019)

Within the TSBC models, two distinct approaches are available and can be distinguished as total strain fixed crack model and total strain rotating crack model (fig 3.8). In both formulations, the crack is initiated when the maximum principal stress equals the tensile strength of the material and its initial orientation is normal to the maximum principal strain. The main difference between these two formulations is related to the crack orientation during the inelastic process. In the fixed model, the coordinate system is fixed upon cracking according to the principal strain directions and remains invariant during the total analysis process. In this model, each integration point admits a maximum of two orthogonal cracks. The rotating model allows a gradual correction of the initial crack direction, as the crack plane can rotate during the analysis. The crack direction rotates with the principal strain axes, ensuring that the crack remains normal to the direction of the maximum principal strain (Lourenço and Pereira, 2018). Regarding the assessment of the Shah Mosque, the rotating crack model has been used, given the shear locking of the fixed crack model.

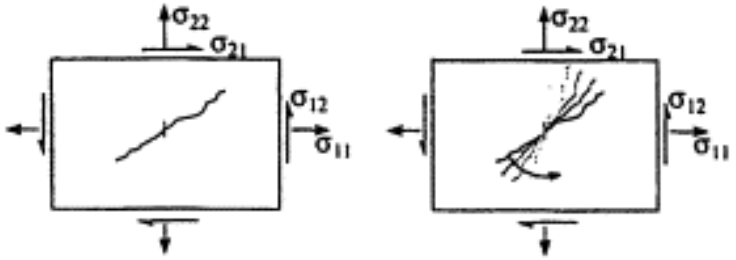

Figure 3.8 Fixed crack model (left) rotating crack model (right)(Milne *et al.*, 2007)

The TSBC constitutive model in DIANA needs the following parameters: density (ρ), Young's modulus I, Poisson coefficient (ν), compressive strength (f_c), compressive fracture energy (G_c), tensile strength (f_t) and mode-I fracture energy (G_f). The material model and the material property applied in DIANA can be summarized in tab. 3.3 and tab. 3.2, given above.

Material model	Crack orientation	Compressive behavior	Tensile behavior
Total Strain-Based Crack model	Rotating	Parabolic	Exponential

Table 3.3 Characteristics of the material model used in DIANA

3.2 Linear static analysis

A first analysis was performed taking into account only the elastic properties of the structure avoiding the non-linear behavior of the material and only the gravitational loads (the self-weight). This analysis was carried out to check if irregularities were present in the model, such as geometric, material or loading inconsistencies. The first control is presented in table 3.5 and it consists in the comparison between the total vertical reaction obtained through the analysis in DIANA and the same resultant value estimated by simple calculation. As expected, the range of results is according to the expected and the difference is less than 3%.

Simple calculation				Fem model	
volume (m^3)	ρ (t/m^3)	Mass (t)	Force (kN)	DIANA (kN)	Δ (%)
14672	1,42	20834	204176	210121	2,8

Table 3.4 Comparison between expected reactions and results in DIANA

Another possible verification is linked to displacement-control. According to the analysis, the maximum vertical displacement of the structure subjected to its self-weight is equal to 4,8 mm (fig 3.9) on the top of the dome. A satisfactory range and distribution of maximum and minimum displacement is also obtained, without abnormal values indicating a meshing inconsistency or inadequate use of material property units.

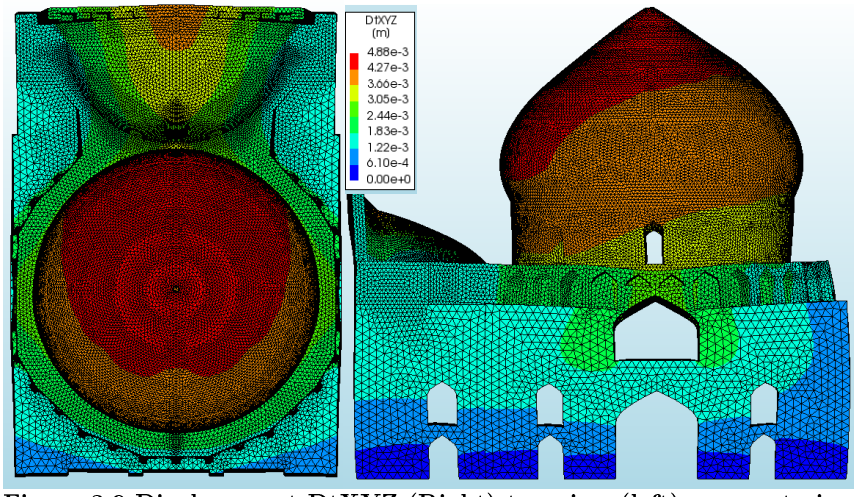

Figure 3.9 Displacement DtXYZ (Right) top view (left) prospect view

A further check to perform is certainly the one concerning the principal strains, to understand, first of all, if the range of values obtained is reliable and if the distribution complies with the prevision (thus being able to further validate the model). As shown in fig 3.10, the range of compression and tensile deformations is in the order of 10^{-4} (typical values within the elastic range). As far as the strain distribution is concerned, it is possible to see an increase in compression deformations (E3) at the base of the structure and the drum but, again, no excessive strain concentrations (or peaks) are found. These usually indicate a meshing inconsistency.

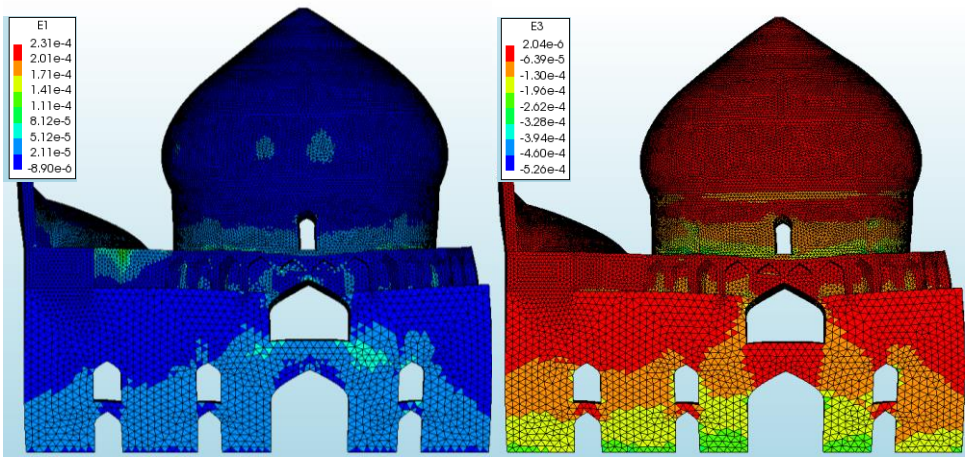

Figure 3.10 Principal strain (left) E1 (right) E3

Secondly, the deformation analysis can be useful to evaluate the presence of possible weaks points where to find stress or strain concentrations. The presence of these zones can guide us towards a refining of the meshes in order to fully understand the behavior of these parts, especially during subsequent non-linear analysis. In fact, as shown in fig. 3.11 a concentration of tensile deformations in the keystone of the great central arch is present and a concentration of compression strain appears in the top of the buttresses. Indeed, as mentioned in section 3.1.4 particular attention is paid to refine the mesh in these areas.

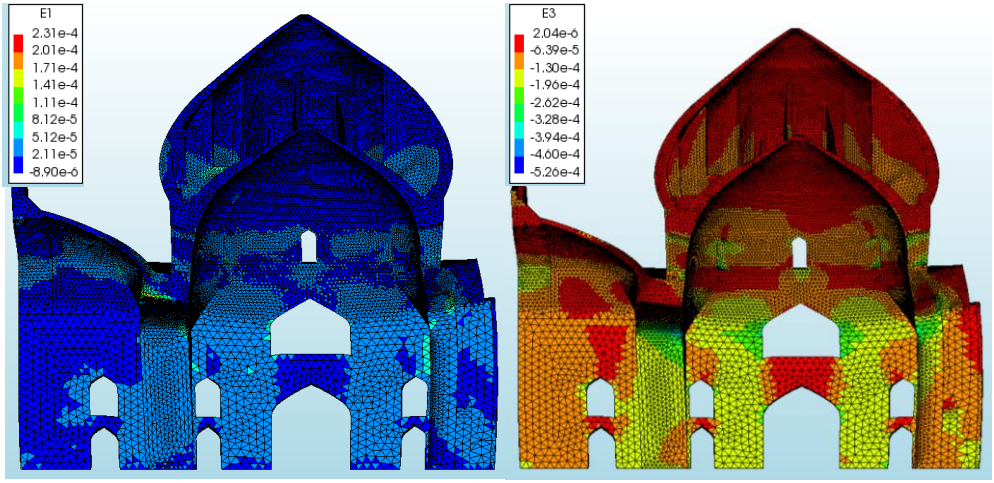

Figure 3.11 Principal strain in the symmetric cross section (left) E1 (right) E3

Even if the stress and strains are directly related in the linear stress range, the principal stress magnitude distribution and range was also verified. The results (fig 3.12) show the expected distribution of stresses, with compression at the base between 0,7 and 0,8 MPa and higher compression stress at the base of the drum with a value of 1,5 MPa. In terms of tensile stress, it is possible to see a consistent range of tension stresses, around 0,1 MPa. The exception is the key stone of the main arch, where a peak of tensile stress is found, with a value around 0,7 MPa. This result suggests decreasing the mesh size in the base of the drum and in the big central arch, in order to better approximate the stress-strain field in this area.

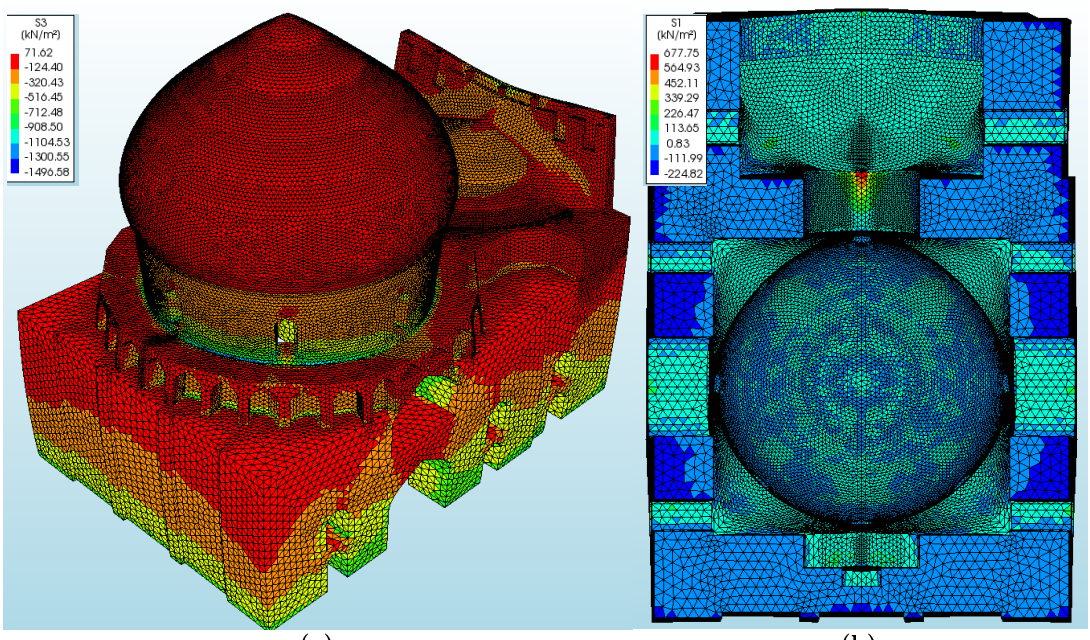

(a) (b)

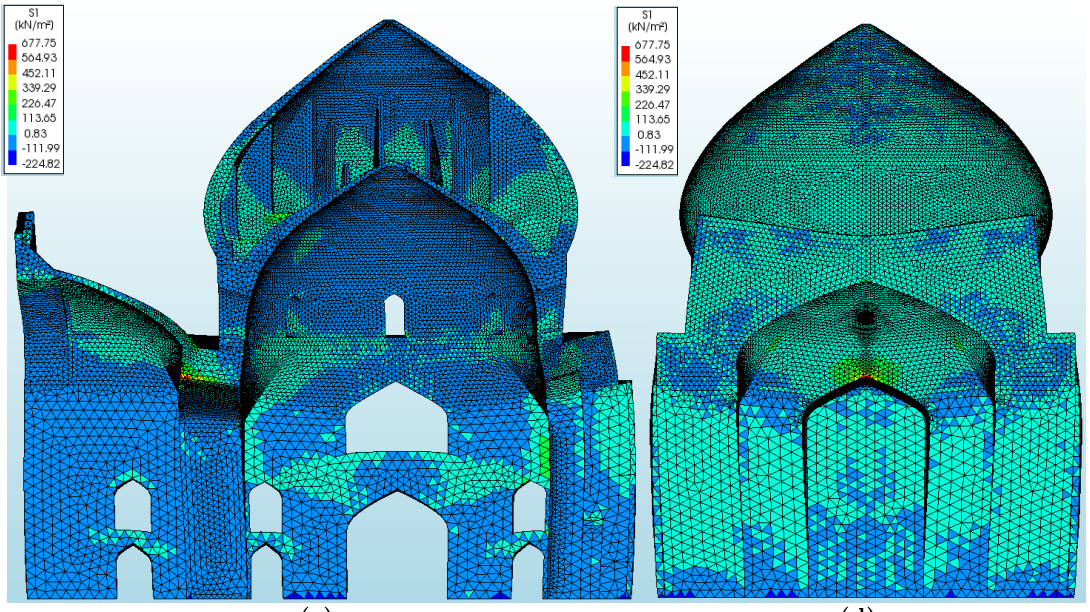

(c) (d)

Figure 3.12 Principal stress (kPa): (a) S3 axonometric view (b) S1 view from below (c) S1 in the symmetric cross section (c) S1 front view

3.3 Incremental vertical analysis

3.3.1 Incremental-Iterative solution procedures for non-linear systems

In non-linear finite element analysis, the relation between forces and displacements becomes non-linear and the displacements depend on the loading history. Just as with a linear analysis, the displacement field, that equilibrates the internal and external forces, has to be calculated. In the linear case, the solution vector can be calculated right away with a single matrix operation but in the non-linearcase it cannot. To determine the state of equilibrium it is not only make the problems discrete in space (with finite elements) but also in "time" (with increments)(DIANA FEA BV, 2019). To achieve equilibrium at the end of the increment, it is needed to use an iterative solution algorithm. The combination of both aspects is called an incremental-iterative solution procedure, which is required to integrate correctly non-linear structural problems. The methods available in Diana for solution procedures are several, but only two iterative procedures, which can be considered the most adequate for the assessment of the Mosque, are presented: the modified Newton-Raphson method and the Secant method. In both procedures, the displacement increment Δu is adapted iteratively by iterative increments δu, until equilibrium is reached, up to a prescribed tolerance. Indicating the iteration number with a right subscript, the incremental displacements at iteration i+1 are calculated as:

$$\Delta u_{i+1} = \Delta u_i + \delta u_{i+1}$$

Equation 3.2 Incremental displacements at iteration i+1

The difference between solution procedures is the way in which δu is determined. The iterative increments are calculated by use of a stiffness matrix $\mathbf{K}$ that represents the linearized form of the relation between the force vector and displacement vector. The used stiffness matrix can change every iteration and the matrix that is used in iteration i is called $\mathbf{K}_i$. A direct approach is to determine the iterative increments by eq. 3.3 (where f_i is the out-of-balance force vector at the start of iteration)(DIANA FEA BV, 2019).

$$\delta u_i = {}^{f_i}/_{K_i}$$

Equation 3.3 Direct calculation of the iterative increments through the stiffness matrix

Newton-Raphson methods use eq. 3.3 to determine the iterative increment of the displacement vector. In a Newton-Raphson method, the stiffness matrix $\mathbf{K}_i$ represents the tangential stiffness of the structure and it is evaluated with eq. 3.4.

$$K_i = {}^{\delta f}/_{\delta \Delta u}$$

Equation 3.4 Evaluation of the stiffness matrix in the modified Newton Raphson method

The modified Newton-Raphson method only evaluates the stiffness relation (eq. 3.4) at the start of the increment (fig 3.13) (different from the regular Newton Raphson where the stiffness matrix

is evaluated for each iteration). This means that the prediction is always based on a converged equilibrium state (DIANA FEA BV, 2019). Usually, this method gives good possibility of convergence. The modified Newton-Raphson method usually needs more iterations than the regular Newton-Raphson method, but each iteration is faster (the stiffness matrix is update only in the beginning of the increment). This method has been used to obtain the post peak behavior of the structure during the vertical incremental analysis.

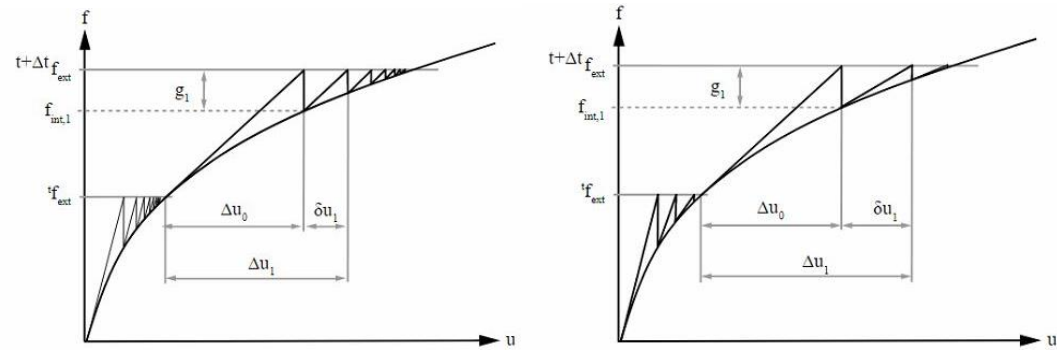

Figure 3.13 Newton Raphson method (left) Secant method (right) (DIANA FEA BV, 2019)

The other method used is the Secant method, which essentially uses the information of previous solution vectors and out-of-balance force vectors during the increment to achieve a better approximation (fig 3.13). Unlike regular Newton-Raphson, the Secant method does not set up a completely new stiffness matrix every iteration. In this case the stiffness of the structure is determined from the known positions at the equilibrium path. If the iterative displacement increment is called δu_i and the change in out-of-balance force vector related to this increment δf_i, the Secant method relation is:

$$K_{i+1}\delta u_i = \delta f_i$$

Equation 3.5 Secant method relation

Basically, in this method the stiffness matrix is determined through the last two convergence states (fig 3.14) and, for this reason, the stiffness matrix can be called secant.

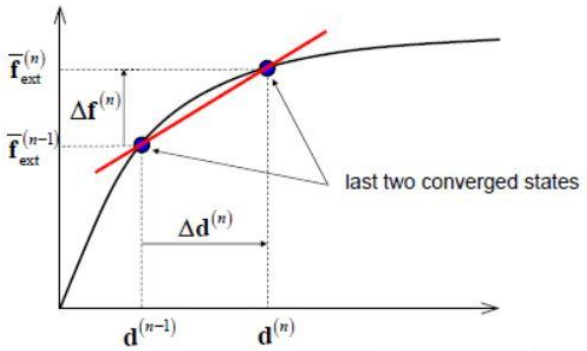

Figure 3.14 Stiffness in Secant method (Jirásek and Lourenço, 2018)

For advanced models, the derivation of the consistent tangent stiffness matrix could be very complicated, so it is, sometimes, necessary to use the Secant method. The method is usually less accurate and slower, but can be more stable an robust for complex structural models like the

masonry structure under study here. The secant method has been used in the analysis to obtain the behavior before the peak. The iteration process must be stopped if the results are satisfactory. For this purpose, Diana offers several convergence norms (force, displacement and energy). In the analysis of the Mosque the energy norm has been chosen. This norm is composed of internal forces and relative displacements as indicated in fig 3.15. To determine convergence, the energy ratio is calculated as the ratio between δE_{i+1} and ΔE_i. In this case, the convergence tollerance was chosen as 10^{-3}.

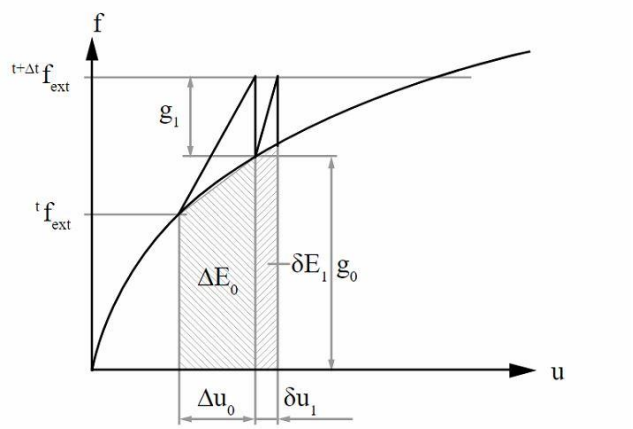

Figure 3.15 Energy based norm (DIANA FEA BV, 2019)

The incremental-iterative solution procedures consists of two parts: the increment part and the iteration part. The iteration was just discussed and, regarding the increment control, DIANA offers many types (such as force control and displacement control). For the analysis of the Mosque, force control is used. For this type of control, to obtain the post-peak behavior it is necessary to use the arc length method (fig 3.16). The characteristics used can be summarized in tab. 3.6

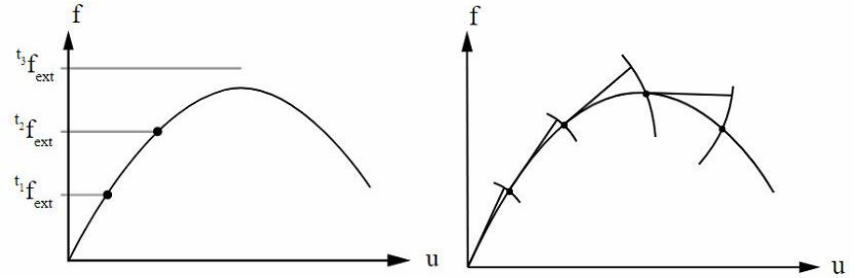

Figure 3.16 Force control (right) arc length method (left) (DIANA FEA BV, 2019)

Analysis	Control type	Convergence criteria	Incremental-iterative method	
Incremental vertical	Force control with arc length method	Energy norm	Secant (pre peak)	modified N.R. (post peak)

Table 3.5 Characteristics used to perform the non-linear analysis

3.3.2 Results of the analysis

After preparing the numerical model and defining the settings for the analysis, it was possible to perform a vertical incremental analysis. Fig 3.17 shows the displacement of the control point (the top of the dome) by increasing the load factor L.F. (considering only the self-weight of the structure).

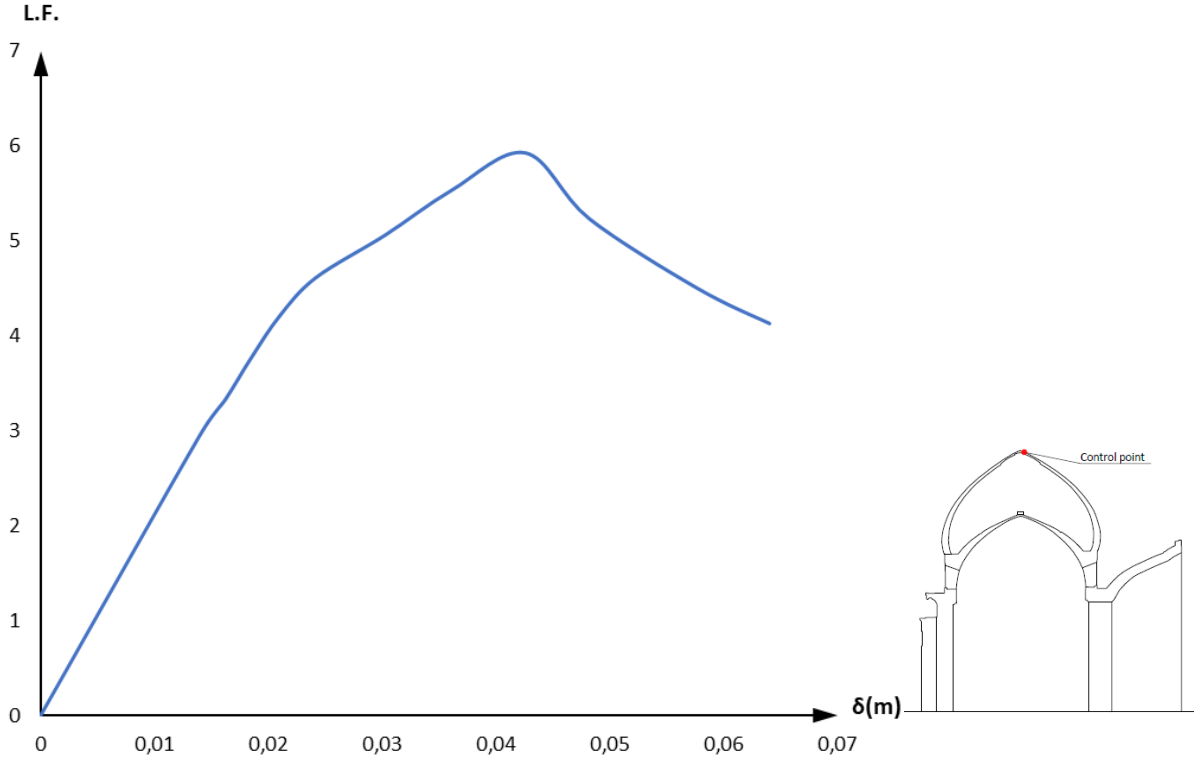

Figure 3.17 Curve F-δ for the incremental vertical analysis. L.F. indicates the load factor magnifying gravity and δ is the displacement at the top of the dome

In order to better understand the results, displacements and principal strains distribution are reported for three specific load stages: the first load stage L.F=4,6 is the beginning of the non-linear behavior, the second L.F.=5,9 is the peak load and the third L.F.=4,7 is the post peak stage. As for the first case, it is immediately clear how the bigger displacements take place for the less rigid parts such as the dome and the *eyvan* (fig 3.18). In terms of strains, it is possible to note peaks of principal tensile strain E1 between the *eyvan* and the dome (fig 3.18) and in the outer shell close to the main arch (fig 3.19). It is also possible to note the presence of shear stress (principal strain in tensiom E1 and compression E3) at the point where the drum rests on the main structure in correspondence with the large closed arch (fig 3.19).

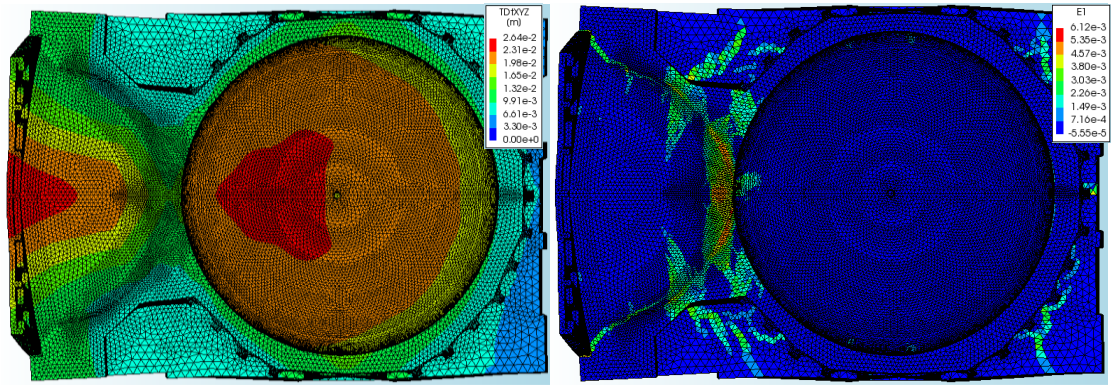

Figure 3.18 Displacement TDtXYZ, (left) principal strain E1 (right), L.F.=4,6

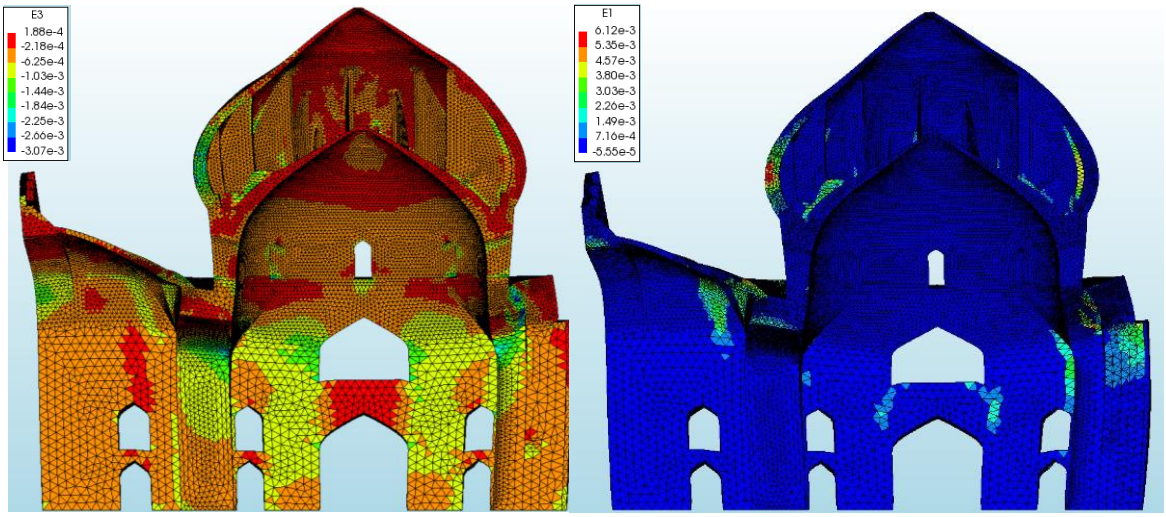

Figure 3.19 Principal strain E3 (left) principal strain E1 (right), L.F.=4,6

The second load stage (L.F. = 5.9) confirms what was said before for the displacements, although they are increasing especially in the dome (fig 3.20). Regarding the principal strains, it is possible to see how several cracks appears in the dome (fig 3.20), especially within the area without the presence of the vertical stiffeners. Fig 3.21 shows the tendency of the dome to push on the underlying elements, causing important compression strains at the base of the drum, confirmed also by the important compression strains at the base of the opened arch (*eyvan* side) and by the shear in the top of the closed arch (patio side).

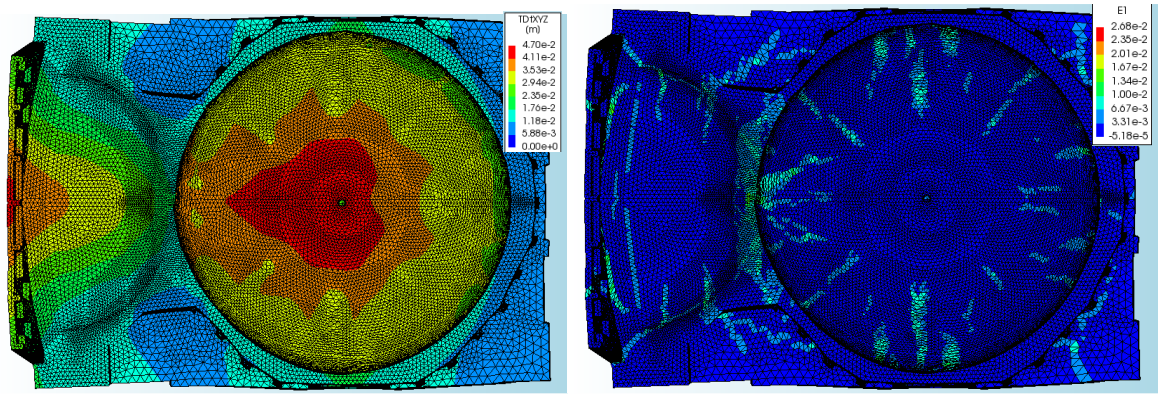

Figure 3.20 Displacement TDtXYZ, (left) principal strain E1 (right), L.F.=5,9

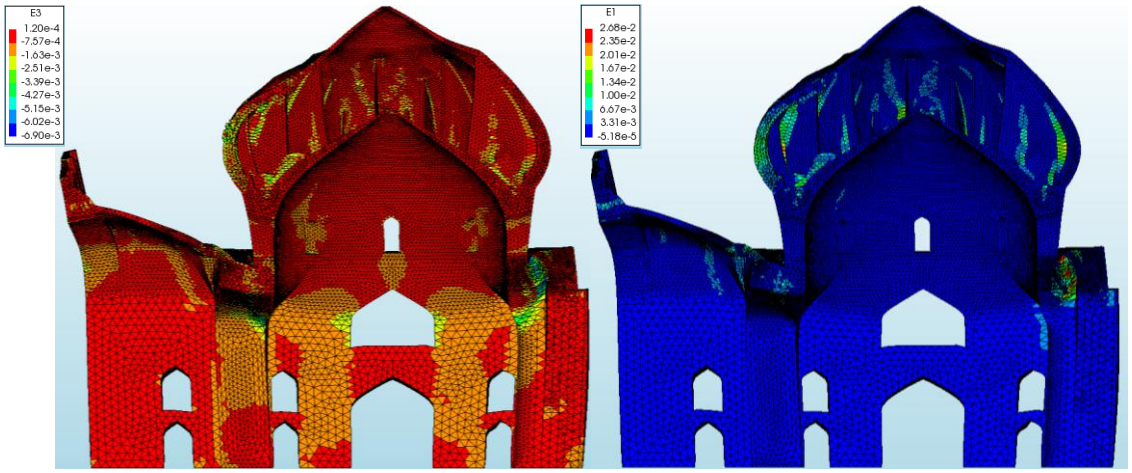

Figure 3.21 Principal strain E3 (left) principal strain E1 (right), L.F.=5,9

The third load stage (L.F. = 4.7) reports the results in the post peak phase. It shows how the displacement is concentrated in the outer shell, especially in the top and in the part close to the main arch (fig 3.22). In terms of strains, it is possible to notice the further increase of the cracks in the dome (fig 3.22). Fig 3.23 shows the tendency of the outer shell of the dome to detach from the stiffener walls. This behavior causes the loss of loadbearing capacity of the structure and it is also confirmed by the incremental displacement for this load step, where the collapse mode is evident (fig 3.24).

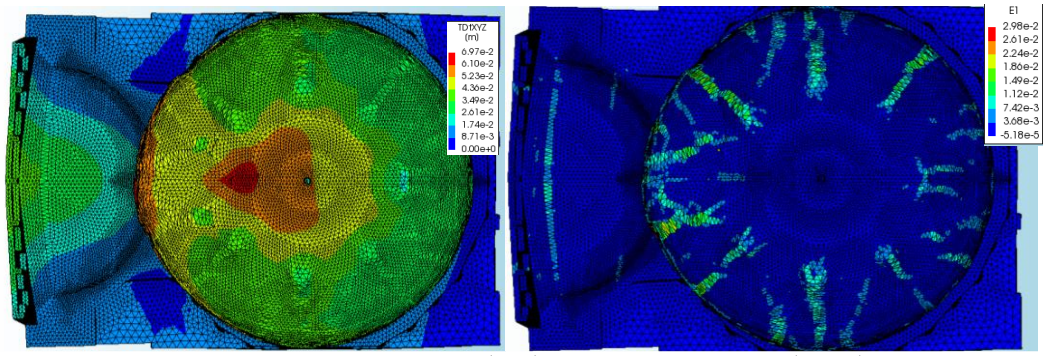

Figure 3.22 Displacement TDtXYZ, (left) principal strain E1 (right), L.F.=4,7

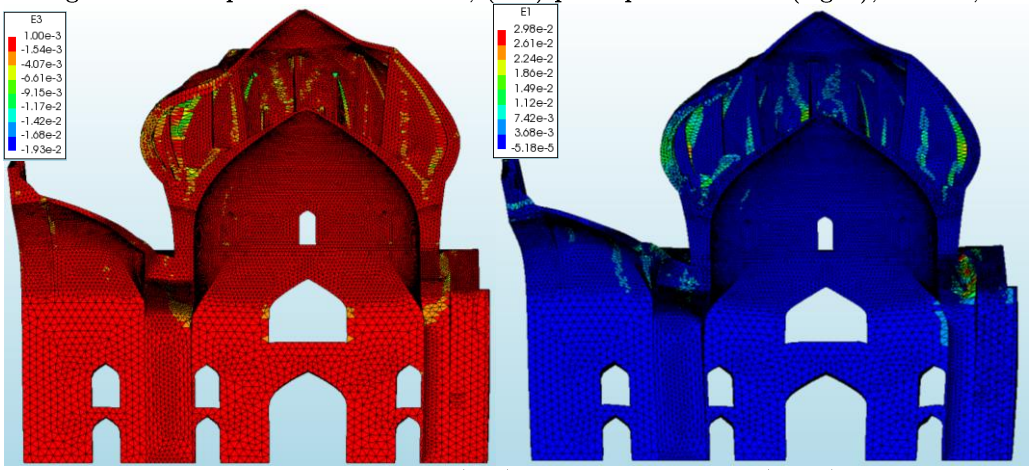

Figure 3.23 Principal strain E3 (left) principal strain E1 (right), L.F.=4,7

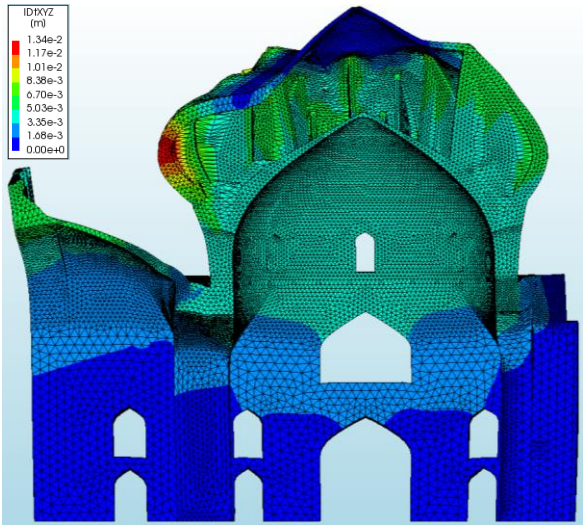

Figure 3.24 Incremental displacement TDtXYZ L.F.=4,7

Fig 3.25 shows the evolution of the principal tensile strains E1 (in the same scale) during the analysis. It is possible to see the damage suffered by the dome especially during the softening behavior. It is also interesting to observe another weak point the structure: the *eyvan*. In fact, as shown, it is possible to see the tendency of this semi-dome (its shape turns out to be its weak point) to exhibit an out of plane mechanism. This appears as a likely problem especially for seismic action, even if the dome is the weakest part of the structure for gravitational loading.

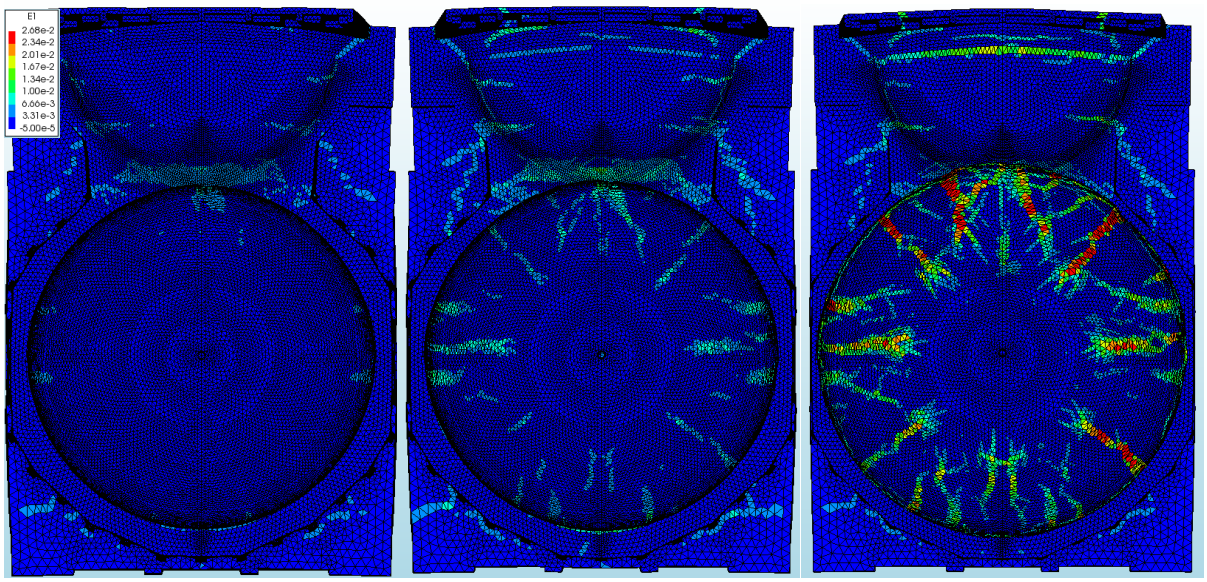

Figure 3.25 Evolution of the principal tensile strain E1 for the 3 load factors (from left to right 4.6, 5.9, 4.7)

3.3.3 Sensitivity analysis

Given the difficulty to reach convergence, particularly in the post-peak regime, and in order to better understand the influence of the fracture energy it is been decided to carry out a sensitivity analysis (fig 3.26). The structural capacity of the structures increases approximately to the double when infinite tensile and compressive fracture energies are used.

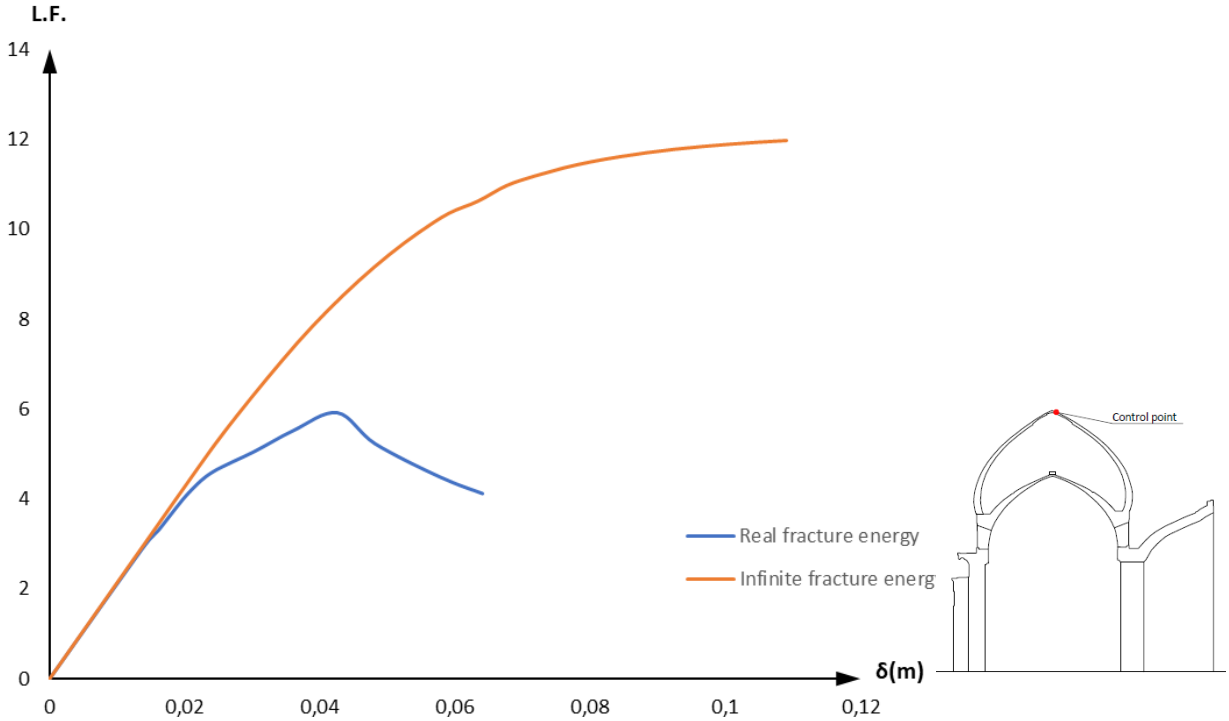

Figure 3.26 Sensitivity analysis for fracture energy

The results highlight the influence of the fracture energy not only in terms of ultimate capacity, but also in the failure mechanism. The results obtained for the infinite fracture energy at ultimate load stage (L.F.=12,1) are compared with the ones obtained for the real fracture energy (L.F.=4,7). The analysis of the displacements, in addition to point out higher displacement (fig 3.26), shows a different distribution. In fact, the displacement is now widely distributed in the dome, especially in proximity of the large opened arch, which is different from the case of the real fracture energy, in which the displacement peak is concentrated in specific parts. This behavior is mainly due to a more global response of the structure.

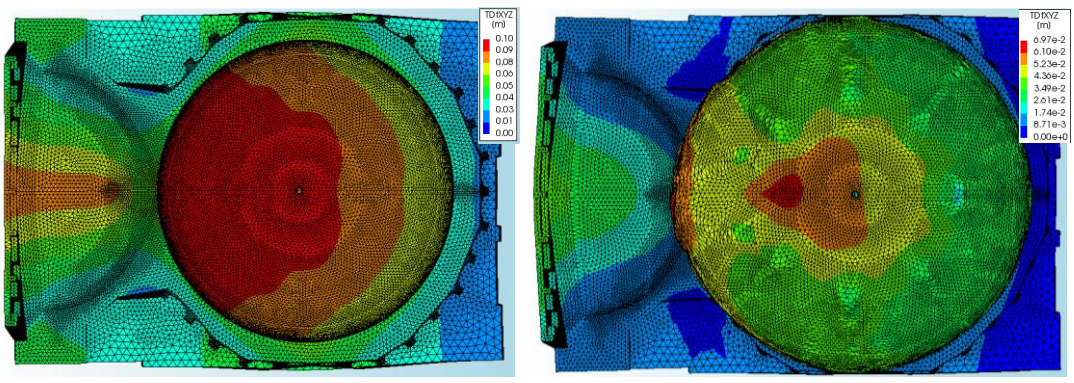

Figure 3.27 Displacement TDtXYZ, (left) infinite fracture energy (right) real fracture energy

The analysis of the deformation confirms what was said before, as the strong increase of the fracture energy can modify, not only the ultimate loadbearing capacity, but also the collapse mechanism. The tensile strains distribution (fig 3.28) point out a strong concentration of tensile strain in the connection between the dome and the *eyvan*, for the case of infinite fracture energy. Rather different is the case of the real fracture energy where the cracks are distributed in the dome. Furthermore, the tensile strain distribution, highlights the concentration of deformation in the keystone of the open arch (fig 3.29), for the infinite fracture energy case. Some differences in the real fracture energy case were observed, as, in this case, the higher tensile strains are present in the connection between the stiffener walls and the dome and in the top of the closed arch (where a concentration of shear stress was observed).

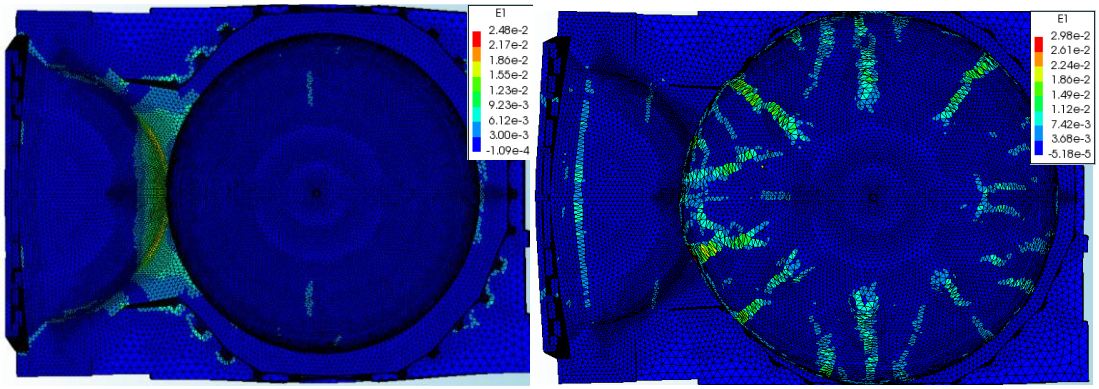

Figure 3.28 Top view Strain E1, (left) infinite fracture energy (right) real fracture energy

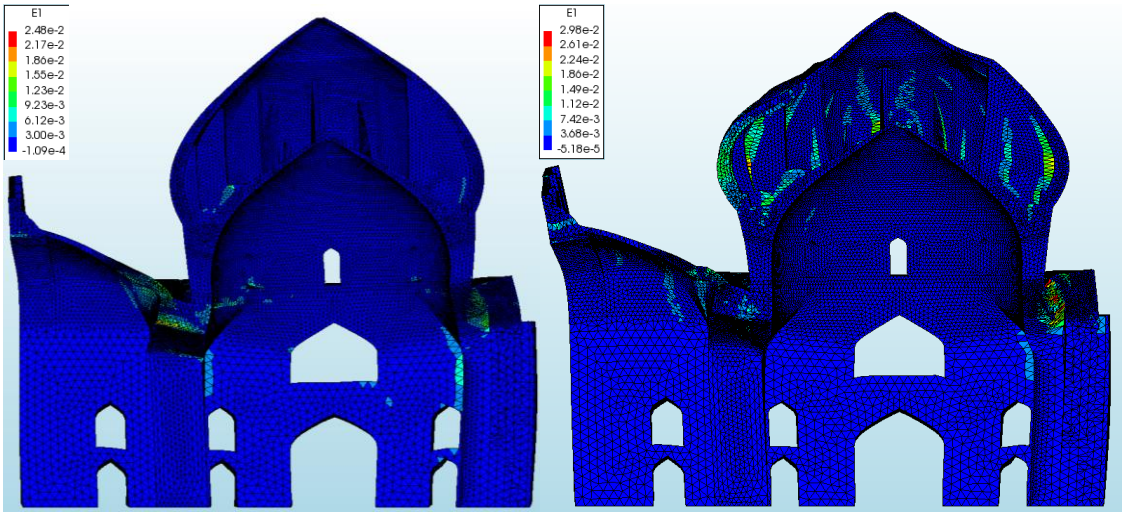

Figure 3.29 Strain E1, (left) infinite fracture energy (right) real fracture energy

The study of the compression strain (fig 3.30) points out what was shown before for the tensile strains. In fact, the peak of compression strain is present only in the top of the buttresses and not in the large partly closed arch (due to shear action) and in the external dome, as in the case of real fracture energy. Furthermore, the value of the maximum compression strain is quite high if compared with the case of real fracture energy (note also that the load factor, i.e compressive stresses, are also much higher in this case). It is this important compressive stress that contributes to failure of the structure in the case of infinite fracture energy.

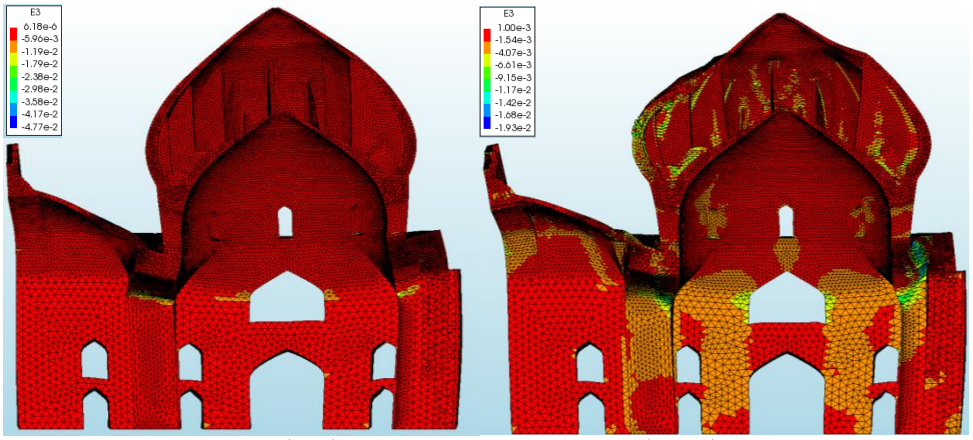

Figure 3.30 Strain E3, (left) infinite fracture energy (right) real fracture energy

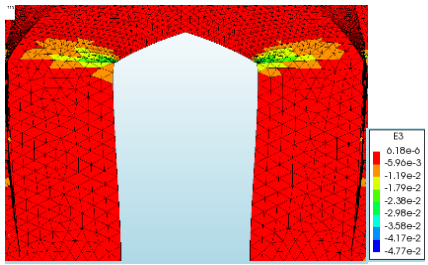

Figure 3.31 Strain E3 infinite fracture energy, Detail of the big open arch

Finally, the analysis of the failure mode and the reason of the different mechanism between the two cases are discussed. For this purpose, the study of the incremental displacement in these two last stages is useful. Fig. 3.32 shows how in the case of real fracture energy the loss of loadbearing capacity is mainly due to the detachment of the outer dome from the stiffener walls. The same picture shows that, for the case of infinite fracture energy, the loss of capacity is due to high displacements in the opened arch, involving also the dome, providing a full rigid block rotation of the dome. In the case of real fracture energy, the concentration of strains is localized in the rigid elements, such as the stiffener walls of the dome and the large closed arch. Regarding the case of infinite fracture energy, the weakest point turns out to be the most flexible part: the opened arch, while the rest of the dome remains mostly elastic.

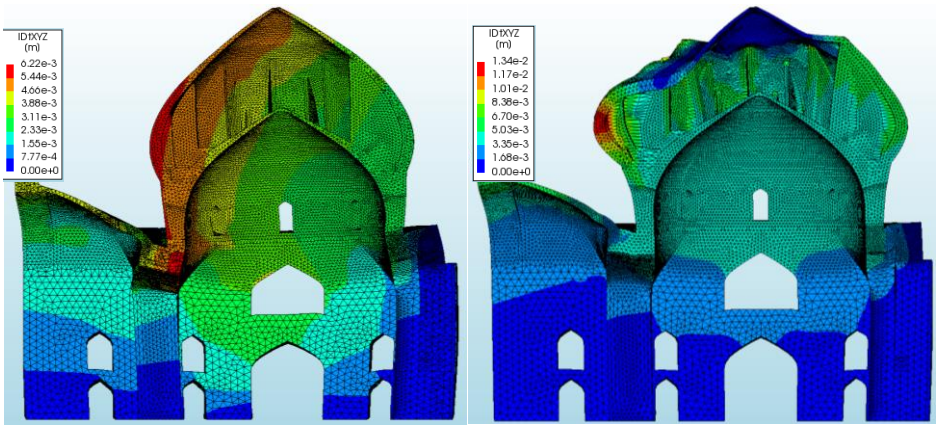

Figure 3.32 Incremental displacement IDtXYZ, (left) infinite fracture energy (right) real fracture energy

3.3.4 Discussion of the results

In conclusion, it is possible to state that the structure when subjected only to gravitational loads appears rather stable (is it recommended to consider also soil-structure interaction in future analyses). The capacity curve for vertical loads reaches a value about six times higher than the real load. It is however right to mention some weaknesses of the structure. First of all, the tendency of the great dome to cause important stresses on the structure on which it rests was observed; this behavior is particularly evident in the two large arches of the structure in which great compression stresses (open arch) and large shear stresses (closed arch) are triggered. Furthermore, it was possible to see how tensile stresses are triggered in the dome, causing it to detach from the stiffener walls. Further, the tendency of the semi-dome (*eyvan*) to have an out of plane mechanism, which could be a weak point especially under seismic actions, was observed. From the analysis of the structure without the modern strengthening elements (how explained in section 2.2). It seems therefore no coincidence that, in 1932, the designer of the reinforcement interventions stabilized the *eyvan* with a net of steel I-beams and applied I-beams steel rings with 90 m perimeter on the extrados of the outer dome in the position of the traditional encircling wooden ties system. It is stressed that these strengthening elements are not considered in the model. Finally, it is possible to say how, in the case of the Shah Mosque, the fracture energy can: not only modify the ultimate load capacity, but also changes the failure mechanism.

4. IN SITU TESTS AND CALIBRATION OF THE MODEL

A fundamental step in the safety assessment of existing structures, in order to obtain reliable results, is the calibration of the model through experimental data gathered directly from the real structure. As stated before, it is hardly possible to develop fully realistic and reliable numerical models representative of the actual structural behavior of a building in the absence of experimentally verified data. For this reason, it is advisable to collect as many information related to the structural behavior as possible. With this aim it was decided to perform non-destructive tests on the Shah Mosque in Isfahan.

4.1 In situ tests

According to (ICOMOS, 1964), the original configuration of a monumental structure shall be respected, and minimum interventions should be applied. In this respect, structural diagnosis should be performed in the most non-destructive way in order to identify existing properties and conditions. There are several experimental methods which are used to identify local or global properties of these structures. Experimental modal identification tests are one of the most common and effective methods, on a more global basis (Aşıkoğlu *et al.*, 2019). Several numerical studies have been carried out by using experimental modal identification tests in historical structures, and identification of the modal parameters was achieved successfully (Aguilar *et al.*, 2012). The choice of tests to be performed in the Mosque is essentially based on two requirements. First of all, given the fact that the Shah Mosque is a building of significant cultural value, destructive or intrusive tests are excluded. Secondly, the logistical point of view plays an important role, as the great distance certainly does not allow the transportation of bulky equipment. The final choice therefore felt on sonic tests, aimed at the characterization of the elastic properties of the material, and on ambient vibration tests, aimed at understanding the overall behavior of the structure.

4.2 Sonic test

In civil engineering the use of wave acoustic methods, more specifically the use of elastic wave propagation, has been adopted in a number of fields such as void and crack detection of concrete structures, or geotechnical laboratory testing (Miranda *et al.*, 2012). In the study of masonry walls the use of wave propagation has also been adopted, but so far the focus has been on qualitative measurements (Binda *et al.,* 2001), such as the relative quality of different wall segments. Sonic and ultrasonic tests can be used to understand the elastic property of the masonry (Miranda *et al.*, 2012). A sonic method, more specifically an impact method, was preferred because the ultrasonic signal's quality is usually insufficient for masonry. For the sonic impact method, an instrumented hammer was used as a strong percussion source and an accelerometer applied on the wall was used as a receiver. The waves from the sonic impact have higher amplitude and wave length, which justifies the better quality of the results when compared with the ultrasounds (Binda *et al.*, 2001).

4.2.1 Equipment

In order to perform the sonic tests a transmitter (the impact hammer), a receiver (the accelerometer), a data acquisition and a personal computer are required. The equipment used included one instrumented impact hammer (PCB Model 086D05) with a measurement range of ±22240 N, one accelerometer (PCB model 352B) with a measurement range of ±5 g and 1000 mV/g sensitivity, a personal computer, cables and a data acquisition system from National Instruments. The signal processing consisted primarily of measuring different wave components travel times. For the sonic impacts, a Labview (LabVIEW, 2013) application (Sonic Analyzer) is used, which enabled the visualization of the transmitted and received signals in the time domain.

4.2.2 Indirect sonic impact method

The indirect sonic impact method (ISIM) of masonry walls, consists then of an indirect, or surface, test with an acoustic hammer as the transmitter and one or more accelerometers as the receivers. In the indirect sonic impact method, the receiving accelerometer is located in the same side of the wall hit with the acoustic hammer. The distance between the instruments must be specified. The P and R wave propagation velocities obtained from the time domain readings are cross-validated and used to estimate the wall's elastic modulus in the direction for which the mechanical behavior is desired, e.g. vertical direction. For the indirect sonic impact method, the impact at the medium's surface was expected to generate only the propagation of R waves on that surface. But, P waves traveling near the surface can also be detected away from the source (Qixian and Bungey, 1996). It is possible to distinguish the P wave and R wave components of the received signal because of their differences; with P wave components having a higher velocity and lower energy than R wave components (Qixian and Bungey, 1996). It is also possible to identify the P wave first arrival of the received signals in time domain as the very first arrival. In summary, the identification of the P and R wave arrival times for the ISIM test, is based on the following three criteria of the time domain received signals (Miranda *et al.*, 2012):

- The P wave always corresponds to the very first arrival in the time domain signal.

- The R wave has considerably more energy than P wave and because of that its arrival is perceptible in a time domain signal (Qixian and Bungey, 1996).
- The relationship between V_p and V_r is approximately 2 (value obtained for granite and concrete in good conditions, but it seems adequate also for masonry in general). Thus, having identified the very first arrival, it is relatively easy to search for the R-wave in a limited time range (Qixian and Bungey, 1996).

These three criteria are summarized in fig 4.1: the very first arrival (P-wave); the arrival of a wave with considerably more energy than P-wave (R-wave); the relationship between the travel time of P wave and the travel time of R-wave (Δt_1; Δt_2).

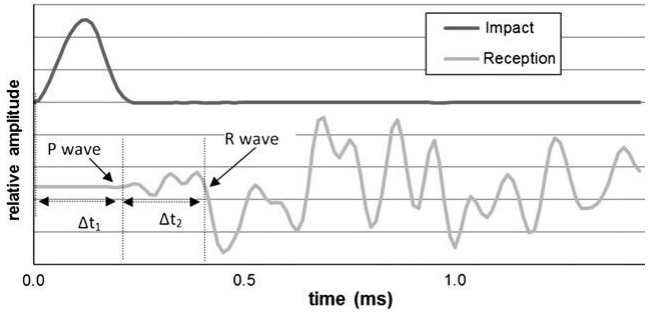

Figure 4.1 Example of a transmitted and corresponding received signals for an indirect sonic test (Miranda et al., 2012)

4.2.3 Test sequence

The strategy followed during this phase was to try to test several structural elements, in order to obtain results that can identify the entire structure. To this end, it was decided to perform the tests inside the dome on all three types of stiffener walls and obviously on both shells constituting the dome. As far as the external part is concerned, the walls constituting the main façade, the constituent shell of the *eyvan*, the minarets, the drum structure and the large lateral arch of the Mosque were tested (fig 4.2).

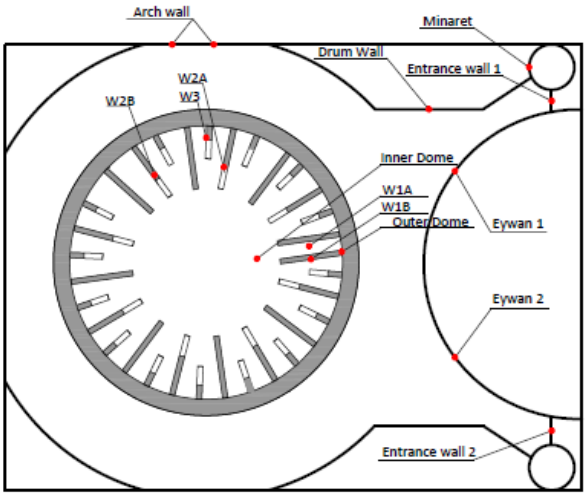

Figure 4.2 Location of the sonic tests

A grid of test points was marked on each part examined (fig 4.3), forming a number of indirect test vertical alignments. The distance between the transmitter and the receiver was generally assumed as 0.75 m, except for the largest stiffener walls (W1A, W1B) where this distance was taken as 1.0 m. In this procedure, the hammer was repeatedly used on the impact point (on average slightly over 10 times for each impact point) and readings are obtained sequentially with an accelerometer placed on the vertical of the impact point. From each reading, the P and R wave travel times could be obtained.

Figure 4.3 Sonic test on the arch of the Mosque. In red the impact point, in blue the receiver point (left) example of sonic test in the another structure in Isfahan (Si-o-se-pol bridge)(right)

4.2.4 Results

The velocities of different types of waves are related with the mechanical properties of materials. For solid, elastic, isotropic, homogeneous, infinite and semi-infinite media, the equations of wave velocity are well known. The velocities of P and R waves for such media are given by:

$$V_P = \sqrt{\frac{E}{\rho} \cdot \frac{1-\nu}{(1+\nu)(1-2\nu)}}$$

Equation 4.1 Velocity of P waves

$$V_R = \frac{0.87 + 1.12\nu}{1+\nu} \cdot \sqrt{\frac{E}{\rho} \cdot \frac{1}{2(1+\nu)}}$$

Equation 4.2 Velocity of R waves

where: V_P is the P-wave velocity, V_R is the R-wave velocity, E is the elastic or Young's modulus, ν is the Poisson's ratio and ρ is the unit weight. If V_P and V_R can be obtained, then it is possible to obtain also the Poisson's ratio. For this purpose, eq. 4.3 is obtained from eq. 4.1 and 4.2:

$$\frac{V_P}{V_R} = \sqrt{\frac{2(1-\nu)}{(1-2\nu)} \cdot \frac{(1+\nu)^2}{(0.87+1.12\nu)^2}}$$

Equation 4.3 P waves and R waves velocity ratio

In practice, once defined the Poisson ratio (ν) and knowing the mass density (ρ) it was possible, through eq. 4.1 and 4.2, to estimate the Young's modulus (E) for all the zones tested (tab. 4.1). Regarding the mass density it was decided to use that value indicate from the Italian code for this type of masonry (Circolare NTC18, 2019) that provides a value of 1800 kg/m^3. Note that this is a dynamic value of the Young's modulus and a moderate difference to the static value of the Young's modulus is expected.

Zone	ρ (kg/m^3)	$\mathbf{V_p}$ (m/s)	$\mathbf{V_r}$ (m/s)	$\mathbf{V_p/V_r}$	ν	**CoV** (%)	**E** (MPa)
W1	1800	1077	462	2,33	0,38	11,1	1083
W2	1800	1110	420	2,64	0,25	13,1	1532
W3	1800	950	559	1,70	0,38	14,6	911
Inner dome	1800	821	373	2,20	0,34	9,0	780
Outer dome	1800	994	424	2,34	0,40	16,1	968
Exterior	1800	936	420	2,23	0,38	22,8	980
Average	1800	980	440	2,21	0,36	14,4	1040

Table 4.1 Results of the sonic test on the Shah Mosque

It is also important to state that in order to obtain reliable results, during the evaluation of the parameters just mentioned, it was decided to define a range outside of which unrealistic values were discarded. This range is explained in eq. 4.4 where σ is the standard deviation, m is the average and x is the value to check.

$$m - \sigma < x < m + \sigma$$

Equation 4.4 Adopted range of acceptable values for sonic test results

4.3 Dynamic characterization test

Dynamic characterization tests are intended to obtain the dynamic properties of a structure in terms of natural frequencies and vibration modes. This type of test can lead to better understand the global behavior of existing structures. Thus, it is a fundamental tool that can be used to calibrate numerical models. For this reason, an ambient vibration test was performed in the Mosque using environmental vibrations as a source of excitation. Following that, Operational Modal Analysis (OMA) was performed, and experimental modal parameters were extracted using (ARTeMIS Modal, 2015).

4.3.1 Equipment

The equipment used to perform the ambient vibration test included accelerometers (PCB model 393B12) with a measurement range of ±0.5 g and 10,000 mV/g, a personal computer, cables and a data acquisition system from National Instruments.

4.3.2 Test sequence

Seven setups were carried out, of which three outside (fig 4.4), two on the outer dome and two on the inner dome of the Shah Mosque (fig 4.5 and 4.6). Each setup was composed of 4 accelerometers. One accelerometer was the reference that must be fixed for all the setups, while

the other three accelerometers can be relocated at different points of the structure. Ambient vibration data were recorded for approximately 20 minutes in each setup. The position of the accelerometers was decided in order to gather information of the dynamic properties of the structure only in the horizontal directions (X and Y), neglecting the vertical component (Z). The location of the accelerometers in the Mosque was decided based on the modal response of a preliminary numerical model, with respect to identification of the translational movements of the structure. About the nomenclature of the setup it was decided to assign the name of "setup ext n" for the measurements outside the dome and "setup n" for those inside the dome, where n is the setup number. Regarding the name of the accelerometers it was decided to give the name "0" for the reference (valid for each setup) and n.1...n.2... for the others, where n is the setup number and the second number is the accelerometer (fig 4.5). Cubic wood blocks (fig 4.4) were used for the installation to fix the accelerometers to the wall, using fast setting glue.

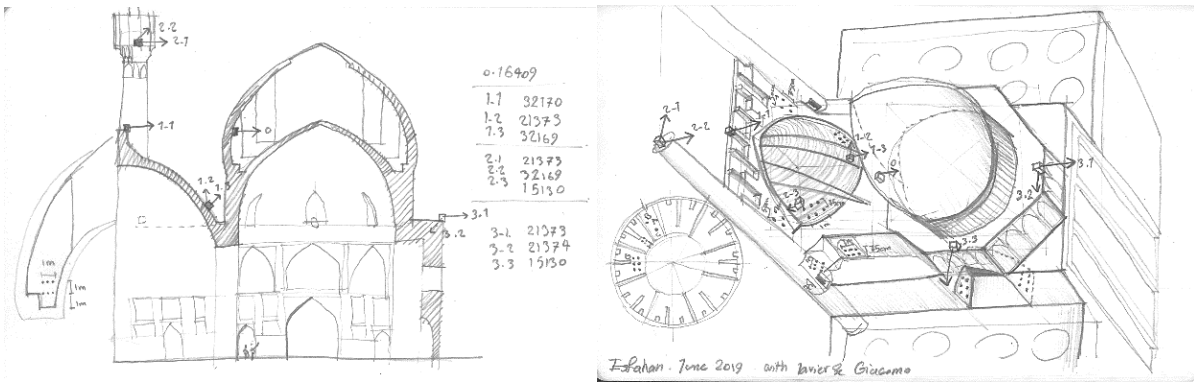

Figure 4.4 Position of the accelerometers and of selected sonic tests (drawings by Ali Tavakoli Dinani)

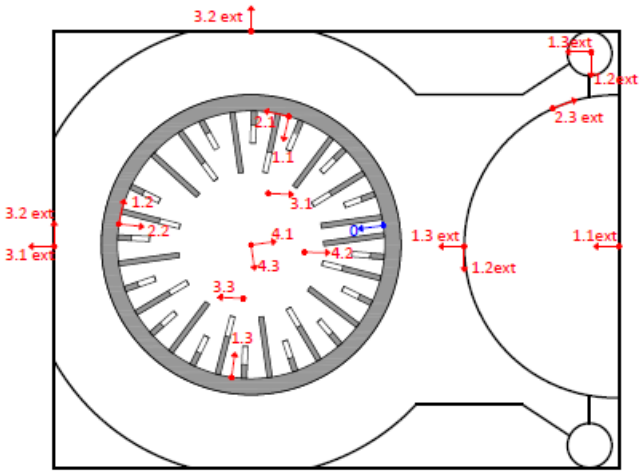

Figure 4.5 Map of the accelerometers in the ambient vibration test in the Mosque

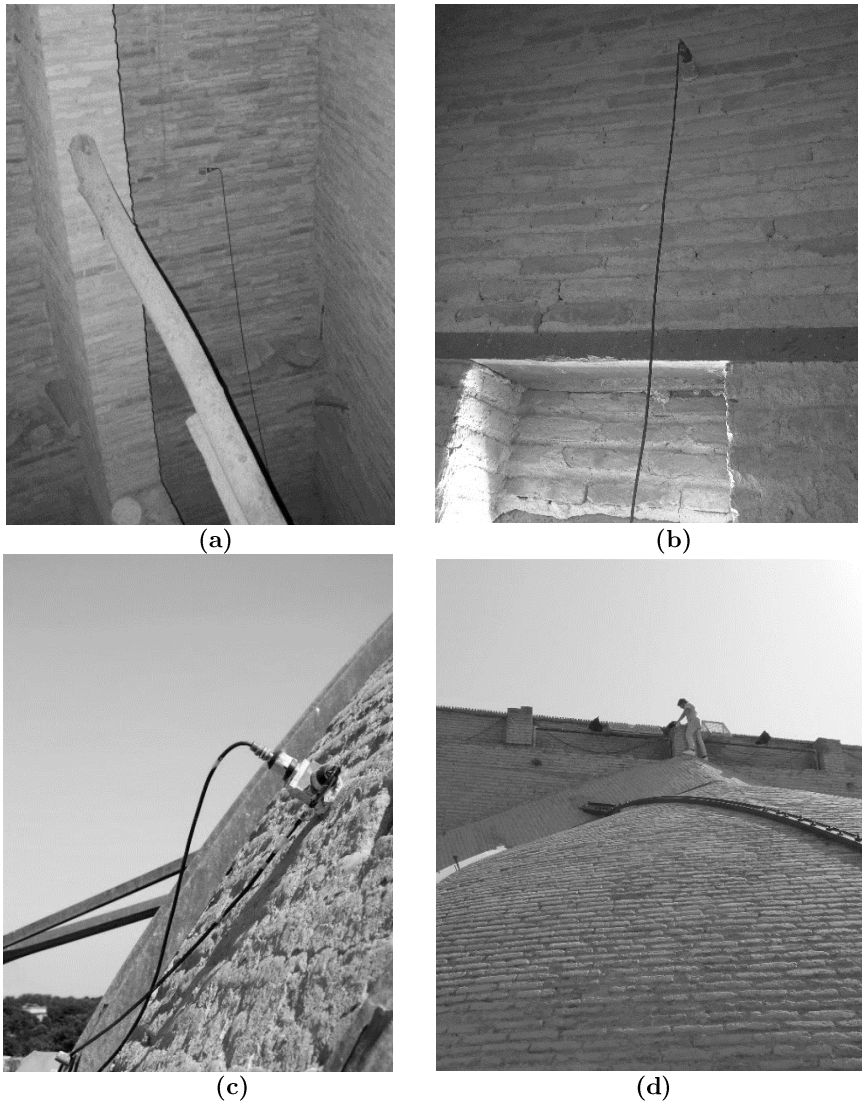

Figure 4.6 Installation of the accelerometers: (a) 2.2 (b) 0, reference (c) 1.2 "ext" and 1.3 "ext" (d) 1.1 "ext" on the top of the *eyvan*

4.4 Operational modal analysis

The modal estimation was carried out using ARTeMIS software (ARTeMIS Modal, 2015), which allows analyzing the results from all test setups simultaneously. The peak values of frequency were selected using two different analysis techniques, in order to compare the results and determine the natural frequencies using the Modal Assurance Criterion (MAC): (a) Enhanced Frequency Domain Decomposition (EFDD); and (b) Stochastic Subspace Identification – Unweighted Principal Components (SSI-UPC) (Maccarini *et al.*, 2018). The reliability of the results mainly depends on the environmental noise, structural components, quality of measurement of the system and technical expertise of the experimental campaign personnel (Aguilar *et al.*, 2012). The EFDD is a non-parametric method, which is developed in the frequency domain, while the SSI is defined as a parametric method, originated from the time domain. Both methods can be used, however, the results of the non-parametric methods are mainly influenced by the quality of the environmental noise, and this drawback can be overcome by using parametric methods (Ramos *et al.*, 2011). For this reason, the final comparison between

the numerical model and the experimental results was performed using the values obtained from the SSI method.

4.4.1 Data preparation in ARTeMIS

The first step was building the model in Artemis. In the software, the geometric model is composed by points, lines and surfaces. To this end it was decided to simplify the shape of the building, especially regarding the double dome and the *eyvan*. These complex elements were discretized in order to avoid curved elements (fig 4.7). The second step was applying the accelerometers in the model, paying attention to the direction and sign, in order to replicate correctly the in-situ configuration. Finally, adequate boundary conditions, i.e. fixed nodes in the base, were applied to the model.

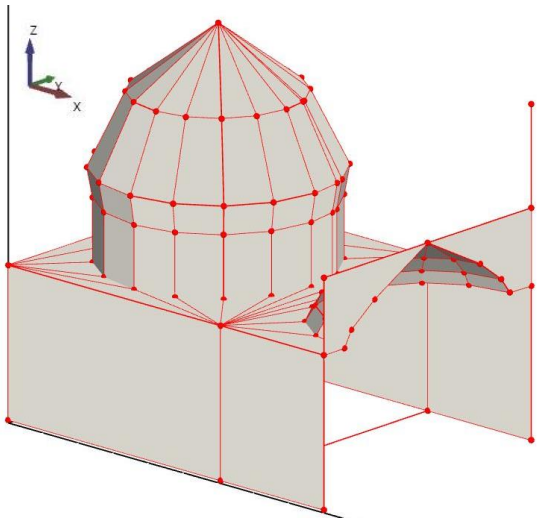

Figure 4.7 Geometric model in ARTeMIS

4.4.2 Modal assurance criterion

The comparison between different mode shape is a fundamental tool in order to assess the reliability of the experimental data. This comparison can be done, for example, between two experimental modes found with different estimation method or between analytical and experimental mode shape. This is possible through the modal assurance criterion (MAC). It is a statistical indicator that is most sensitive to large differences and relatively insensitive to small differences in the mode shapes. This yields a good statistic indicator and a degree of consistency between mode shapes. The MAC is often used to pair modes shapes derived from analytical models with those obtained experimentally. It is easy to apply and does not require an estimate of the system matrices. It is bounded between 0 and 1, with 1 indicating fully consistent mode shapes. It can only indicate consistency and does not indicate validity or orthogonality. A value near 0 indicates that the modes are not consistent (Pastor *et al.*, 2012). The MAC is calculated as the normalized scalar product of the two sets of vectors $\{\varphi_A\}$ and $\{\varphi_X\}$, as shown in eq. 4.5.

$$MAC(A,X) = \frac{\left|\sum_{j=1}^{n}\{\varphi_A\}_j\{\varphi_X\}_j\right|}{\left(\sum_{j=1}^{n}\{\varphi_A\}_j^2\right)\left(\sum_{j=1}^{n}\{\varphi_X\}_j^2\right)}$$

Equation 4.5 MAC comparation

Once extracted the vectors (which describe the mode shape) from the numerical and the experimental model, it was possible to compare them through the MAC comparation.

4.4.3 Modal estimation

To define the main vibration modes of the structure, the analysis of the model with the seven setups at the same time appeared too complicated and inducing excessive perturbation in the results. So, it was decided to analyze the setups separately. To this scope, it was possible to define three configurations as a function of the location:

- Exterior part
- Inner dome
- Outer dome

In each configuration only the accelerometers of the specific zone were analyzed. For all the three configurations one main mode, with a frequency around 2,6 Hz (fig 4.8), was found. Comparing the estimation method EFDD and SSI, through the modal assurance criterion it was possible to insure the reliability of the data (tab 4.2). Furthermore, the presence of this mode in the three configurations stresses its reliability. This approach was very useful to understand possible problems (noise, inaccurate readings...) in the recording for each accelerometer. In fact, the need for dismissal of selected accelerograms was evident from the post-processing.

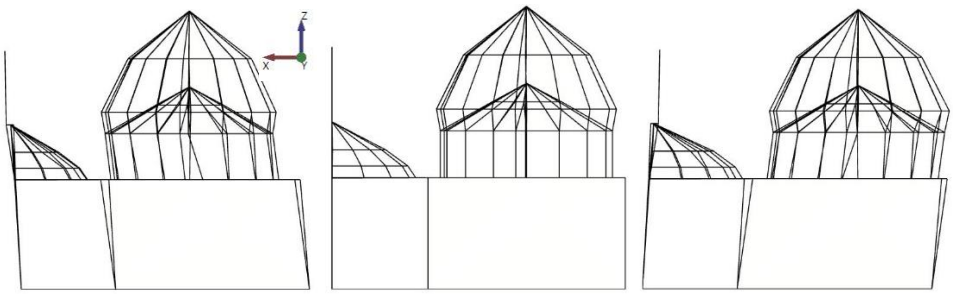

Figure 4.8 Mode 1, outer dome configuration, SSI method, f=2,57 Hz

Configuration	MAC Comparison	
Exterior	EFDD f= 2,54 Hz	SSI f=2,53 Hz MAC= 0,92
Outer dome	EFDD f= 2,55 Hz	SSI f=2,57 Hz MAC= 0,96
Inner dome	EFDD f= 2,59 Hz	SSI f=2,56 Hz MAC= 0,98

Table 4.2 MAC comparation of the first mode, for the three configurations

The subsequent step was that to analyze all the setups at the same time. In order to confirm the results obtained in the three configurations. For the complete configuration (where all the setups are applied on the model), the procedure is explained with more accuracy, but the same approach was used for each setup. The estimation of frequencies and modes is performed using a frequency range between 0 Hz and 20 Hz, in order to reduce the computational burden and

increase the accuracy, neglecting non-significant vibration modes. The peak value of the first frequency was selected first using the EFDD method (fig 4.9) and then using the SSI-UPC method (fig 4.10). The mode found reflects the prevision made during the estimation in the simplified configurations. This first vibration mode identified, with a frequency around 2,6 Hz, is a translational mode in the direction of the symmetry axis (X) (fig 4.11 and 4.12). The last step to perform, in order to compare the results and determine the natural frequencies, is the MAC evaluation (tab 4.3).

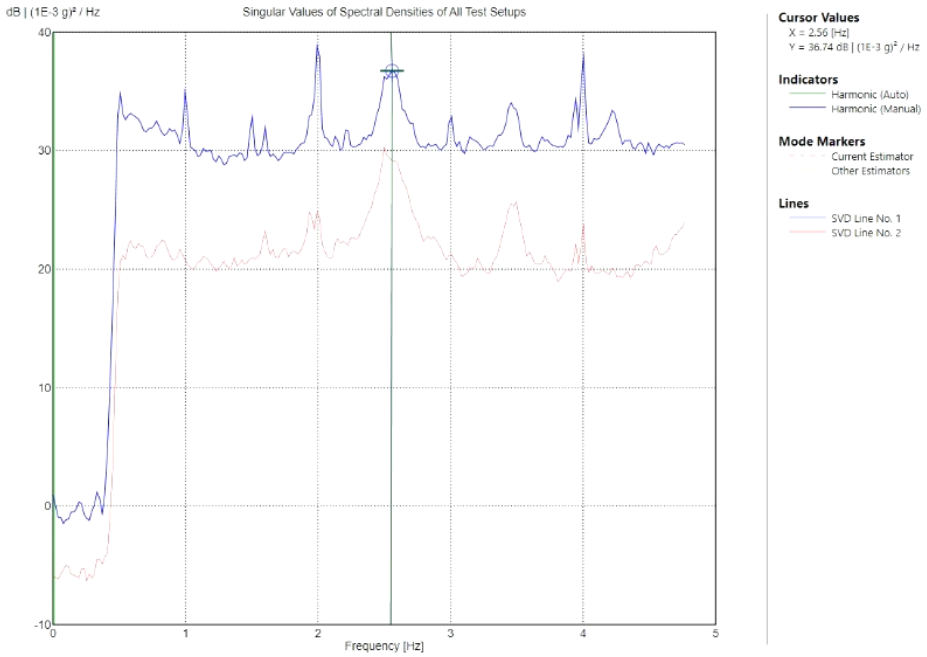

Figure 4.9 EFDD method, with singular value of spectral densities of all setups

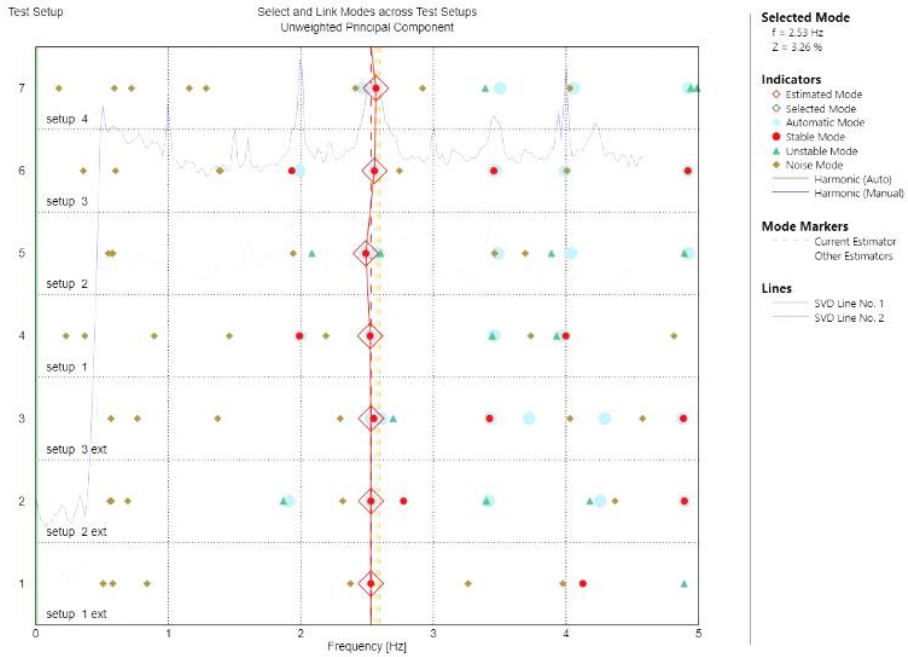

Figure 4.10 The SSI-UPC method, with selection and linking process of modes across all test setups

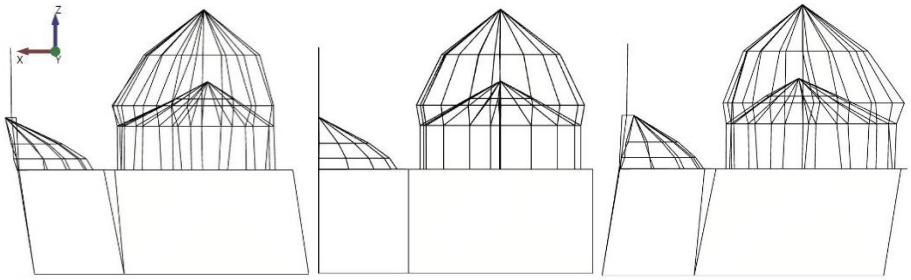

Figure 4.11 Mode 1, complete configuration, SSI method, f=2,55 Hz, prospect view

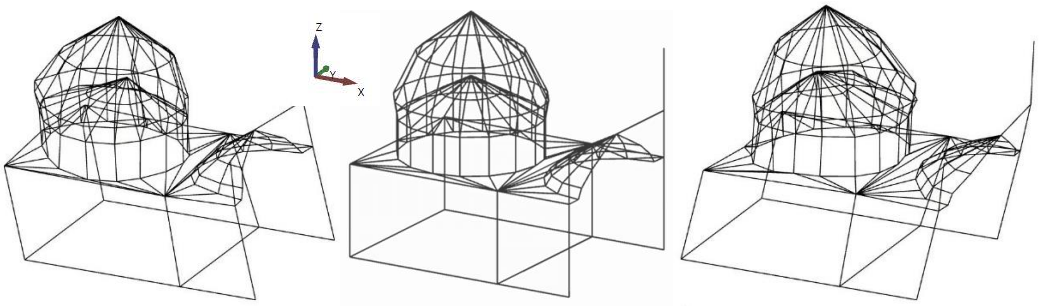

Figure 4.12 Mode 1, complete configuration, SSI method, f=2,55 Hz, axonometric view

Configuration	MAC Comparison	
Complete	EFDD f= 2,58 Hz	SSI f=2,55 Hz
	MAC= 0,91	

Table 4.3 MAC comparison of the first mode, for the complete configuration

4.5 Calibration of the model

Once the dynamic properties of the structure have been identified, the correlation between the experimental and the numerical modal responses should be examined. The numerical model was calibrated by an updating process so that the model would achieve a higher reliability and would closely simulate the real behavior of the structure. Assuming that the elastic properties of the material (E, G and ν) were obtained through the sonic tests, the only way to modify the dynamic property of the numerical model is acting on the boundary condition. As stated in the previous section, not the entire building was modelled. To take into account the influence of the rest the structure, adequate boundary conditions may be used.

4.5.1 Evaluation of the boundary condition

In order to evaluate the boundary conditions, the calculation of the axial rigidity provided by the adjoining structure was made. The stiffness of the element is obtainable taking into account both flexural and shear deformation (Timoshenko's theory), as a first approximation. If the element is free to translate only in the top, the stiffness is given by eq. 4.6.

$$K = \frac{12EI}{h^3} + \frac{GA}{1{,}2h}$$

Equation 4.6 Stiffness evaluation

The contribution of the adjoining structure is divided in three sectors, called K1, K2 and K3 (fig 4.13). Also, the uniform distributed stiffness is calculated and given in tab 4.4.

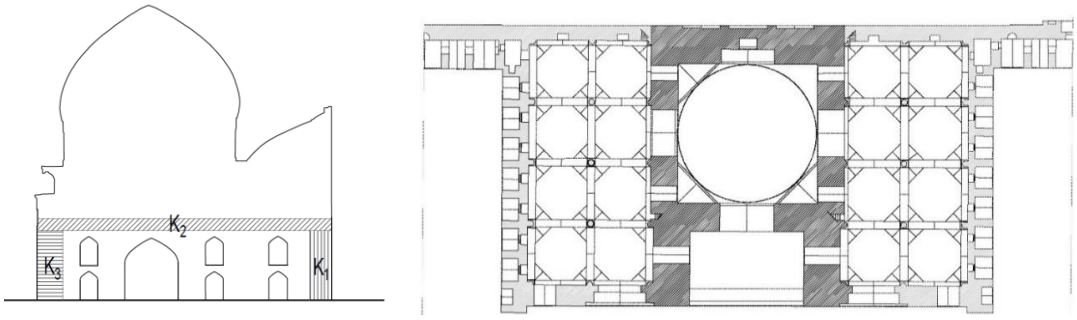

Figure 4.13 Sectors of lateral stiffness (left) plan of the entire structure (right)

The shear stiffness is initially estimated as 40% of the normal stiffness (given by a normal Poisson's ratio in a continuum). Subsequently, it is modified in order to minimize the difference between the experimental and numerical model. This is made by modifying the shear stiffness and by running an eigenvalue analysis in DIANA. In conclusion, it is possible to state that: (a) uniform stiffness in all walls gave results closer to the experimental results, possibly due to the large rigidity of the walls and of the floor; (b) the lateral stiffness is increased up to the 50% of the normal one to reach a similar behavior between experimental and numerical.

K_1 (N/mm^3)	K_2 (N/mm^3)	K_3 (N/mm^3)	$K_{uniform}$ (N/mm^3)
105,5	48,0	850,2	313,7

Table 4.4 Stiffness provided by the adjoining structure

4.5.2 Eigenvalue analysis of the calibrated model

After the calibration of the model, through the boundary condition, a full eigenvalue analysis was performed (fig 4.14) (tab 4.5). The results, in terms of frequency and shape of the first mode, were consistent with the experimental data. The analysis showed also a second mode, very close in terms of frequency to the first but with a different shape. This mode was a translational mode, but in the opposite direction of the first. Remembering that experimental and the numerical model are strongly dependent (sometimes the FE model can give a suggestion on possible unidentified vibrating modes in the experimental results), a further check on the experimental data was made.

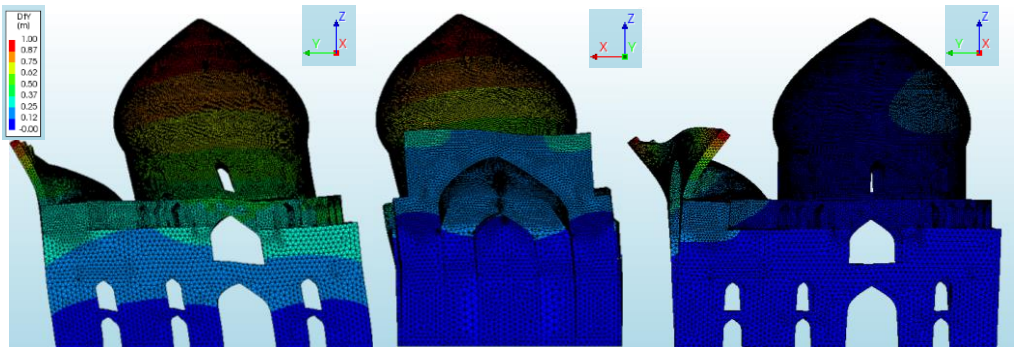

Figure 4.14 Modal shape (from left to right) mode 1, mode 2, mode 3

Mode	f (Hz)	Eff, mass X (%)	Eff, mass Y (%)
Mode 1	2,46	0	62,92
Mode 2	2,75	33,12	0
Mode 3	3,05	1,27	0

Table 4.5 Results of the eigenvalue analysis, first three modes

Through the additional control of the experimental data, the second mode was found (fig 4.15) (tab 4.6). This mode tends to excite mainly the dome of the Mosque (or is not captured in the external dome). Also, for this behavior, this mode cannot be very useful to calibrate the normal stiffness provided by the adjoining structure. Still, the information gathered from this vibrating mode can help in a further validation of the numerical model. Regarding the higher modes, it was observed that they are basically local modes, e.g. mode 3, and, for this reason, it was possible to neglect them (appendix B shows the results for the first 100 modes).

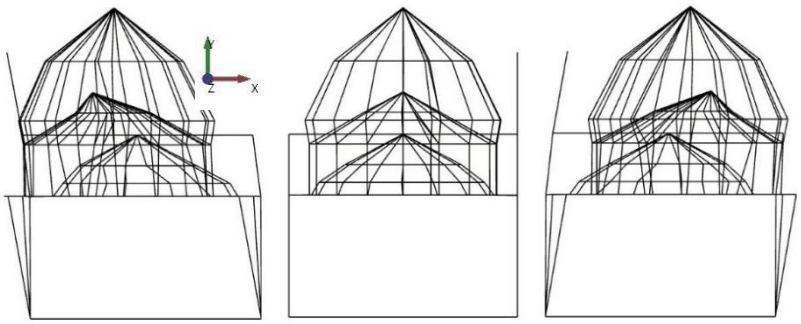

Figure 4.15 Mode 2, inner dome configuration, SSI method, f=3,02 Hz

Configuration	MAC Comparison	
Inner dome	EFDD f= 2,99 Hz	SSI f=3,02 Hz
	MAC= 0,95	

Table 4.6 MAC comparation of the second mode, for the inner dome configuration

4.5.3 Modal assurance criterion between numerical and experimental models

The last step to perform, in order to validate the model, is the comparison between the numerical model and the experimental results. This is possible again through the modal assurance criterion (MAC). Once extracted the vectors (which describe the mode shape) from the numerical and the experimental model, it was possible to compare them through the MAC comparation (tab 4.7). The comparison between the experimental and numerical model provides a good result. Regarding the first mode the MAC value is 0,86, value that indicates a consistent of the FE model if compare with the experimental one. Also, for the second mode the results in term of coherence between the two mode shapes appears adequate with a MAC value of 0,81. It is important to remember, how during the extraction of the data, an accurate coincidence between the nodes of the numerical and experimental model is required. The mode shape used for the experimental model is obtained from the SSI method, given its lower sensitivity to environmental noise (Ramos *et al.*, 2011).

Mode	Model	f (Hz)	MAC
Mode 1	Numerical	2,46	0,86
	Experimental	2,55	
Mode 2	Numerical	2,75	0,81
	Experimental	3,02	

Table 4.7 MAC comparation between experimental and numerical model

4.6 Conclusion

The results (tab 4.7) showed a good correspondence between the models with a MAC value of 0,86 for the first mode and 0,81 for the second mode. The results confirm the reliability of the calibration of the model. Unfortunately, a translational mode, in the same direction of the second mode, able to excite the entire structure was not found. For this reason, some doubts remain about the normal stiffness provided by the adjoining structure. But it is possible to say that the comparison in terms of mode shapes and frequencies provide a good level of reliability of the numerical model. Furthermore, it is possible to confirm the relevance of in-situ tests for improving the numerical model with the aim to have a more realistic behavior. In fact, substituting the Young's modulus obtained with the sonic test, it was been possible to increase the first period of the structure approaching the experimental data. Then, through the boundary condition updating, it was possible to get a closer response in terms of mode shapes. To conclude, it is important to remember: (a) despite initial skepticism of the author, the experimental data provided excellent and reliable information about the real behavior of the structure; (b) that the numerical and the experimental parts must go hand in hand during the entire process of model validation and updating, in order to obtain sufficient and reliable results.

5. FINAL STRUCTURAL ANALYSIS

The previous chapters were a path aimed at achieving the widest possible knowledge about the structure. This path has had from the beginning as the main target to want to understand the static behavior of the structure. Through a historical research the structure's past was understood: its history, the external events that affected it and the interventions suffered. Athwart a preliminary structural analysis, it was understood the possible weak points. The last step was the one that most distinguishes applied sciences, such as engineering, from pure sciences, such as mathematics and physics: the study of the real behavior of the system, system which in this case is the structure. To this end, a local and global characterization of the structure was carried out using experimental data gathered in situ.

5.1 Numerical model

The final numerical model exploits the setups used for the preliminary analysis (section 3), although some modify are necessary. Basically, the differences applied to the model are: (a) the material properties are changed after the characterization of the elastic properties through the sonic test; (b) the boundary condition are changed as a result of the calibration of the model.

5.1.1 Material property

The evaluation of the mechanical properties of the masonry of the mosque is based on the information gathered through the in situ sonic tests (section 4). Regarding the elastic properties, the average values obtained from the experimental data were used. Regarding the strength, the Italian code (Circolare NTC18, 2019) provides the average properties for this type of masonry. Based on these values, the strength for the mosque was obtained proportionately, comparing the elastic modulus of the tests with that of the code.

Masonry type		$\wp$ (t/m^3)	**E** (MPa)	**G** (MPa)	f_c (MPa)	τ_0 (MPa)
Masonry with solid bricks and lime mortar / "*Muratura in mattoni pieni e malta di calce*"	Min	1,8	1200	400	2,4	0,060
	Max		1800	600	4,0	0,092

Table 5.1 Material properties for brick masonry with lime mortar (Circolare NTC18, 2019)

Basically, through the ratio between the elastic module found with the test (1050 MPa) and the minimum from the code (1200 MPa), it is possible to obtain the proportional values for the other properties. Unfortunately, the code does not provide all the data required in DIANA for the total strain crack based model, such as: the tensile strength (ft), the compressive (Gc) and the tensile (Gf) fracture energy. Conventionally, it is possible to assume the tensile strength (ft) equal to 1,5 times the shear strength (τ0) (eq 5.1) (Vinci, 2018).

$$f_t = 1{,}5 \cdot \tau_0$$

Equation 5.1 Relation between shear strength and tensile strength

Regarding the compressive fracture energy, the approach provided by (Lourenço, 2018) can be used. In this case, the evaluation of the fracture energy is based on the ductility index (d_u), given by the ratio between the fracture energy (G_f) and the tensile strength (f_t) (Lourenço, 2009). The ductility index can be evaluated from eq. 5.2, where f_c is the compressive strength in MPa. Subsequently, it is possible to calculate the compressive fracture energy through eq. 5.3.

$$d = 2{,}8 - 0{,}1 f_c$$

Equation 5.2 Ductility index (Lourenço, 2018)

$$G_c = d \cdot f_c$$

Equation 5.3 Compressive fracture energy

For the tensile fracture energy, given the macro modelling approach and the scarce information about brick, mortar and their interface, an average value of 0,012 N/mm can be assumed (Lourenço, 2018). The final material properties are summarized in tab. 5.2.

	ρ (t/m^3)	**E** (MPa)	ν	$\mathbf{f_c}$ (MPa)	$\mathbf{G_c}$ (N/mm)	$\mathbf{f_t}$ (MPa)	$\mathbf{G_f}$ (N/mm)
Masonry	1,8	1050	0,35	2,1	5,4	0,08	0,012

Table 5.2 Material properties adopted for the final model

It is also important to emphasize that, given the experimental nature of this thesis, it was decided to neglect the safety coefficients on the materials specified in the codes. The same was also done for the actions.

5.1.2 Element type

As stated before, in order to calibrate the model, adequate boundary conditions are applied. To this end, interface elements able to replicate the stiffness provided by the adjoining structure are used. It is possible to see the interface properties required in DIANA in section 4.5.1. Structural interface element types in DIANA are sets of points, sets of lines, or sets of triangles or quadrilaterals. The lines, triangles and quadrilaterals may have linear, quadratic, or cubic interpolation functions for the displacement field. For elements with linear interpolation functions there are only two nodes at each edge, whereas for elements with quadratic interpolation functions there are three nodes at each edge, and elements with cubic interpolation functions have four nodes along each edge (DIANA FEA BV, 2019). In this case, a plane triangular tridimensional element is chosen (T18IF). The T18IF element is an interface element between two planes in a three-dimensional configuration (fig 5.1). The local XYZ axes for the displacements are evaluated in the first node with X from node 1 to node 2 and z perpendicular to the plane. The element is based on linear interpolation. By default, Diana applies a 3-point integration scheme (DIANA FEA BV, 2019).

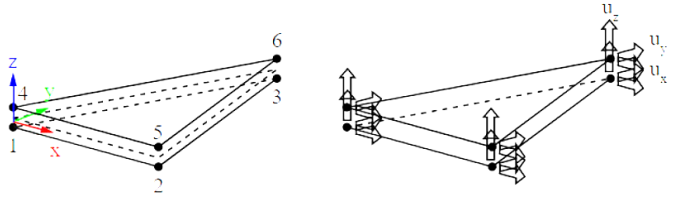

Figure 5.1 T18IF element (left) topology (right) displacements (DIANA FEA BV, 2019)

5.2 Incremental vertical analysis

After calibrating the numerical model and defining the settings for the analysis (the same used in section 3), it was possible to perform a vertical incremental structural analysis. Fig 5.2 shows the displacement of the control point (the top of the dome) by increasing the load factor L.F. (considering only the self-weight of the structure).

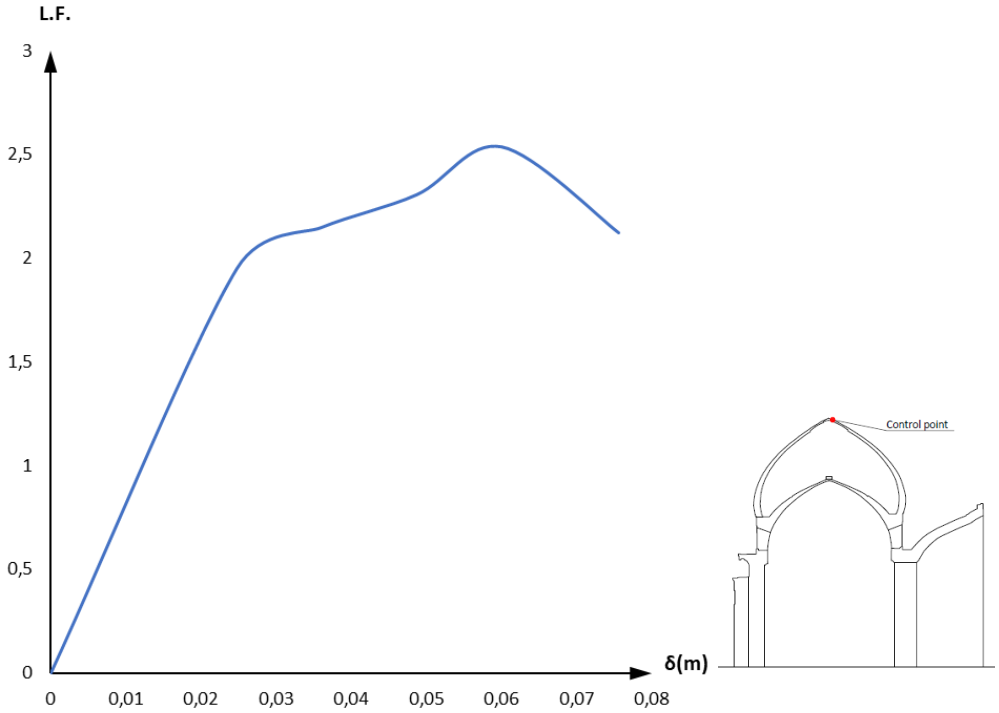

Figure 5.2 Curve F-δ for the incremental vertical analysis. L.F. indicates the load factor magnifying gravity and δ is the displacement at the top of the dome

In order to better understand the results, displacements and principal strains distribution are reported for two specific load stages: the first load stage L.F.=2,54 is the peak load and the second L.F.=2,12 is the post peak stage. As for the first case, it is possible to observe how the larger displacements take place on the top of the dome (fig 5.3). In terms of strains, it is possible to note concentration of principal tensile strain E1 in the dome, especially in the outer shell close to the opened arch (*eyvan* side) (fig 5.3). Furthermore, it is possible to note the presence of large shear stresses at the point where the drum rests on the main structure in correspondence with the large closed arch (fig 5.4). The analysis of the strain field inside the dome, shows also high values in the connection points between the stiffener walls and the outer shell of the dome. This behavior highlights the tendency of the dome to detach from the stiffener walls. These results are consistent with those obtained with the provisional model in section 3, although using different material property, meaning that the loadbearing capacity and the global behavior are different.

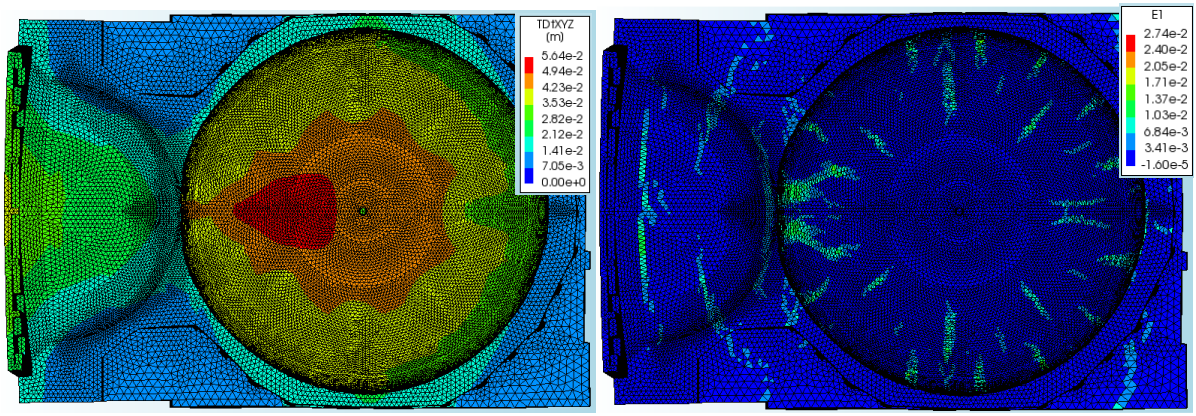

Figure 5.3 Displacement TDtXYZ, (left) principal strain E1 (right), L.F.=2,54

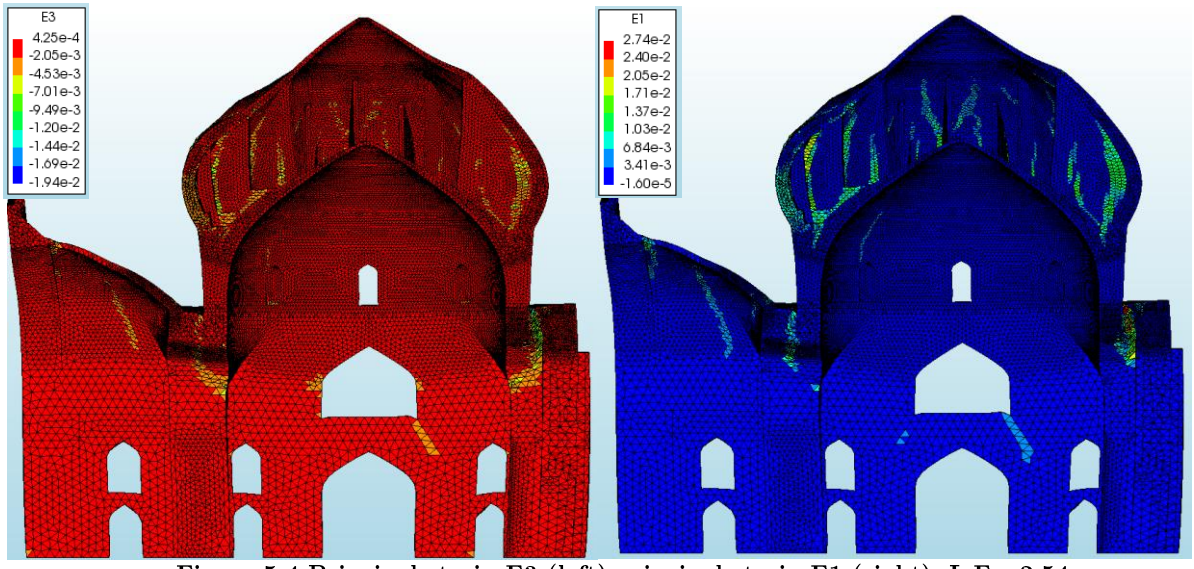

Figure 5.4 Principal strain E3 (left) principal strain E1 (right), L.F.=2,54

The second load stage (L.F. = 2,12) confirms what was said before for the displacements, although they are increasing especially in the most flexible part of the dome, that one without the stiffener effect provides by the walls inside the dome (fig 5.5). Regarding the principal strains, it is possible to see how several cracks appear in the dome (fig 5.5), especially in the area over the opened arch (*eyvan* side). Fig 5.6 confirms the tendency of the outer shell of the dome to detach from the stiffener walls, causing high level of tensile strain. As observed before for the case of the provisional model, shear in the top of the closed arch (patio side) is present. The analysis of the incremental displacement is a fundamental tool to understand the possible reason of the final loss of loadbearing capacity. In this case, the incremental displacement (fig 5.7) confirms this tendency of the outer dome to detach from the stiffener walls. This behavior is mainly due to the particular bulbous shape of the dome, as this form triggers tensile strains in the shell, able to withstand only to compression. This effect is compensated by the stiffener walls, but once the dome is detached from them the capacity decreases quickly.

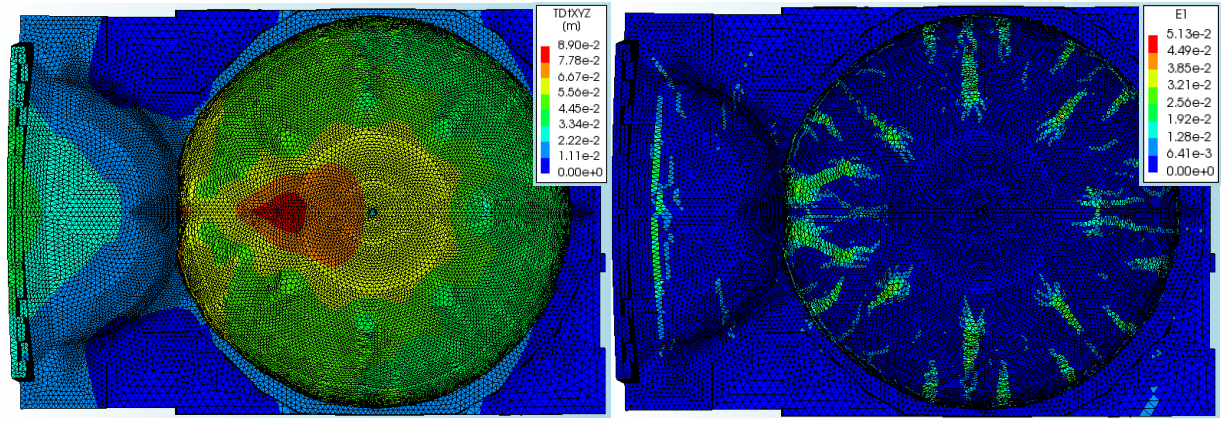

Figure 5.5 Displacement TDtXYZ, (left) principal strain E1 (right), L.F.=2,12

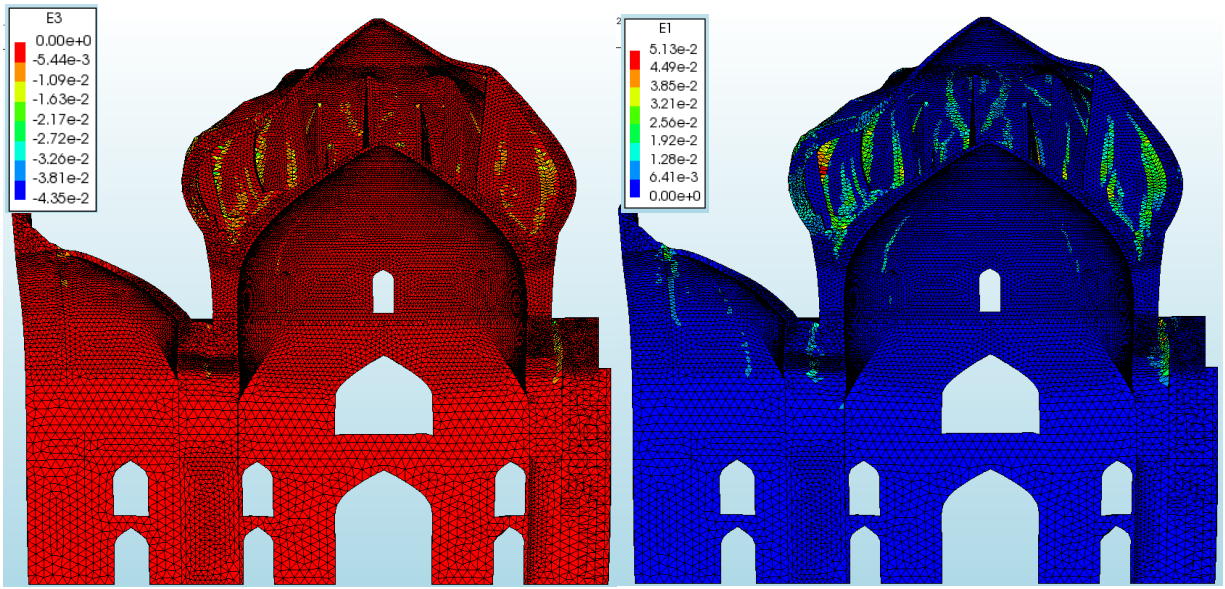

Figure 5.6 Principal strain E3 (left) principal strain E1 (right), L.F.=2,12

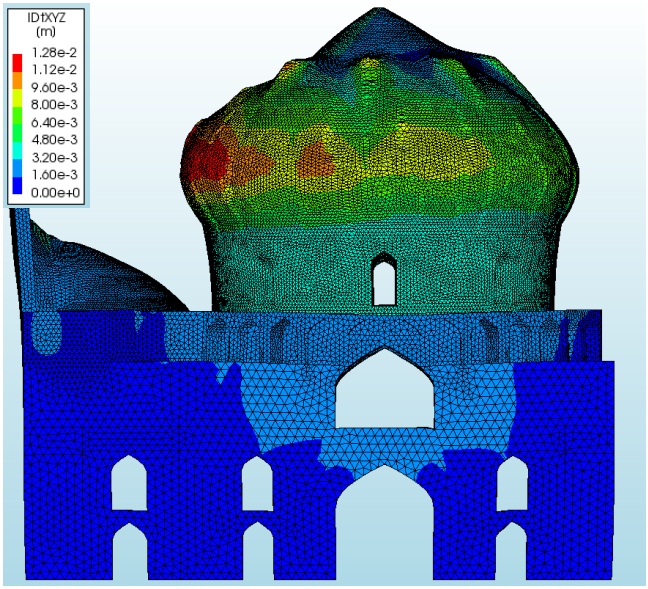

Figure 5.7 Incremental displacement TDtXYZ L.F.=2,12

5.2.1 Comparison final and provisional model

As shown in section 3, a comparison between the results obtained through a model built with the data found in literature and the one built through the experimental data is interesting. The main difference between the models are the material and the boundary condition. In the case of an incremental vertical analysis, the main role is certainly played from the material properties. Tab. 5.3 compares the properties of the two model and evaluates the difference (Δ) for each value. It is clear how the final model has characteristics in terms of strength and elastic property clearly lower. Also, the specific weight is increased. Furthermore, it is possible to see a strong decrease of the compressive fracture energy, even if less than strength, which means an increase in ductility. The only different case is the tensile fracture energy, increased of the 33%.

Model	ρ (t/m^3)	E (MPa)	ν	f_c (MPa)	G_c (N/mm)	f_t (MPa)	G_f (N/mm)
Provisional	1,42	2834	0,2	5,75	9,2	0,28	0,008
Final	1,8	1050	0,35	2,1	5,4	0,08	0,012
Δ (%)	21	-170	43	-174	-69	-256	33

Table 5.3 Comparison between material properties in the final and provisional model

As shown in the previous section, the behavior of the structure under an increasing vertical load is quite similar between the two cases. But the comparison of the two capacity curves (fig 5.8) highlights some important differences. First of all, the influence of the elastic modulus is clear, in fact the stiffness of the final model is drastically reduced. Furthermore, the maximum capacity is reduced to about the half, consistently with the reduction if the strength properties and increase of the specific weight. The only advantage obtained with the new properties is ductility, as the final model shows a higher capacity of deformation, probably due to the increase of the tensile fracture energy and the ductility in compression.

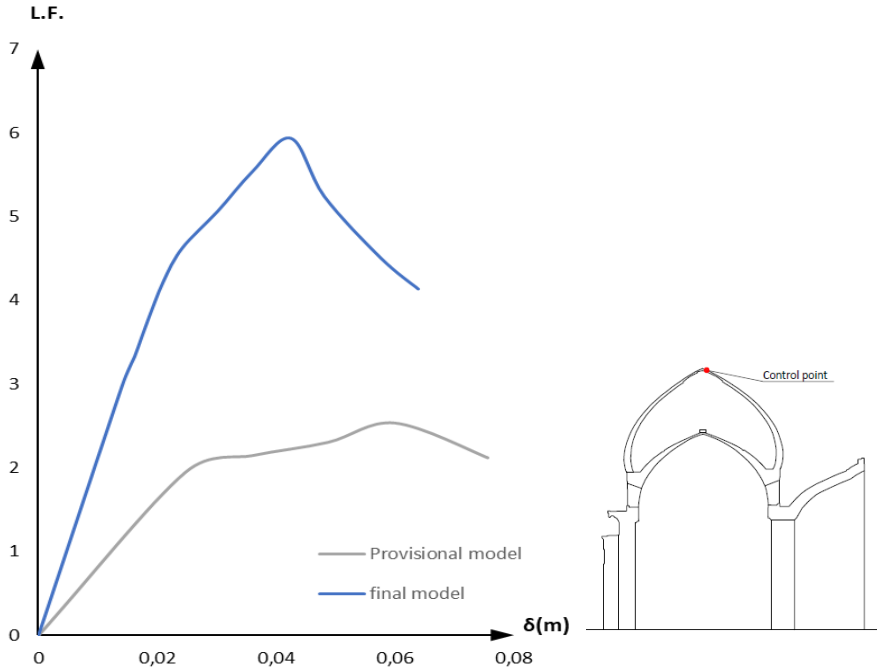

Figure 5.8 Final and provisional model comparison for vertical capacity

5.3 Incremental horizontal analysis

To assess the response of a structure under seismic actions, several methods exists. In this thesis, a pushover analysis with load profile proportional to the mass is used. Pushover analysis consists of a non-linear static analysis in which horizontal forces represent seismic actions. The method uses an incremental-iterative procedure assuming conditions of constant gravity loads and monotonically increasing the horizontal loads. This method can be used to estimate the failure mechanisms of a structure, to analyze the distribution of damage, to assess the structural performance of existing buildings and to predict the capacity curve of a structure (EN 1998-1, 2004). Two pushover analyses in the Y direction (positive and negative) were carried out. The reason of this choice is due to two main reasons: (a) the calibration of the model is particularly reliable in this direction (a second mode able to excite the entire structure in the X direction was not found); (b) as observed previously, the weakest point seems to be the out of the plane mechanism of the *eyvan*. The results will be expressed in terms of base shear factor (α) versus control point displacement (δ). The factor α is given by eq. 5.4.

$$\alpha = \frac{\sum F_V}{\sum F_H}$$

Equation 5.4 Base shear factor

where $\sum F_v$ is the sum of the vertical reactions and $\sum F_H$ is the sum of the horizontal reactions. Regarding the numerical model, the properties and the setting discussed in section 5.2 are used.

5.3.1 Pushover +Y direction

In order to better understand the results, displacements and principal strains distribution are reported for two specific load stages: the first load stage L.F.=0,2 is the peak load and the second L.F.=0,18 is the post peak stage. The capacity curve showed in fig 5.9 points out a maximum base shear factor of 0,2 and a good ductility given by a substantial softening behavior only at a late stage.

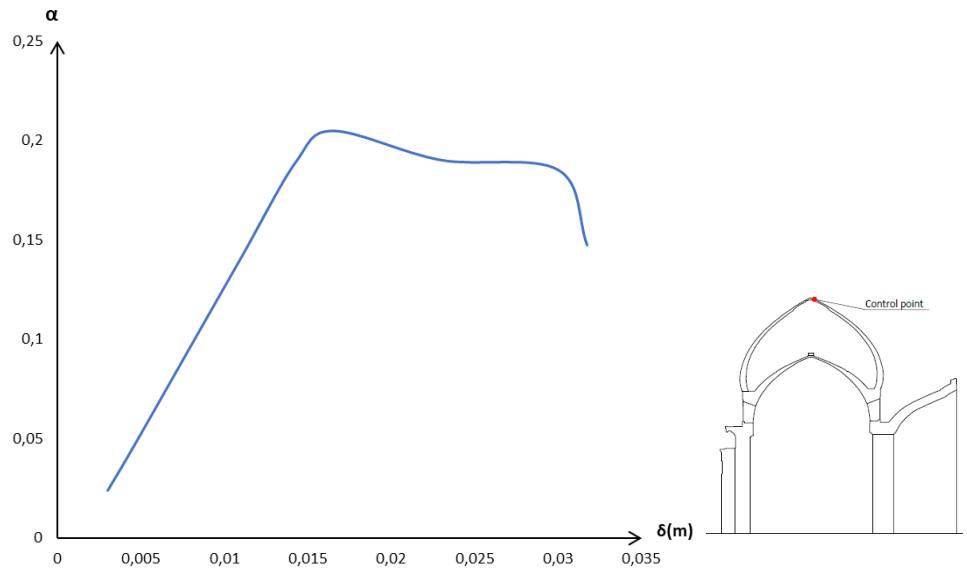

Figure 5.9 Capacity curve for pushover in +Y direction

Regarding the first case (the peak of the capacity curve) it is possible to observe how the larger displacements take place in the dome and mainly on the *eyvan* (fig 5.10). The analysis of the incremental displacements highlights the tendency of the *eyvan* to move out of plane. As concerns the tensile strain, fig. 5.11 confirms how this tendency trigger peaks of tensile deformation between the structure that support the *eyvan* and the structure that support the dome. The analysis of the compression strain (fig 5.11) indicates the presence of large compression at the base of the drum concentrated in the *eyvan* side. This concentration of strain highlights the tendency of the dome to overturn.

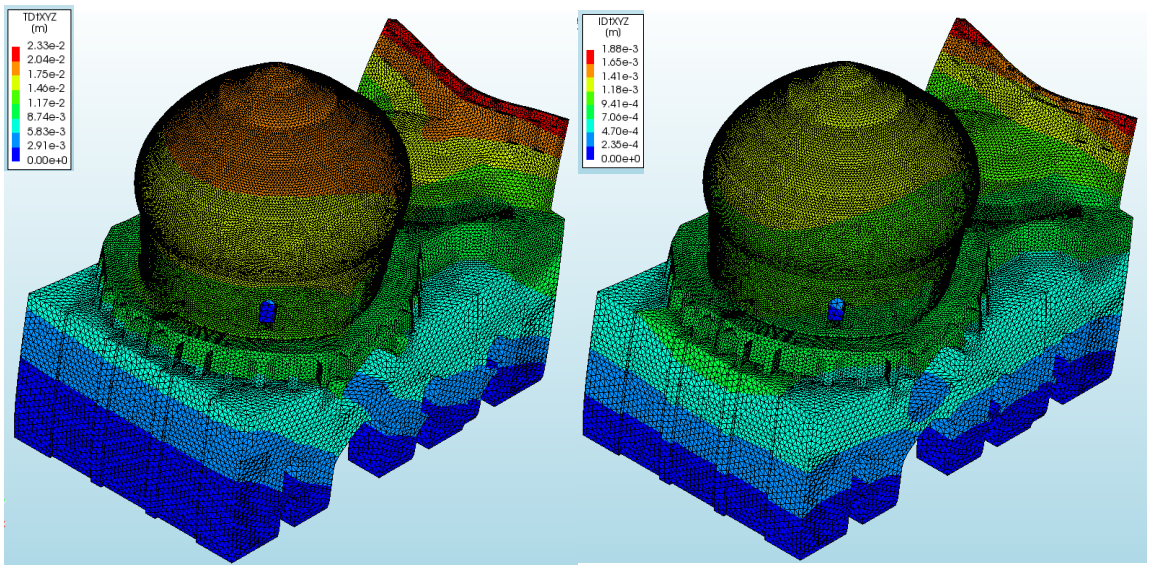

Figure 5.10 Pushover L.F.=0,2, displacement TDtXYZ (left) incremental displacement IDtXYZ (right)

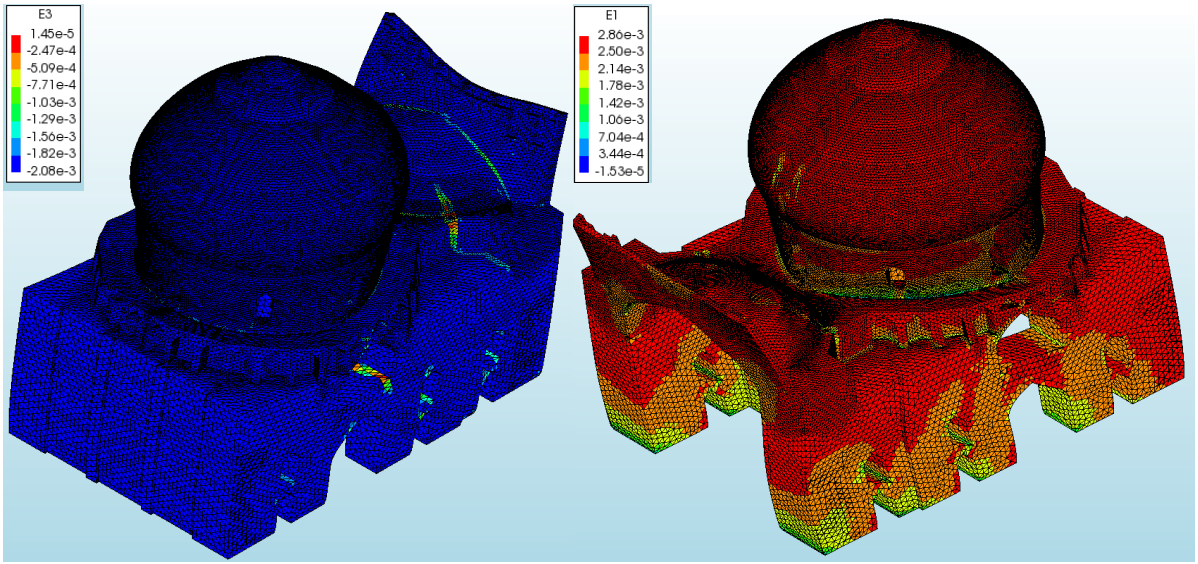

Figure 5.11 Pushover L.F.=0,2 (left) strain E1 (right) strain E3

The second load stage (L.F. = 0,18) shows clearly the collapse mechanism of the mosque under the horizontal load in +Y direction. The analysis of the displacements (fig 5.12) demonstrates how, at this stage, only the *eyvan* is moving. The incremental displacement (fig 5.12) confirms how the collapse is due to the out of plane mechanism of the *eyvan*. The results in terms of compression and tensile strains (fig 5.13), put in evidence how this collapse mechanism is mainly due to the detachment of the crown wall of the *eyvan* from the semi-dome.

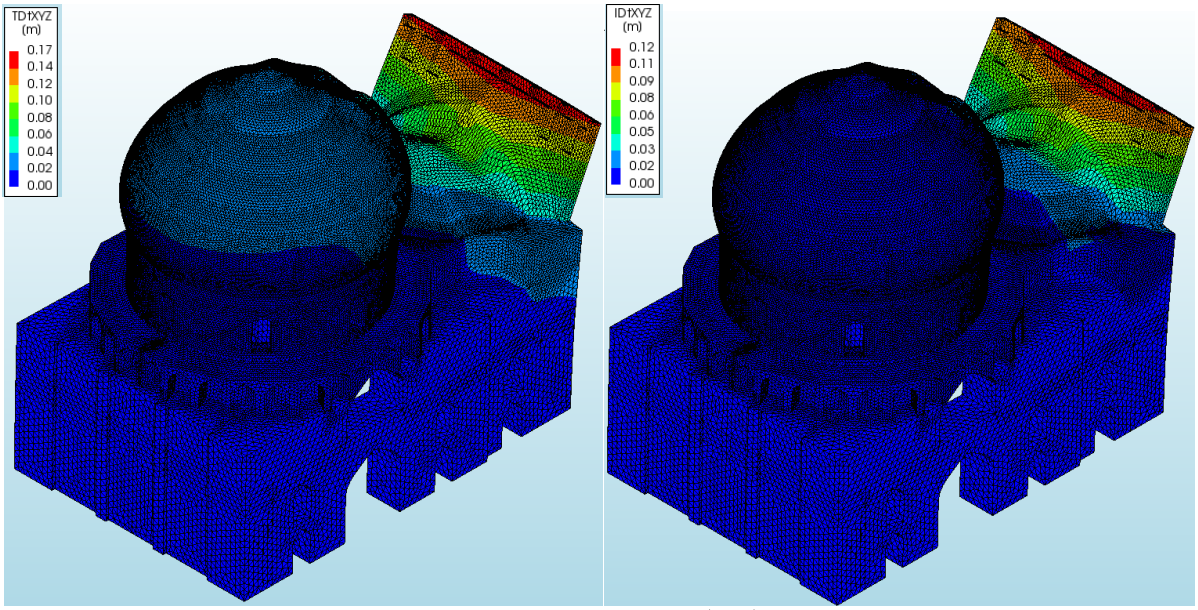

Figure 5.12 Pushover L.F.=0,18 displacement TDtXYZ (left) incremental displacement IDtXYZ (right)

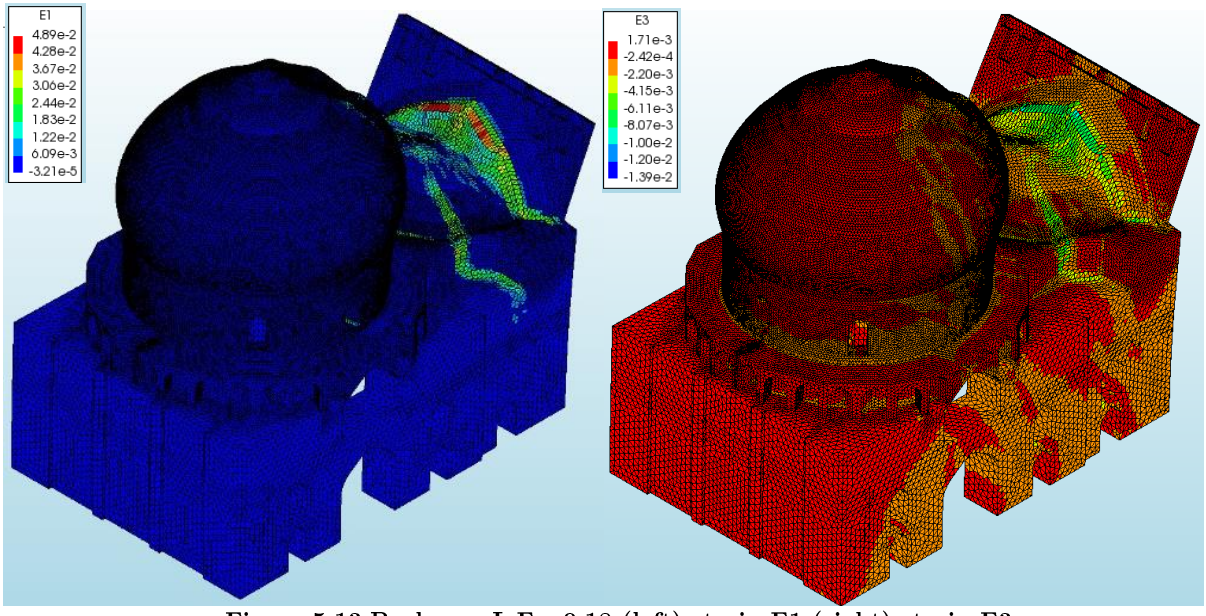

Figure 5.13 Pushover L.F.=0,18 (left) strain E1 (right) strain E3

5.3.2 Pushover -Y direction

In order to better understand the results, displacements and principal strains distribution are reported for two specific load stages: the first load stage L.F.=0,23 is the peak load and the second L.F.=0,21 is the post peak stage. Fig 5.14 shows the capacity curve for the horizontal loading in -Y direction. The curve highlights a maximum base shear factor around 0,23. In comparison with the pushover in +Y direction, it is possible to say that the maximum capacity is higher in this case, but the ductility is decreased. As for the first case, it is possible to observe how the bigger displacements take place on the dome (fig 5.15). Also the incremental displacements (fig 5.15) confirm how in this stage the main role is played from the dome. The tensile principal strains (fig 5.16) are concentrated in the main body of the mosque, especially in the less stiff parts, such as the big openings on the edge. The analysis of the compressive strains (fig 5.16) confirms what was just said, clearly showing a peak of strains in the base of the drum.

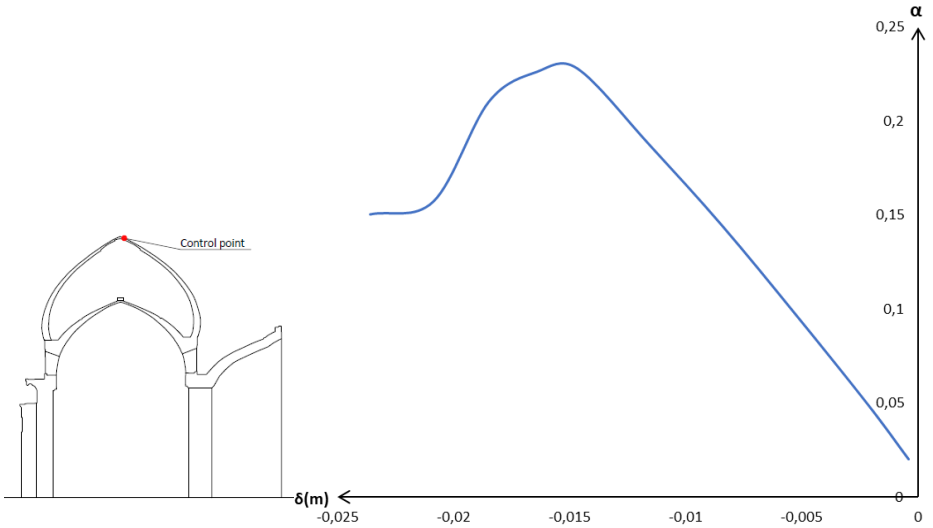

Figure 5.14 Capacity curve for pushover in -Y direction

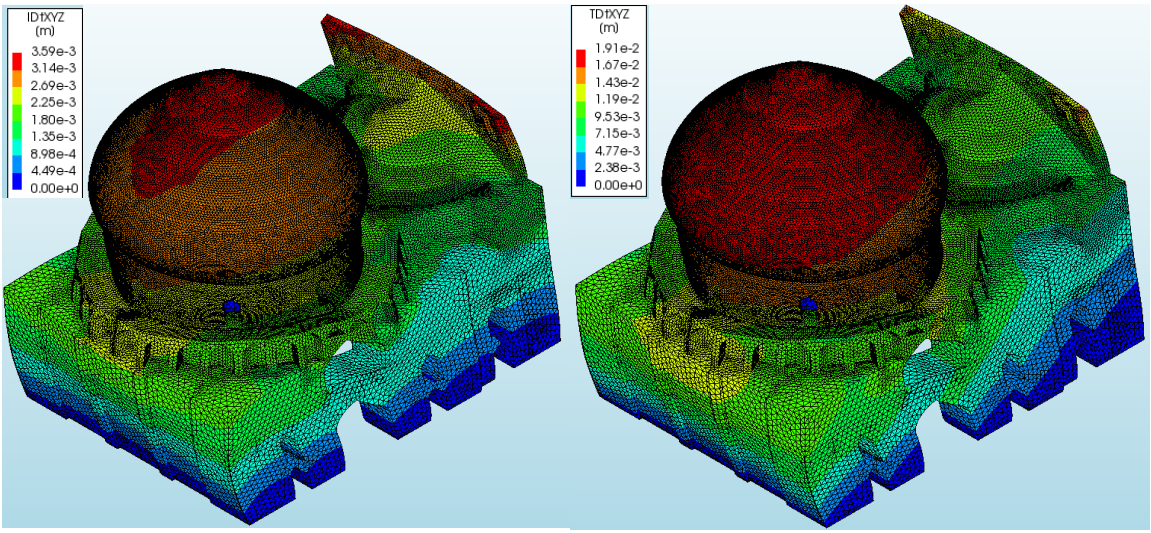

Figure 5.15 Pushover L.F.=0,23 displacement TDtXYZ (left) incremental displacement IDtXYZ (right)

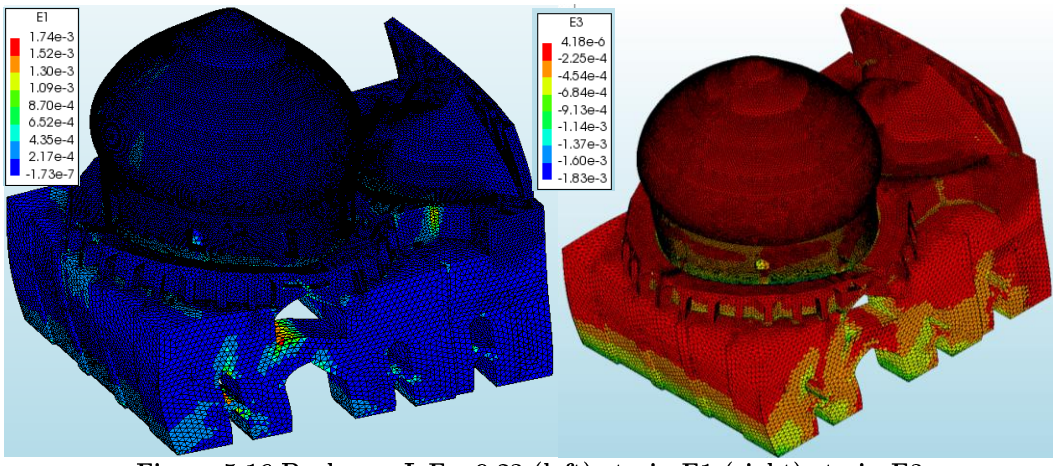

Figure 5.16 Pushover L.F.=0,23 (left) strain E1 (right) strain E3

Even in the second load stage (L.F. = 0,21) the higher displacements are focused on the dome of the mosque (fig 5.17). The analysis of the incremental displacements (fig 5.17) indicates large values in the dome in correspondence of the closed arch (patio side). In this case, the failure mechanism is not so clear as in the pushover in +Y direction, involving significant shear in the walls and curved elements. The study of the principal strains (fig 5.18) indicates the tendency of the structure it supports the dome to separate from the structure it supports the *eyvan.* The analysis of the principal strains inside the dome (fig 5.19) and the incremental displacements (fig 5.17) indicate as a possible failure mechanism the detachment of the stiffener walls (patio side) from the inner dome.

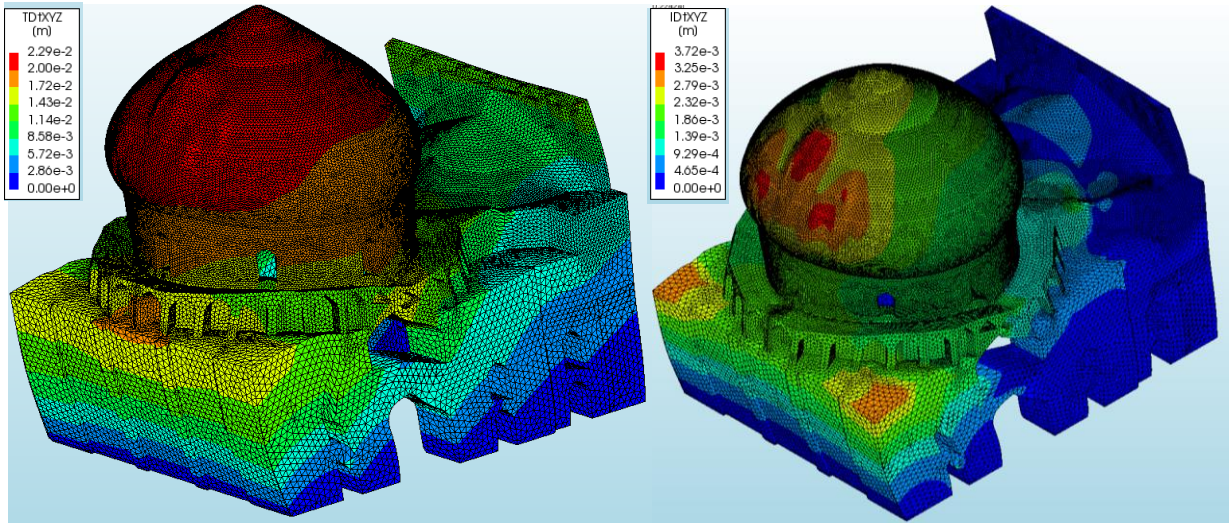

Figure 5.17 Pushover L.F.=0,21 displacement TDtXYZ (left) incremental displacement IDtXYZ (right)

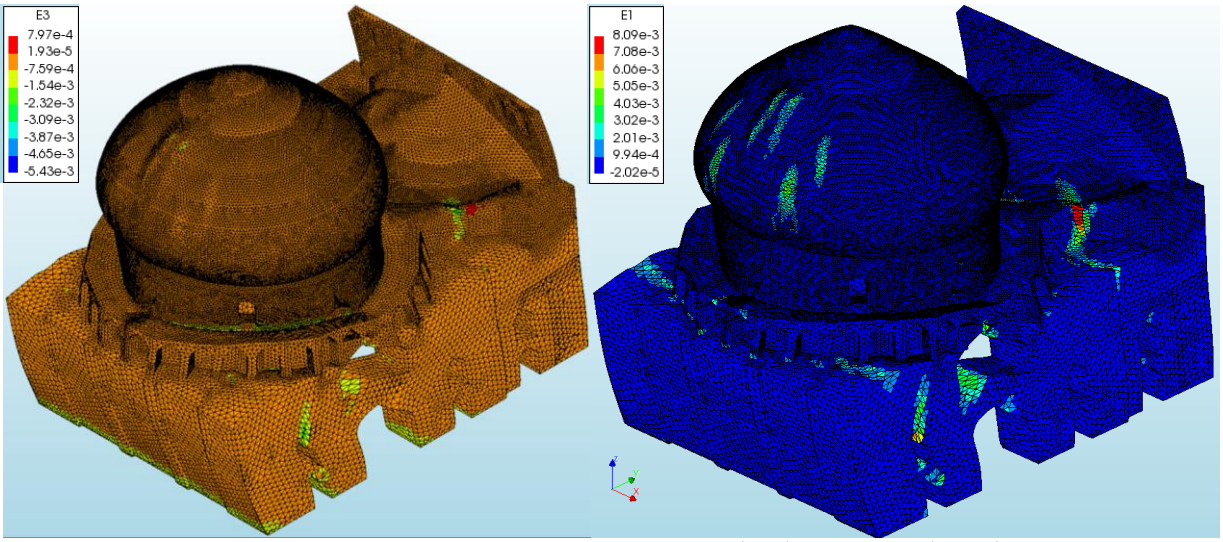

Figure 5.18 Pushover L.F.=0,21 strain E1 (left) strain E3 (right)

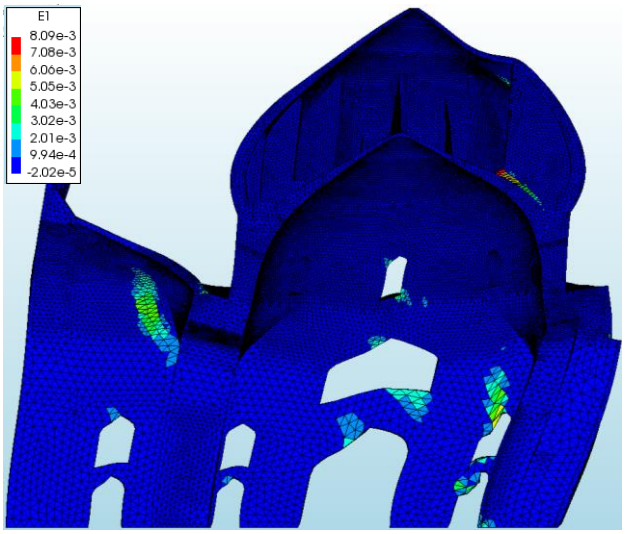

Figure 5.19 Pushover L.F.=0,21 strain E1, symmetric cross section

5.3.3 Ductility

The seismic analysis results point out the collapse mechanisms due to a horizontal action in the Y direction. The response of the structure in the +Y direction is quite ductile. The evaluation of this quantity appears very useful. For this reason, a simplified approach is used. To assess the performance of the structures under seismic action is often used the N2 method. This method, suggested also by (EN 1998-1, 2004), is born for concrete multistory building, it is based on the transformation of the real system with multi degrees of freedom (MDOF) in a simplified model with one degree of freedom (SDOF). The name N2, where "N" means non-linear and 2 the two systems used, MDOF and SDOF (Mezzina, 2011), represent in fact the basic concepts of the method. In the N2 method, seismic demand is determined by using response spectra. Inelastic behavior is taken into account explicitly. Consequently, the structure should, in principle, be modeled as a SDOF system (Fajfar, 2000). In the method the next step is the approximation of the capacity curve (modified for the SDOF system) by a bilinear law. Finally, the bilinear

capacity curve is compared with the demand through the acceleration-displacement-response-spectrum (ADRS). Unfortunately, this approach results very reliable for multistory building where each floor can be approximate as a rigid diaphragm. The method appears unreliable for masonry building without the "box behavior", so, it is clear, how for a structure such as the Shah Mosque, it is inapplicable. Despite these considerations, the second part of the method (bilinearization of the capacity curve) can be a very useful tool to understand the ductility of the system. As regards the assessment of the Shah Mosque, the transformation from MDOF to SDOF system was neglected, passing directly to the bilinearization of the capacity curve. The ductility of the structure was evaluated in the +Y and -Y directions. To this scope a bilinear elastic perfectly plastic approximation (based on the equal energy principle) was used following the (NTC, 2018) approach. Remembering that; (a) the capacity curve is expressed with the relation base shear force (F_b) vs. displacement (δ) (b) the maximum displacement of the system (δ_u) is reached when, in the softening stage, the maximum base shear force (F_{bmax}) is decreased of the 20%. It is possible to divide this procedure in two phases; (a) the elastic part (b) the plastic part. The elastic segment must pass at 0 and at in the point where the base shear force reach the value of $0{,}6F_{bmax}$ (fig 5.20), then, it is also possible to evaluate the stiffness (K) of the bilinear system.

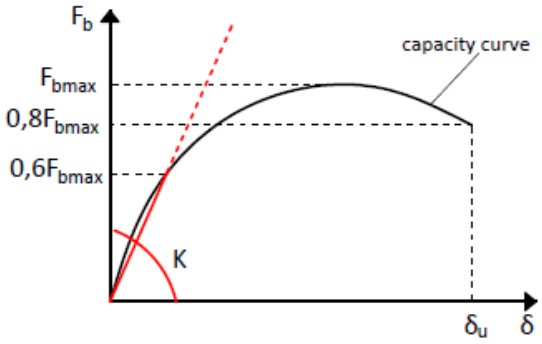

Figure 5.20 Bilinearization, elastic part (drawings by author, 2019)

The second phase, the plastic part (fig 5.21), aims at determination of the missing parameters of the bilinear curve; the displacement (δ_y) and the base shear force in the yielding point (F_y). These parameters are obtainable equaling the area under the capacity curve and the area subtended by the bilinear curve.

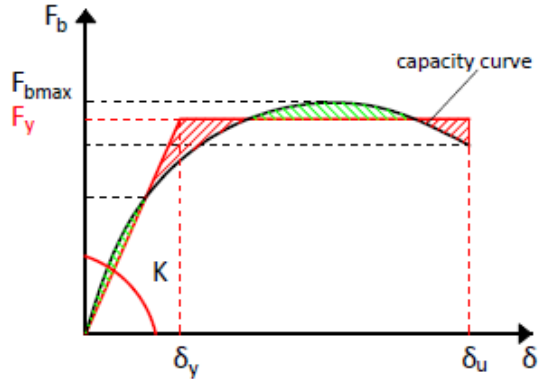

Figure 5.21 Bilinearization, plastic part (drawings by author, 2019)

The bilinearization of the capacity curve for the mosque (fig 5.22) highlights an important difference in terms of ductility (μ) between +Y and -Y response, around 40% (tab 5.4). The capacity in the -Y direction, despite the lower ductility, shows a higher maximum capacity, around 10% (tab 5.4). In terms of stiffness, the behavior of the structure is similar in the two directions.

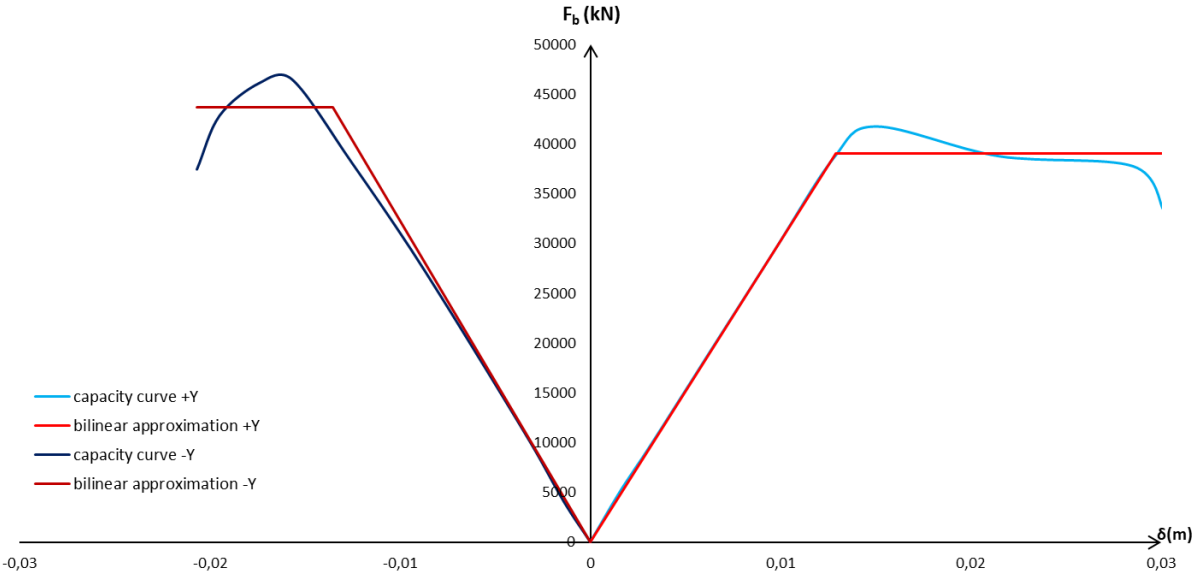

Figure 5.22 Bilinearization of the capacity curve in +Y and -Y directions

Direction	$\mathbf{F}_y$(kN)	δ_y(m)	δ_u(m)	**K**(kN/m)	μ
(+Y)	39054	0,014	0,030	3033789	2,2
(-Y)	43690	0,013	0,021	3125342	1,6
Δ (%)	11	-5	-46	3	-38

Table 5.4 Comparison between the bilinear parameters in +Y and -Y directions

5.3.4 Discussion of the results

The seismic analysis results point out the collapse mechanisms due to a horizontal action in the Y direction. The response of the structure in the +Y direction is quite ductile, if compared with the behavior in the other direction. In this case the collapse is due to the out of plane mechanism of the *eyvan*. The response of the building in the -Y direction highlights a higher loadbearing capacity, although a lower ductility is observed. In this case, the failure seems to be reached by the detachment of the stiffener walls from the inner dome, together with shear failure of the base walls. Finally, is important to underlined how this study is made without take into account the codes, just think about the fact that (EN 1998-1, 2004) needs regularity to perform pushover analysis. This is due to the strong experimental nature of the thesis. For this reason, it is strongly recommended to carry out a further seismic analysis, in all the directions (±X and ±Y) using time history analysis to compare the results with the expected earthquakes in the region. Information about the seismic hazard in the region are reported in annex C.

6. CONCLUSIONS AND RECOMMENDATIONS

During the development of this thesis it was attempted to reach the highest possible level of knowledge on the Shah Mosque. For this reason, a careful study of the building as a whole was made. The first step regarded the state-of-the-art, aimed at collecting all available information about the building. In this phase, particular attention was paid to the historical research, as it leads us to understand better the structural performance of the building. This research was focused on typological and historical geneses of the building, in terms of construction methods, interventions made on the building and actions suffered by the structure during its life. The second step was a preliminary structural analysis made using the data collected in the literature through the state-of-the-art process. This phase was a fundamental tool in order to understand the possible behavior of the structure. The preliminary structural analysis was useful specially to reach a high knowledge level of the structure. In fact, given the distance between the building and Portugal, having a great knowledge before the survey campaign was important. For this purpose, before the in-situ tests were performed:

- Detailed analysis of the geometry was made, to understand what was necessary to check with more accuracy.
- Eigenvalue analysis was made, to prepare an adequate ambient vibration test plan. In fact, the knowledge of the dynamic behavior of the structure can help in: (a) understanding the best positions for the accelerometers in order to obtain good records; (b) check, during the test, if the results are consistent with the preliminary numerical model.

The third step was the in-situ tests and the subsequent data process. During this phase, dynamic identification and sonic tests were performed in situ. The distance to the building and the limited time available required a precise organization. A good action plan made day by day and an excellent teamwork were a winning strategy to obtain reliable experimental data. Subsequently, the processing of the data stressed the importance of the numerical model in the analysis of the experimental results. As mentioned above, the numerical and the experimental model must go hand by hand to reach good information. To finalize this phase, the model was calibrated. This path had as a target the assessment of the static condition of the mosque. The last step performed was the structural analysis of the Shah Mosque. The results obtained shows a reasonable condition of the mosque under gravitational loads. The structure can withstand more than two times its self-weight. Regarding the response of the structure under seismic actions, even if not enough studied in this thesis, the earliest failure mechanism found is the out of plane mechanism of the *eyvan* with a base shear factor around 0,2. As a result of the previous works and in order to understand deeply the static behavior of the Shah Mosque the following recommendations for further studies were proposed:

- Geometry, the numerical model can be updated with the elements neglected in this study. The main parts do not consider in this thesis are the minarets, which could be the weakest elements especially under seismic action, and the adjoining structure, considered in this thesis only as a boundary condition

- Material, the mechanical properties of the masonry constituent the Shah Mosque are not precise enough, because the properties in terms of strength are missing.
- Soil, the specific geotechnical characterization for foundation of the mosque is only partly present. The information about the soil is the one related to the Metro project in Isfahan, which describes the soil in a zone close to the mosque. For this reason, a geotechnical survey of the foundation of the mosque is useful.
- Boundary condition, in order to understand the real behavior of the structure adequate boundary condition are necessary. To this end the updating of the model with the soil property is required and more careful process of the dynamic identification data obtained.
- Modern strengthening intervention, the response of the structure can be reliable only if all the structural elements are characterized. For this reason, the implementation of the model with the strengthening elements is suggested.
- Seismic hazard, the knowledge of the probability that an earthquake will occur in a given geographic area, within a given window of time, and with ground motion intensity exceeding a given threshold is necessary to assess the performance of the structure. A study of the seismic hazard in the Isfahan region seems fundamental.
- Seismic analysis, the seismic analysis of this type of buildings need particularly attention. For this reason, the following analysis are suggested: (a) pushover analysis in the X and Y direction (positive and negative). For this type of analysis also the use of at least two load profiles is suggested; (b) dynamic non-linear analysis with a real or spectrum-compatible accelerogram
- Seismic assessment, an adequate comparison between the capacity of the structure and the demand required from the possible earthquake is necessary, in order to establish the safety level of the structure
- Strengthening proposal, the evaluation of the past strengthening design and the proposal of new strengthening interventions on the structure (either if needed or only conceptually for research sake) is interesting.

REFERENCES

Aguilar, R., Torrealva, D., Ramos, L., and Lourenço, P., (2012) 'Operational Modal Analysis Tests on Peruvian Historical Buildings: The Case Study of the 19th Century Hotel Comercio', in Proceedings of the 15th World Conference on Earthquake Engineering.

Ambraseys, N. N. (1979) 'A Test Case of Historical Seismicity: Isfahan and Chahar Mahal, Iran', The Geographical Journal, 145(1), p. 56.

Ardalan, N. and Bakhtiar, L. (1973) 'The sense of unity: the Sufi tradition in Persian architecture', University of Chicago press, 9.

ARTeMIS Modal (2015) '"SVS-Structural Vibration Solutions A/S"'. Aalborg, Denmark.

Ashkan, M. and Ahmad, Y. (2009) 'Persian Dome : History, Morphology and Typologies', International Journal of Architectural Research-IJAR, 3(3), pp. 98–115.

Ashkan, M. and Ahmad, Y. (2010) 'Discontinuous double-shell domes through Islamic eras in the Middle East and Central Asia: History, morphology, typologies, geometry, and construction', Nexus Network Journal, 12(2), pp. 287–319.

Aşıkoğlu, A., Lourenco, P. B., Avşar, Ö., and Silva, L. C.,(2019) 'Finite Element Modeling and Operational Modal Analysis of a Historical finite element modeling and operational modal', University of Minho, Guimaraes.

Binda, L., Saisi, A. and Tiraboschi, C. (2001) 'Application of sonic tests to the diagnosis of damaged and repaired structures', NDT and E International, 1, pp. 123–138.

Blake, S. P. (1999) Half the world : the social architecture of Safavid Isfahan, 1590-1722, Islamic art and architecture series, V.9. Edited by M. Pub. Costa Mesa (California): Mazda Pub ed.

Circolare NTC18 (2019) Circolare 21 gennaio 2019 n.7 " Istruzioni per l'applicazione dell'«Aggiornamento delle "Norme tecniche per le costruzioni"» di cui al decreto ministeriale 17 gennaio 2018", Ministero delle Infrastrutture.

Coste, P. (1867) 'Drawings'. The New York Public Library collection.

DIANA FEA BV (2019) 'Diana User's Manual, Release 10.3', DIANA FEA BV. Delft.

Dinani, A. T. (2019) Hybrid double dome: building performance and cable-net strengthening of Esfahan Shah Mosque's dome. PhD thesis. PoliMi.

Dinani, A. T., Sadeghi, S. and Lourenco, P. B. (2019) 'A Double Dome Through the Ages', in Springer (ed.) Structural Analysis of Historical Constructions. Cham, pp. 87–95.

EN 1998-1 (2004) '8: Design of structures for earthquake resistance—Part 1: General rules, seismic actions and rules for buildings (EN 1998-1: 2004)', European Committee for Normalization, Brussels.

Fajfar, P. (2000) 'A Nonlinear Analysis Method for Performance-Based Seismic Design', Earthquake Spectra, Vol.16, No, pp. 573–592.

Hamzehloo, H. et al. (2012) 'Seismic Hazard Maps of Iran', International Institute of Earthquake Engineering and Seismology. Tehran, I.R.Iran.

Hejazi, M. and Mehdizadeh Saradj, F. (2012) Persian architectural heritage: form, structure and conservation. Southampton: WIT Press.

Herdeg, K. (1990) 'Formal structure in Islamic architecture of Iran and Turkistan'. Rizzoli Intl Pubns.

Hillenbrand, R. (1994) Islamic architecture: form, function, and meaning, Columbia University Press. New York: New York : Columbia University Press.

ICOMOS (1964) 'International Charter for the conservation and restoration of monuments and sites', in The Venice Charter 1964.

ICOMOS Report of the Bureau (1979). Paris. Available at: http://whc.unesco.org/archive/repbur79.htm.

Jirásek, M. and Lourenço, P. B. (2018) 'SA2-08: Solution procedures for nonlinear analysis'. University of Minho, Guimaraes: Slideshow presentation, Advanced Masters in Structural Analysis of Monuments and Historical Constructions program.

Kavak Consulting Engineers (2009) 'Study of structural damages of the Allahvardi Khan Bridges by the Finite Element Method'.

LabVIEW (2013) 'LabVIEW - National Instruments', Austin, Texas, United States.

Lourenço, P. . (2018) 'SA2 14a: Material Data to Use, Slideshow presentation'. University of Minho, Guimaraes: Slideshow presentation, Advanced Masters in Structural Analysis of Monuments and Historical Constructions program.

Lourenço, P. B. (1996) Computational strategies for masonry structures, PhD Thesis. Delft University of Technology.

Lourenço, P. B. (2009) 'Recent advances in masonry modelling: micromodelling and homogenisation', University of Minho, Guimaraes, pp. 251–94.

Lourenço, P. B. and Pereira, J. M. (2018) Seismic Retrofitting Project: Recommendations for Advanced Modeling of Historic Earthen Sites. Guimaraes.

Maaref-I Salnameh-I Esfahan (1936) 'Sal-i Tahsili 1313-1314', Report of the Esfahan Ministry of Education.

Maccarini, H., Vasconcelos, G., Rodrigues, H., Ortega, J., and Lourenço, P. B.,(2018) 'Out-of-plane behavior of stone masonry walls: Experimental and numerical analysis', Construction and Building Materials. Elsevier Ltd, 179, pp. 430–452.

Mainstone, R. J. (2001) 'Vaults, domes, and curved membrances. In Developments on Structural Form', Architectural Press, (London), p. 124.

Mezzina, M. (2011) Progettazione sismo-resistente di edifici in cemento armato. Edited by D. Agostini. Novara.

Milne, I., Ritchie, R. O. and Karihaloo, B. (2007) Comprehensive Structural Integrity, Comprehensive Structural Integrity. Elsevier Science.

Miranda, L. F., Rio, J., Miranda Guedes, J., and Costa, A., (2012) 'Sonic Impact Method - A new technique for characterization of stone masonry walls', Construction and Building Materials, 36, pp. 27–37.

NTC (2018) Norme tecniche delle costruzioni - D.M. 17/01/2018, Ministero Infrastrutture e Trasporti. Roma.

Pastor, M., Binda, M. and Harčarik, T. (2012) 'Modal assurance criterion', Procedia Engineering, 48, pp. 543 – 548.

Pirnia, K. (1987) 'Joints and Vaults', Asar Magazine, No 24(Tehran), pp. 5–192.

Pirnia, K. (1991) 'Dome in architecture of Iran', Asar Magazine, No 20(Tehran).

Qixian, L. and Bungey, J. (1996) 'Using compression wave ultrasonic transducers to measure the velocity of surface waves and hence determine dynamic modulus of elasticity for concrete', Construct Build Mater, 10, pp. 237–242.

Ramos, L. F., Aguilar, R. and Lourenço, P. B. (2011) 'Operational modal analysis of historical constructions using commercial wireless platforms', Structural Health Monitoring 10(5). Printince Hall, pp. 511–521.

Roca, P., Cervera, M., Gariup, G., and Pela', L., (2010) 'Structural analysis of masonry historical constructions. Classical and advanced approaches', Archives of Computational Methods in Engineering, 17(3), pp. 299–325.

Standard No. 2800 (2007) Iranian code of practice for seismic resistant design of buildings. Theran: BHRC Publication No. S – 465.

Varjavand, P. (1976) 'How the Masjed-e shah survived from the demolition', Art and people magazine, 164(Ministry of Culture and people, Theran).

Vecchio, F. J. and Collins, M. P. (1986) 'The Modified Compression-Field Theory for Reinforced Concrete Elements Subjected to Shear', ACI Journal Proceedings, 83, pp. 219–231.

Vinci, M. (2018) Metodi di calcolo e di consolidamento per edifici in muratura. Palermo: Dario Flaccovio Ed.

Yarshater, E. (1983) The Cambridge History of Iran. Cambridge, Massachusets: Columbia University. Center for Iranian Studies.

ANNEX A

Table containing a list of all instrumentally located earthquakes of the past century in the region of isfahan and Chahar Mahal, an area limited by the 31st and 33rd degrees of north latitude and the 50th and 52nd degrees of east longitude. The magnitude of the events was calculated using either amplitude-period data or P and S distances of recording [Ambraseys 1979].

TABLE I

Instrumentally located epicentres within 31° and 33°N, and 50° and 52°E

Date		Time (GMT)	Epicentre N	E	m	h	I₀
1922 Mar	21	1656	31·75°	−51·14° k	5·5	n	VII
1934 Mar	13	2333	31·00	−51·50 k	5·3	n	VII+
1958 July	26	1553	32·00	−50·60 k	4·2	n	VII
1960 Mar	2	1218	32·00	−50·25 e	4·0	n	
Mar	24	2321	31·50	−51·00 e	4·2	n	
Apr	23	0026	31·13	−50·33 b	4·3	i	
May	10	2152	31·80	−50·80 e	4·5	n	
June	7	2209	31·00	−51·00 e	4·2	n	
June	27	1251	32·00	−50·00 e	4·2	n	
Sept	21	2305	31·92	−50·82 k	5·0	n	VI+
1961 Oct	1	2057	32·00	−52·00 d	3·9	n	
1962 Aug	6	0232	32·17	−50·64 k	3·6	n	V
Nov	20	1156	31·95	−51·30 k	3·8	n	V
1964 Feb	19	2034	31·57	−50·62 b	4·2	n	
1965 Mar	25	1954	32·26	−50·41 b	4·7	n	
June	7	1606	31·00	−50·40 e	4·3	n	
1966 Jan	16	2002	31·00	−50·50 e	4·4	i	
1967 July	27	0140	31·61	−50·40 e	4·9	i	IV
1968 Nov	6	1706	31·84	−50·76 e	4·6	n	
1969 Feb	19	2212	32·20	−50·70 f	3·5	n	
May	30	1128	32·90	−50·30 f	4·4	n	
June	20	1728	31·00	−50·00 f	4·5	n	
July	15	1249	32·80	−50·30 f	3·8	n	
Nov	30	1911	32·40	−51·70 f	4·2	n	
1971 Oct	5	2245	31·65	−50·70 e	4·1	n	IV
1972 Aug	6	0700	31·80	−50·10 g	5·0	n	
1973 Jan	10	1730	31·02	−51·32 e	4·7	i	
July	22	0947	31·20	−50·10 e	3·3	i	
Aug	5	0944	31·06	−50·30 e	4·7	i	
Aug	23	1226	31·87	−51·01 e	5·0	n	
Aug	28	1227	31·60	−50·80 e	4·7	n	
1974 Mar	1	0614	31·10	−51·20 e	4·3	i	
Mar	12	0145	32·25	−50·15 e	4·3	n	
May	4	2208	31·85	−50·62 e	4·0	i	
May	17	1946	31·29	−51·22 e	4·9	n	
Sept	10	0550	32·40	−50·40 g	3·9	i	
1975 Sept	21	1416	31·60	−51·04 g	5·2	n	VII
Oct	22	0441	31·64	−50·22 g	3·6	i	
Nov	13	0055	31·78	−50·94 g	4·1	n	
1976 Feb	26	0922	31·40	−50·08 g	4·1	n	
Apr	13	2200	31·49	−50·30 g	3·8	i	
Sept	6	1604	31·13	−50·37 g	5·0	n	
1977 Jan	12	0149	31·83	−50·49 g	4·2	i	
Mar	26	0306	31·27	−50·01 g	4·4	n	
Apr	6	1336	31·92	−50·64 g	5·6	n	VII+
Apr	12	2312	31·98	−50·74 g	4·9	n	
May	4	0201	31·79	−50·86 g	4·8	n	VI+

Note: Epicentral locations: (a) Institute of Geological Sciences, Edinburgh; (b) Nowroozi, 1976; (c) Institut de Physique du Globe, Strasbourg; (d) Station Seismologique de Chiraz, 1962–1963; (d) International Seismological Centre; (f) Goudarzi, 1972; (g) PDE U.S. Geological Survey; (k) Macroseismic locations.
m = body-wave magnitude; h = focal depth, n(normal), i(intermediate);
I = epicentral Intensity (MM)

ANNEX B

Table containing the first 100 modes of the calibrated model.

Modes		X			Y		
n	f (Hz)	Eff. Mass (t)	Eff. Mass (%)	Cumulative (%)	Eff. Mass (t)	Eff. Mass (%)	Cumulative (%)
1	2,46	9,11E-06	4,45E-08	4,45E-08	1,29E+04	6,29E+01	6,29E+01
2	2,75	6,78E+03	3,31E+01	3,31E+01	2,12E-08	1,04E-10	6,29E+01
3	3,51	2,60E+02	1,27E+00	3,44E+01	2,61E-05	1,28E-07	6,29E+01
4	3,68	1,34E-04	6,53E-07	3,44E+01	8,31E+02	4,06E+00	6,70E+01
5	4,29	2,58E+01	1,26E-01	3,45E+01	2,86E-01	1,40E-03	6,70E+01
6	4,31	1,61E-02	7,86E-05	3,45E+01	1,43E+03	6,96E+00	7,39E+01
7	4,53	1,42E+03	6,96E+00	4,15E+01	1,08E-02	5,28E-05	7,39E+01
8	4,67	5,20E-03	2,54E-05	4,15E+01	4,22E+02	2,06E+00	7,60E+01
9	5,05	5,53E+02	2,70E+00	4,42E+01	2,98E-05	1,46E-07	7,60E+01
10	5,23	8,84E-03	4,32E-05	4,42E+01	2,77E+02	1,35E+00	7,74E+01
11	5,32	6,67E+02	3,26E+00	4,74E+01	1,08E-02	5,29E-05	7,74E+01
12	5,48	3,65E-02	1,78E-04	4,74E+01	1,25E+02	6,08E-01	7,80E+01
13	5,55	2,80E+02	1,37E+00	4,88E+01	4,56E-03	2,23E-05	7,80E+01
14	5,75	4,11E-04	2,01E-06	4,88E+01	2,32E+01	1,14E-01	7,81E+01
15	6,77	4,29E+02	2,10E+00	5,09E+01	2,22E-05	1,08E-07	7,81E+01
16	6,92	1,13E-03	5,53E-06	5,09E+01	1,22E+02	5,94E-01	7,87E+01
17	7,26	3,38E-05	1,65E-07	5,09E+01	9,51E+02	4,64E+00	8,33E+01
18	7,47	1,60E+01	7,84E-02	5,10E+01	7,86E-02	3,84E-04	8,33E+01
19	7,48	1,34E-01	6,54E-04	5,10E+01	1,50E+01	7,33E-02	8,34E+01
20	7,65	2,92E+01	1,42E-01	5,11E+01	4,84E-03	2,36E-05	8,34E+01
21	7,73	1,78E-03	8,67E-06	5,11E+01	1,55E+02	7,59E-01	8,42E+01
22	8,03	6,80E-02	3,32E-04	5,11E+01	8,22E-02	4,02E-04	8,42E+01
23	8,03	1,63E+01	7,97E-02	5,12E+01	2,25E-04	1,10E-06	8,42E+01
24	8,24	1,06E+02	5,16E-01	5,17E+01	6,18E-06	3,02E-08	8,42E+01
25	8,43	4,18E-04	2,04E-06	5,17E+01	4,64E+01	2,27E-01	8,44E+01
26	8,79	4,76E-01	2,33E-03	5,17E+01	6,92E-03	3,38E-05	8,44E+01
27	8,90	3,72E+00	1,82E-02	5,17E+01	1,13E-03	5,51E-06	8,44E+01
28	8,96	1,37E+02	6,71E-01	5,24E+01	8,20E-03	4,01E-05	8,44E+01
29	8,99	5,46E-04	2,67E-06	5,24E+01	1,63E+01	7,97E-02	8,45E+01
30	9,16	2,08E+00	1,02E-02	5,24E+01	9,24E+00	4,52E-02	8,45E+01
31	9,31	2,09E+02	1,02E+00	5,34E+01	1,19E+01	5,81E-02	8,46E+01
32	9,32	1,88E+02	9,18E-01	5,43E+01	2,49E+01	1,22E-01	8,47E+01
33	9,38	6,37E+00	3,11E-02	5,44E+01	4,37E-01	2,13E-03	8,47E+01
34	9,41	7,34E+01	3,59E-01	5,47E+01	2,05E+00	1,00E-02	8,47E+01
35	9,44	1,02E+02	5,00E-01	5,52E+01	1,27E+00	6,20E-03	8,47E+01
36	9,46	3,47E+02	1,69E+00	5,69E+01	2,32E-02	1,13E-04	8,47E+01
37	9,50	4,15E+01	2,03E-01	5,71E+01	7,61E-02	3,72E-04	8,47E+01
38	9,56	6,94E+01	3,39E-01	5,75E+01	3,16E-01	1,54E-03	8,47E+01
39	9,78	5,89E+02	2,88E+00	6,03E+01	9,63E-05	4,71E-07	8,47E+01

40	10,11	5,29E+01	2,58E-01	6,06E+01	4,14E-06	2,02E-08	8,47E+01
41	10,19	4,38E-03	2,14E-05	6,06E+01	2,21E-02	1,08E-04	8,47E+01
42	10,32	2,80E-03	1,37E-05	6,06E+01	2,02E+01	9,89E-02	8,48E+01
43	10,34	5,84E-04	2,85E-06	6,06E+01	1,40E-01	6,85E-04	8,48E+01
44	10,47	6,75E-07	3,30E-09	6,06E+01	1,34E+02	6,54E-01	8,55E+01
45	10,71	9,83E-04	4,80E-06	6,06E+01	5,64E-01	2,75E-03	8,55E+01
46	10,82	8,77E-01	4,29E-03	6,06E+01	5,25E-03	2,57E-05	8,55E+01
47	10,92	2,24E-03	1,10E-05	6,06E+01	5,37E+01	2,62E-01	8,57E+01
48	11,03	8,29E-01	4,05E-03	6,06E+01	3,92E-04	1,91E-06	8,57E+01
49	11,11	1,87E+01	9,12E-02	6,07E+01	1,22E-03	5,95E-06	8,57E+01
50	11,27	7,84E-03	3,83E-05	6,07E+01	1,88E+01	9,17E-02	8,58E+01
51	11,31	2,50E+01	1,22E-01	6,08E+01	1,23E-03	6,02E-06	8,58E+01
52	11,50	8,25E-08	4,03E-10	6,08E+01	2,43E+02	1,19E+00	8,70E+01
53	11,75	6,26E+00	3,06E-02	6,09E+01	7,56E-01	3,69E-03	8,70E+01
54	11,75	8,00E-02	3,91E-04	6,09E+01	6,70E+01	3,27E-01	8,73E+01
55	12,03	7,03E+02	3,43E+00	6,43E+01	1,86E-03	9,10E-06	8,73E+01
56	12,08	9,64E-03	4,71E-05	6,43E+01	4,02E+00	1,97E-02	8,74E+01
57	12,24	5,80E-05	2,83E-07	6,43E+01	1,03E+00	5,02E-03	8,74E+01
58	12,35	7,55E-03	3,69E-05	6,43E+01	7,29E+00	3,56E-02	8,74E+01
59	12,49	3,31E+01	1,62E-01	6,45E+01	2,42E-02	1,18E-04	8,74E+01
60	12,49	1,22E+00	5,95E-03	6,45E+01	5,30E-01	2,59E-03	8,74E+01
61	12,68	4,41E-03	2,16E-05	6,45E+01	1,62E+02	7,90E-01	8,82E+01
62	12,69	5,63E+01	2,75E-01	6,47E+01	2,59E-05	1,27E-07	8,82E+01
63	12,81	6,20E-02	3,03E-04	6,47E+01	2,64E-02	1,29E-04	8,82E+01
64	12,87	2,18E+02	1,06E+00	6,58E+01	3,78E-02	1,85E-04	8,82E+01
65	12,90	1,66E+00	8,10E-03	6,58E+01	1,55E+01	7,58E-02	8,83E+01
66	12,93	4,82E+02	2,36E+00	6,82E+01	1,40E-02	6,86E-05	8,83E+01
67	13,18	1,94E+00	9,48E-03	6,82E+01	9,35E+00	4,57E-02	8,83E+01
68	13,19	1,55E+02	7,58E-01	6,89E+01	1,26E-01	6,17E-04	8,83E+01
69	13,40	1,96E+01	9,60E-02	6,90E+01	2,21E-03	1,08E-05	8,83E+01
70	13,53	4,54E-02	2,22E-04	6,90E+01	2,22E-01	1,08E-03	8,83E+01
71	13,64	3,68E+02	1,80E+00	7,08E+01	1,07E-03	5,22E-06	8,83E+01
72	13,72	1,36E-01	6,65E-04	7,08E+01	2,13E+01	1,04E-01	8,84E+01
73	13,88	3,39E+01	1,65E-01	7,10E+01	4,46E-03	2,18E-05	8,84E+01
74	14,02	1,55E+02	7,56E-01	7,18E+01	9,27E-02	4,53E-04	8,84E+01
75	14,06	2,27E-01	1,11E-03	7,18E+01	5,09E+01	2,49E-01	8,87E+01
76	14,12	2,84E-01	1,39E-03	7,18E+01	1,18E+01	5,79E-02	8,87E+01
77	14,26	1,89E+02	9,26E-01	7,27E+01	2,77E-02	1,35E-04	8,87E+01
78	14,28	1,63E+00	7,98E-03	7,27E+01	1,58E+01	7,70E-02	8,88E+01
79	14,33	1,59E-01	7,75E-04	7,27E+01	2,75E+01	1,34E-01	8,89E+01
80	14,48	1,18E+02	5,77E-01	7,33E+01	1,08E-02	5,27E-05	8,89E+01
81	14,54	2,62E-01	1,28E-03	7,33E+01	1,07E+01	5,21E-02	8,90E+01
82	14,56	3,08E+00	1,51E-02	7,33E+01	8,45E-01	4,13E-03	8,90E+01
83	14,66	2,93E+00	1,43E-02	7,33E+01	2,99E+00	1,46E-02	8,90E+01
84	14,71	4,43E+02	2,16E+00	7,55E+01	3,43E-01	1,68E-03	8,90E+01
85	14,73	8,55E+01	4,18E-01	7,59E+01	4,09E+00	2,00E-02	8,90E+01

86	14,74	5,78E+00	2,82E-02	7,59E+01	3,37E+00	1,64E-02	8,90E+01
87	14,87	1,25E+02	6,11E-01	7,65E+01	3,09E-01	1,51E-03	8,90E+01
88	14,88	2,18E+01	1,06E-01	7,66E+01	1,27E+00	6,20E-03	8,91E+01
89	14,97	6,69E+02	3,27E+00	7,99E+01	4,14E-02	2,02E-04	8,91E+01
90	15,08	4,44E+02	2,17E+00	8,21E+01	1,36E+00	6,66E-03	8,91E+01
91	15,15	6,05E+01	2,96E-01	8,24E+01	8,72E+00	4,26E-02	8,91E+01
92	15,17	8,80E+01	4,30E-01	8,28E+01	5,63E-01	2,75E-03	8,91E+01
93	15,23	3,21E-02	1,57E-04	8,28E+01	2,32E+00	1,13E-02	8,91E+01
94	15,32	9,74E+01	4,76E-01	8,33E+01	5,96E+00	2,91E-02	8,91E+01
95	15,32	4,66E+01	2,28E-01	8,35E+01	1,03E+01	5,02E-02	8,92E+01
96	15,44	3,53E+00	1,72E-02	8,35E+01	1,91E-03	9,33E-06	8,92E+01
97	15,46	7,40E+00	3,61E-02	8,35E+01	1,47E-01	7,19E-04	8,92E+01
98	15,50	4,36E-02	2,13E-04	8,35E+01	1,31E-01	6,38E-04	8,92E+01
99	15,57	2,74E+01	1,34E-01	8,37E+01	2,00E+01	9,79E-02	8,93E+01
100	15,59	8,10E+01	3,96E-01	8,41E+01	1,65E+01	8,05E-02	8,94E+01

ANNEX C

A new seismic hazard maps have been developed for Iran based on probabilistic earthquake hazard analysis. The hazard map depict peak horizontal ground acceleration with 10% and 2% probability of exceedance in 50 years, corresponding to return period of 475 and 2475 years, respectively (Hamzehloo et al., 2012).

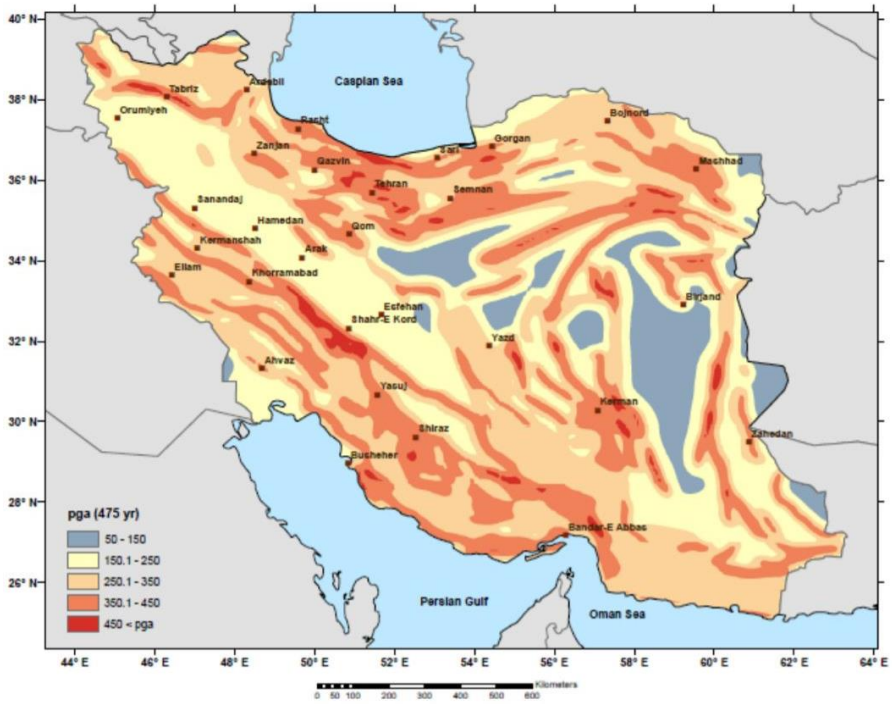

Figure C.1 PGA (cm/s^2) with a return period of 475 years

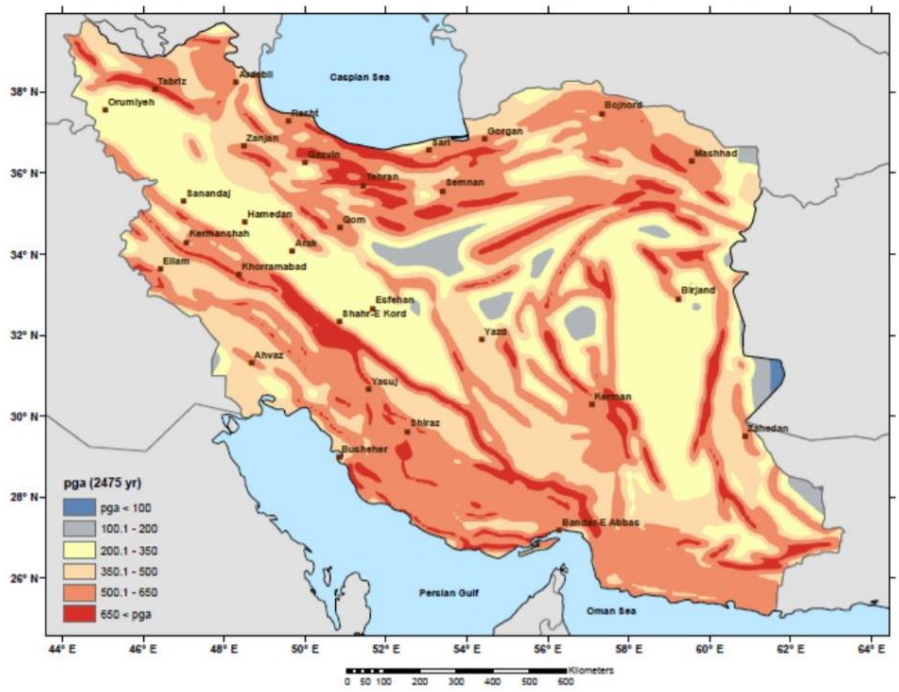

Figure C.2 PGA (cm/s^2) with a return period of 2475 years

Further, the Iranian code for seismic action (Standard No. 2800, 2007) provides the peak ground acceleration for several level of seismic hazard (fig C.3). Then, for each city in the country, the code provides the type of seismic hazard (fig C.4). These values are made to be used with an equivalent static analysis, but is for sure, a useful tool to evaluate the possible magnitude of the expected earthquake.

Zone	Description	Design base acceleration(/g)
1	Very high level of relative seismic hazard	0.35
2	High level of relative seismic hazard	0.30
3	Intermediate level of relative seismic hazard	0.25
4	Low level of relative seismic hazard	0.20

Figure C.3 Design base acceleration ratio for various seismic zone

Item	City	Province	Seismic relative hazard			
			VH	H	I	L
1	Eghlid	Fars		×		
2	Eivan	Ilam			×	
3	Eivanekey	Semnan		×		
4	Esfahan	Esfahan			×	
5	Esfarayen	N. Khorasan		×		
6	Eshtehard	Tehran	×			

Figure C.4 Seismic Hazard for the cities with the "E" in Iran